

# MVDC Distribution Fed High Power Multi-Motor Drives

THÈSE N° 8517 (2018)

PRÉSENTÉE LE 29 JUIN 2018

À LA FACULTÉ DES SCIENCES ET TECHNIQUES DE L'INGÉNIEUR  
LABORATOIRE D'ÉLECTRONIQUE DE PUISSANCE  
PROGRAMME DOCTORAL EN GÉNIE ÉLECTRIQUE

ÉCOLE POLYTECHNIQUE FÉDÉRALE DE LAUSANNE

POUR L'OBTENTION DU GRADE DE DOCTEUR ÈS SCIENCES

PAR

**Uzair JAVAID**

acceptée sur proposition du jury:

Prof. M. Paolone, président du jury  
Prof. D. Dujic, Dr W. van der Merwe, directeurs de thèse  
Dr S. Colombi, rapporteur  
Prof. E. Levi, rapporteur  
Dr R. Cherkaoui, rapporteur



ÉCOLE POLYTECHNIQUE  
FÉDÉRALE DE LAUSANNE

Suisse  
2018

École Polytechnique Fédérale de Lausanne  
Power Electronics Laboratory  
Station 11  
1015 Lausanne, Switzerland  
<http://pel.epfl.ch>  
© 2018 by Uzair Javaid

*Dedicated to my family*





# Acknowledgements

*“Do not go where the path may lead, go instead where there is no path and leave a trail”*

Ralph Waldo Emerson

The Ph.D. journey, I undertook four years ago, was inspired by this quote and during this journey a number of people played very important role. I would like to take this opportunity to acknowledge their efforts and support which played a direct or indirect role in this accomplishment.

First of all, I would like to express my gratitude to Prof. Dražen Dujic for providing me the opportunity to do research in the newly established Power Electronics Laboratory (PEL) at EPFL and showing his faith in my abilities as a researcher. His confidence in me and guidance over the last four years have helped me overcome the challenges of research. As one of the first Ph.D. students in the lab, I had the opportunity to observe and learn from the challenges he faced to provide a research conducive and relaxed environment in the lab. Apart from the scientific discussions, it was a pleasure to share ideas with him on various topics.

I would like to thank Dr. Wim van der Merwe (ABB MV Drives) for his guidance during the Ph.D., and also making it possible for me to understand the practical aspects of my research by arranging my stay at ABB MV Drives, where I had the opportunity to see high power MV drives and appreciate the engineering effort involved in producing them. I would also like to thank ABB MV Drives for sponsoring the Ph.D. work.

In addition to my supervisors, Dr. Francisco D. Freijedo provided his valuable insights in the power electronics control and stability. He also introduced me to some very well written books on the complex topic of control systems, which helped in understanding the challenges of power electronics control. These played a pivotal role in the compilation of this thesis.

I would like to thank the jury members, Prof. Mario Paolone (EPFL), Dr. Rachid Cherkaoui (EPFL), Dr. Silvio Colombi (GE Industrial Solutions) and Prof. Emil Levi (Liverpool John Moores University) who agreed to evaluate my work, dedicated time for it and provided their valuable feedback on my work that helped in improving the quality of the thesis.

Over the last four year, I have shared many wonderful experiences with and learned from all the members of PEL. Emilien and Yan Kim have helped me with the french language on various occasions and especially while writing this thesis. I would like to thank the serbian crew (Marko M., Marko P., Dragan, Stefan and Ozrenko) for all the long conversations and insights they have shared with me. It was truly a pleasure to spend all those times with them.

On a personal note, I would also like to express my gratitude to all my friends in EPFL, Switzerland and all over the world. I would especially like to thank Mateen, Sina, Damiano, Merel, Nauman and Kunal for their support and close friendship.

In the end, I would like to thank my family for their constant support and unconditional love which enabled me to pursue Ph.D. in the first place.

February 2018

Uzair



# Abstract

High power variable speed drives play a major role in many industrial applications. At the moment, these high power loads are supplied by the source (grid/generator) through the state-of-the-art medium voltage ac (MVAC) power distribution network (PDN). The voltage levels, in these systems, are dependent on the power levels of the loads, other technical (standards) or historical requirements. These MVAC PDNs are used for energy intensive land based industrial and offshore applications that include, e.g., hot and cold rolling mills for metal industry, ore mining, processing plants, liquefied natural gas (LNG) tankers, drill ships and exploration platforms, etc., and, in such systems, the installed power capacity can reach up to 250 MW.

With the recent improvements in the power electronic technologies, medium voltage dc (MVDC) PDNs are being promoted for such installations, especially marine applications. There are a number of motives behind such a push, one of them being the opportunity to optimize the use of prime movers (diesel-generator-sets) by operating them at the most optimal speed/efficiency with respect to the loading conditions, thus improving fuel efficiency. As today these prime movers are driving generators that are all synchronized to the same MVAC PDN, hence, to achieve decoupling of the speeds of the different prime movers there is a need to remove synchronization requirement first. This is easily achievable if generator's output ac voltages are rectified and connected together to the MVDC PDN. Another motivation is the removal of the bulky transformers, which would lead to space and installation cost savings. Additionally, MVDC PDN provides flexibility in design of these systems and possibilities to include new technologies, e.g., gas turbines, permanent synchronous generators, energy storage, high power dc-dc converters, etc.

In this thesis, a number of technical issues pertaining to a possible MVDC PDN are discussed and multi-converter dynamic interactions are investigated. In the first part of the thesis, a discussion and evaluation of the possible technologies is provided, commercially available or proposed in the literature, which can be adopted by the MVDC PDNs, e.g., prime movers, generators, rectifiers, cables, filters, inverters and motors. This is followed by a critical discussion on the adoption of MVDC PDN by analyzing the opportunities and the challenges of replacing the state-of-the-art MVAC PDN in the existing *LNG tanker* and *drill ship*. These two systems work in entirely different conditions, thus they provide distinct technological challenges for the adoption of the MVDC PDN. Taking into account the earlier evaluation, possible high quality multi-phase multi-pulse MVDC supplies, for different power levels, are proposed, designed, and simulated.

In the second part, small signal models (*impedance models*) are developed for different commercially available rectifiers (diode, thyristor, active, MMC) and inverters, mapping the impact of their respective control schemes. These small signal models are then used to investigate the dynamic interactions between the sources and the loads that are connected through distribution cables. The effects of the variations of the different passive elements are studied, which show that lower filtering effort and higher inductance in the system lead to instability. Furthermore, state space modeling techniques are investigated for developing models to analyze multi-converter interactions in multi-port MVDC PDNs. This analysis is further used to identify unstable system configurations.

**Keywords:** *MVAC Distribution, MVDC Distribution, Power Electronic Converters, Control, Small Signal Modeling, Impedance Modeling, Nyquist Criteria, Multi-Port System Stability, Sensitivity Matrix.*



# Résumé

Les unités de commande de moteur électrique forte puissance à vitesse variable jouent un rôle prépondérant dans nombre d'applications industrielles. Actuellement, ces charges de forte puissance sont alimentées depuis la source (réseau ou génératrice électrique) au travers d'un réseau de distribution alternatif moyenne tension (MT) des plus modernes. Dans ces systèmes, les niveaux de tension sont dépendants des niveaux de puissance de la charge ainsi que d'autres critères techniques ou historiques. Ces réseaux de distribution alternatifs MT sont utilisés par l'industrie lourde dans des installations terrestres ou extraterritoriales : laminage à chaud ou à froid du métal, extraction de minerais, usines de transformation, pétroliers de gaz naturel liquéfié (GNL), navires de forage, plateformes d'exploration, etc. Dans de telles installations, la puissance installée peut atteindre 250 MW.

Avec les récentes améliorations des technologies d'électronique de puissance, les réseaux de distribution continue MT sont encouragés pour ce genre d'installation, notamment dans les applications maritimes. De nombreuses raisons expliquent cet engouement, l'une d'entre elles étant la possibilité d'optimiser l'utilisation des moteurs primaires (groupes diesel) en les faisant fonctionner à leur régime vitesse/rendement idéal en fonction de leur condition de charge, améliorant par conséquent leur consommation de carburant. Il est d'usage d'utiliser ces moteurs primaires pour entraîner les génératrices électriques qui sont, elles-mêmes, toutes synchronisées sur un seul réseau alternatif MT, c'est pourquoi il n'est possible de varier la vitesse des moteurs primaires qu'après s'être affranchi des contraintes de synchronisation électrique. Ceci est facilement réalisable si les tensions alternatives de sortie de la génératrice sont redressées et reliées ensemble à un réseau de distribution continu MT. Une autre motivation est l'élimination des transformateurs lourds et volumineux, ce qui amènerait à des gains d'espace et des réductions du coût d'installation. De plus, les réseaux de distribution continus MT amènent de la flexibilité dans la conception de ces systèmes et la possibilité d'intégrer des technologies innovantes comme des turbines à gaz, des génératrices synchrones à aimants permanents, du stockage d'énergie, des convertisseurs de forte puissance, etc.

Dans cette thèse, un certain nombre de questions techniques relatives à une éventuelle distribution électrique continue MT sont discutées et les interactions dynamiques inter-convertisseurs sont examinées. Dans une première partie de la thèse, une discussion et un examen des différentes solutions possibles pour l'adoption de ce type de réseaux sont apportés, qu'elles soient disponibles dans sur le marché ou proposées dans la littérature ; comme par exemple, moteurs primaires, génératrices, redresseurs, câbles, filtres, onduleurs et moteurs. Suit un débat critique sur l'adoption des réseaux de distribution continus MT qui analyse les opportunités et les défis de remplacer les réseaux de distribution alternatifs MT de dernière génération dans les pétroliers GNL et les navires de forage existants. Ces deux systèmes de distribution œuvrent dans des conditions complètement différentes, et par conséquent soulèvent des enjeux technologiques distincts pour l'adoption des réseaux de distribution continus MT. En considérant cette première évaluation, d'éventuelles alimentations multi-phase multi-pulse, pour divers niveaux de tension, sont proposées, modélisées et simulées.

Dans une seconde partie, des modèles petits signaux (modèles d'impédance) sont développés pour divers redresseurs (diode, thyristor, actif, MMC) et onduleurs disponibles sur le marché, modélisant l'impact sur leur stratégie de contrôle respective. Ces modèles sont ensuite utilisés pour étudier les interactions dynamiques entre les sources et les charges connectées au travers de câbles de distribution. L'incidence de la variation des éléments passifs sur la stabilité est évaluée, ceci montre que des filtres

plus faibles et des inductances plus importantes dans un système peuvent le rendre instable. De plus, les techniques de modélisation d'espace d'état sont examinées dans le but de développer des modèles pour l'étude des interactions entre les convertisseurs dans les réseaux de distribution continus MT à ports multiples. Cette analyse est ensuite utilisée pour l'identification des configurations instables de ce genre de systèmes.

**Mots-clés:** Distribution Moyenne Tension Alternative, Distribution Moyenne Tension Continue, Convertisseurs d'Electronique de Puissance, Contrôle, Modélisation Petits Signaux, Modélisation d'Impédances, Critère de Nyquist, Stabilité de Systèmes Multi-Ports, Matrice de Sensibilité.

# List of Abbreviations

|      |  |
|------|--|
| ac   | alternating current                    |
| ANPC | active neutral point clamped converter |
| ARU  | active rectifier unit                  |
| AVR  | automatic voltage regulator            |
| CHB  | cascaded h-bridge converter            |
| CPL  | constant power load                    |
| DAC  | dynamic ac                             |
| dc   | direct current                         |
| DP   | dynamic positioning                    |
| DRU  | diode rectifier unit                   |
| DTC  | direct torque control                  |
| DVC  | direct voltage control                 |
| ES   | energy storage                         |
| ESAC | energy source analysis consortium      |
| FC   | flying capacitor converter             |
| FOC  | field-oriented control                 |
| GE   | General Electric                       |
| GHG  | green house gas                        |
| GMPM | gain margin and phase margin           |
| GT   | gas turbine                            |
| HFO  | heavy fuel oil                         |
| HVDC | high voltage dc                        |
| ICE  | internal combustion engine             |
| IM   | induction machine                      |
| IMO  | International Maritime Organization    |

|      |                                      |
|------|--------------------------------------|
| LCC  | line commutated converters           |
| LF   | low frequency                        |
| LHP  | left half plane                      |
| LNG  | liquefied natural gas                |
| LV   | low voltage                          |
| LVDC | low voltage dc                       |
| MIMO | multiple input multiple output       |
| MMC  | modular multilevel converter         |
| MV   | medium voltage                       |
| MVAC | medium voltage ac                    |
| MVDC | medium voltage dc                    |
| NPC  | neutral point clamped converter      |
| PDN  | power distribution network           |
| PM   | prime mover                          |
| PMSM | permanent magnet synchronous machine |
| RHP  | right half plane                     |
| SFOC | specific fuel oil consumption        |
| SISO | single input single output           |
| SM   | synchronous machine                  |
| TRU  | thyristor rectifier unit             |
| VCT  | voltage coordination transformer     |
| VSC  | voltage source converter             |
| VSD  | variable speed drive                 |
| VSI  | voltage source inverter              |



# Contents

|  |            |
|--|------------|
| <b>Acknowledgements</b>  | <b>iii</b> |
| <b>Abstract</b>  | <b>v</b>   |
| <b>Résumé</b>  | <b>vii</b> |
| <b>List of Abbreviations</b>   | <b>ix</b>  |
| <b>1 Introduction</b>  | <b>1</b>   |
| 1.1 AC vs DC Power Distribution Network                                | 1          |
| 1.2 Ship On-Board Power Distribution Network                           | 2          |
| 1.2.1 Evolution of the Ship Propulsion                                 | 2          |
| 1.2.2 Ship On-Board MVAC Power Distribution Network                    | 3          |
| 1.2.3 Ship On-Board DC Power Distribution Network                      | 4          |
| 1.3 Ship On-Board LVDC Power Distribution Network                      | 7          |
| 1.4 Ship On-Board MVDC Power Distribution Network                      | 7          |
| 1.4.1 Objectives of the Thesis   | 8          |
| 1.4.2 Contributions of the Thesis                                      | 9          |
| 1.5 Outline of the Thesis  | 9          |
| 1.6 List of Publications   | 10         |
| <b>2 Technologies - Marine On-Board Power Distribution Networks</b>    | <b>13</b>  |
| 2.1 Introduction   | 13         |
| 2.2 Power Generation System  | 14         |
| 2.2.1 Prime Movers   | 14         |
| 2.2.2 Generators   | 16         |
| 2.2.3 Transformers   | 18         |
| 2.2.4 Rectifiers   | 19         |
| 2.3 Distribution System  | 22         |
| 2.3.1 Filters  | 22         |
| 2.3.2 Cables   | 23         |
| 2.4 Propulsion Loads   | 23         |
| 2.4.1 Inverters  | 24         |
| 2.4.2 Motors   | 24         |
| 2.5 Energy Storage Technologies and High Power dc-dc Converters        | 24         |
| 2.6 Summary  | 25         |
| <b>3 Case Studies - Ship On-Board MVDC Power Distribution Networks</b> | <b>27</b>  |
| 3.1 Introduction   | 27         |
| 3.1.1 MVAC PDN - LNG Tanker  | 28         |
| 3.1.2 MVAC PDN - Drill Ship  | 29         |
| 3.2 Architectures - MVDC Power Distribution Network                    | 31         |
| 3.2.1 LNG Tanker - Possible PDNs                                       | 32         |
| 3.2.2 Drill Ship - Possible Architectures                              | 35         |
|  | xi         |

|          |  |           |
|----------|--|-----------|
| 3.3      | Summary  | 36        |
| <b>4</b> | <b>Multi-Phase Multi-Pulse Power Supplies for MVDC Power Distribution Networks</b> | <b>39</b> |
| 4.1      | Introduction   | 39        |
| 4.2      | MVDC Supply - 3-phase, 6-pulse   | 40        |
| 4.3      | MVDC Supply - $N \times 3$ -phase, $N \times 6$ -pulse                             | 40        |
| 4.3.1    | Multi-Pulse - Parallel Connection  | 41        |
| 4.3.2    | Multi-Pulse - Series Connection  | 42        |
| 4.4      | Multi-Phase Multi-Pulse MVDC Supply  | 43        |
| 4.4.1    | Design of DRU Sub-module   | 43        |
| 4.4.2    | Case 1: 18 MW, 5 kV, 12-Pulse Parallel Rectifier                                   | 45        |
| 4.4.3    | Case 2: 27 MW, 15 kV, 18-Pulse Series Rectifier                                    | 45        |
| 4.4.4    | Fault Withstand Capabilities   | 47        |
| 4.5      | Summary  | 49        |
| <b>5</b> | <b>Source - Load Interactions in the MVDC Power Distribution Network</b>           | <b>51</b> |
| 5.1      | Introduction   | 51        |
| 5.2      | Overview of Stability Criteria   | 52        |
| 5.3      | Small Signal Modeling of the MVDC PDN  | 55        |
| 5.4      | Source/Load Impedance/Admittance Measurement                                       | 57        |
| 5.4.1    | Load Admittance - Propulsion Drive   | 57        |
| 5.4.2    | Source Impedance - Diode Rectifier Unit  | 58        |
| 5.4.3    | Source Impedance - Thyristor Rectifier Unit  | 61        |
| 5.4.4    | Source Impedance - Active Rectifier Unit   | 61        |
| 5.5      | Dynamic Assessment of the MVDC PDN   | 64        |
| 5.6      | Summary  | 67        |
| <b>6</b> | <b>Interactions of the MMC and CPLs in the MVDC Power Distribution Network</b>     | <b>69</b> |
| 6.1      | Introduction   | 69        |
| 6.2      | System Description   | 70        |
| 6.3      | Dynamic Assessment of MVDC Power Distribution Network                              | 71        |
| 6.3.1    | Load Admittance  | 72        |
| 6.3.2    | Source Impedance   | 72        |
| 6.4      | MMC Control Structure  | 73        |
| 6.5      | Impedance Stability Assessment   | 77        |
| 6.6      | Time Domain Simulations  | 78        |
| 6.7      | Summary  | 78        |
| <b>7</b> | <b>Dynamic Stability of the Multi-port MVDC Power Distribution Network</b>         | <b>81</b> |
| 7.1      | Introduction   | 81        |
| 7.2      | Multiple Input Multiple Output Systems   | 82        |
| 7.2.1    | State Space Representation of MIMO System  | 82        |
| 7.2.2    | Stability of the MIMO Systems  | 83        |
| 7.3      | Modeling of Multi-Terminal MVDC PDN  | 84        |
| 7.3.1    | Case 1 - One Drive Connected Remotely  | 85        |
| 7.3.2    | Case 2 - Two Drives Connected Remotely   | 88        |

|          |   |            |
|----------|---|------------|
| 7.4      | Dynamic Analysis of Multi-Terminal MVDC PDN | 90         |
| 7.4.1    | Analysis and Discussion - Case 1            | 91         |
| 7.4.2    | Analysis and Discussion - Case 2            | 95         |
| 7.5      | Time Domain Simulation                      | 99         |
| 7.6      | Summary                                     | 101        |
| 7.6.1    | Future Work                                 | 101        |
| <b>8</b> | <b>Conclusions and Future Work</b>          | <b>103</b> |
| 8.1      | Summary and Contributions                   | 103        |
| 8.2      | Overall Conclusion                          | 105        |
| 8.3      | Future Work                                 | 105        |
| <b>A</b> | <b>Time Domain Models</b>                   | <b>107</b> |
| A.1      | DRU time domain model                       | 107        |
| A.2      | TRU time domain model                       | 109        |
| A.3      | ARU time domain model                       | 110        |
| A.4      | MMC time domain model                       | 111        |
|          | <b>References</b>                           | <b>113</b> |
|          | <b>Curriculum Vitae</b>                     | <b>119</b> |



# 1

## Introduction

*This chapter discusses the increasing popularity of direct current (dc) power distribution networks (PDNs), the enabling technologies, and the underlying benefits and challenges of adopting them. Additionally, ship on-board power distribution network is discussed, as an early adoption area of the medium voltage dc (MVDC) PDN. Based on these motivations, the objectives and the outline of the thesis are provided.*

### 1.1 AC vs DC Power Distribution Network

The ‘War of the Currents’, as it is now known, started in the late 1880’s when Thomas Edison and Nikola Tesla promoted two competing technologies, dc and alternating current (ac), for electrical power generation and distribution [1]–[3]. DC generation and distribution, implemented by Edison in partnership with General Electric (GE), became popular for providing electricity to buildings and street lights. The dc network lacked the technologies for increasing/decreasing dc voltage levels and, therefore, suffered higher losses when transmitting electricity over large distances [2]. Nikola Tesla, on the other hand, in partnership with George Westinghouse claimed that ac technology is a cheaper alternative to the dc system for generation and transmission of electricity. The invention of ac machines, e.g., generators and transformers, and the successful display of ac technology by Tesla and Westinghouse at a Chicago fair, led to the selection of ac technology by the Niagara Falls Power Company to generate electricity and supply the city of Buffalo [1], [3]. From that time onward, dc technology was put aside (largely used for special purposes, e.g., telephone exchanges etc.), while, ac technology was further developed and became the main source of power generation, transmission and distribution [1], [2].

The introduction of *mercury valves*, in 1914, caused a shift in the conception of few transmission projects that were designed around dc [4]. These projects considered line commutated converters (LCC) for conversion of ac to dc for the transmission of electrical power. This concept got more attention after the introduction of semiconductor thyristor valves and led to many new large distance (greater than 500 km) dc transmission projects. Additionally, these projects benefited from the lack of synchronization requirement of the ac sources, and the lack of skin effect inherent to ac, leading to higher power density of the installed transmission lines. Thus reducing the required equipment, compared to a similar ac transmission, and costs in the implementation of such projects [1]. Furthermore, the improvement in the semiconductor technology and the development of numerous power electronic converters, over the last four decades, has made it possible to generate and transmit electricity from unconventional and renewable resources, e.g., solar and wind energy. In an effort to reduce carbon footprint of the conventional power plants, an even higher penetration of the renewable and storage technologies is expected in the electricity grid. DC transmission and distribution networks

provide relatively easy interface of these technologies with the electricity grid, therefore, they have become an attractive alternative to the ac networks.

One possible early adoption area of the dc power distribution network (PDN) are the industrial PDNs. In these applications, medium voltage ac (MVAC) PDN (1 - 36 kV) interfaces the ac source/grid with the loads that are usually high power four-quadrant variable speed drives (VSDs). In some commercial offerings of these multi-motor VSDs, multiple inverters are interfaced to a common dc-link (e.g., ACS6000 [5]). Furthermore, the manufacturers of the four-quadrant VSDs can also create separate commercial offers for rectifiers and inverters, facilitating the adoption of dc PDN. These applications, involving multiple high power drives, are usually land based, e.g., hot and cold rolling mills for metal industry, ore mining, processing plants and so on. In metal industry, a number of drives are operated, in a coordinated manner, for producing hot or cold rolled steel. For mining operations, multiple drive sets may be involved in a single process and usually a significant number of processes are being carried out in parallel. The total installed power, in such instances, can easily exceed 250 MW, where the bulk of this power is consumed by medium voltage (MV) VSDs.

Additionally, multi-motor VSD configurations are also found in off-shore applications, e.g., oil exploration platforms, off-shore support vessels, LNG tankers and so on. Here, the installed power capacity is in the range of 20 - 100 MW, depending on the function and operational requirements of the vessel. These high power MV VSDs are usually offered for a defined voltage class (e.g., 3.3, 6.6, 11 kV), while the distribution voltage of the MVAC PDN may be higher due to large power requirement. This leads to the requirement of voltage coordination transformers (VCTs), which also provide galvanic isolation, to adjust the MVAC PDN's voltage to a suitable level for the rectifier stage of the drive. Therefore, these VCTs add to the overall footprint and installation cost in such applications, where space is already constrained.

As discussed earlier, MVDC PDNs (3 - 50 kV) are being promoted as power collection grids for renewable energy for their easy interface. Additionally, they are being considered for setting up industrial level grids for connecting multiple inverters with common dc-bus for better power utilization and regeneration from different loads, leading to reduced operational cost and footprint of the equipment, while making the system more efficient and environmentally friendly. In this thesis, the MVDC PDNs are discussed and analyzed for marine on-board applications for their expected benefits.

## 1.2 Ship On-Board Power Distribution Network

### 1.2.1 Evolution of the Ship Propulsion

Electric ship propulsion has existed since the last century. The first electrically propelled ship was constructed in 1911 called USS Jupiter. In the early 20<sup>th</sup> century, on board electricity usage was little as compared to the propulsion system. The electrical system worked as a gearbox to operate the ship at different speeds. Sophisticated high power mechanical gearboxes were not available at that time due to complicated manufacturing process. With the advancement in mechanical gear manufacturing, after World War II, and the non-availability of electrical VSDs, mechanical propulsion systems replaced electrical propulsion [6], [7]. The mechanical propulsion system has a diesel engine connected to a controllable gearbox, which is then connected to a propeller. A schematics of a typical mechanical propulsion system is given in **Fig. 1.1(a)**. It should also be noted that these systems

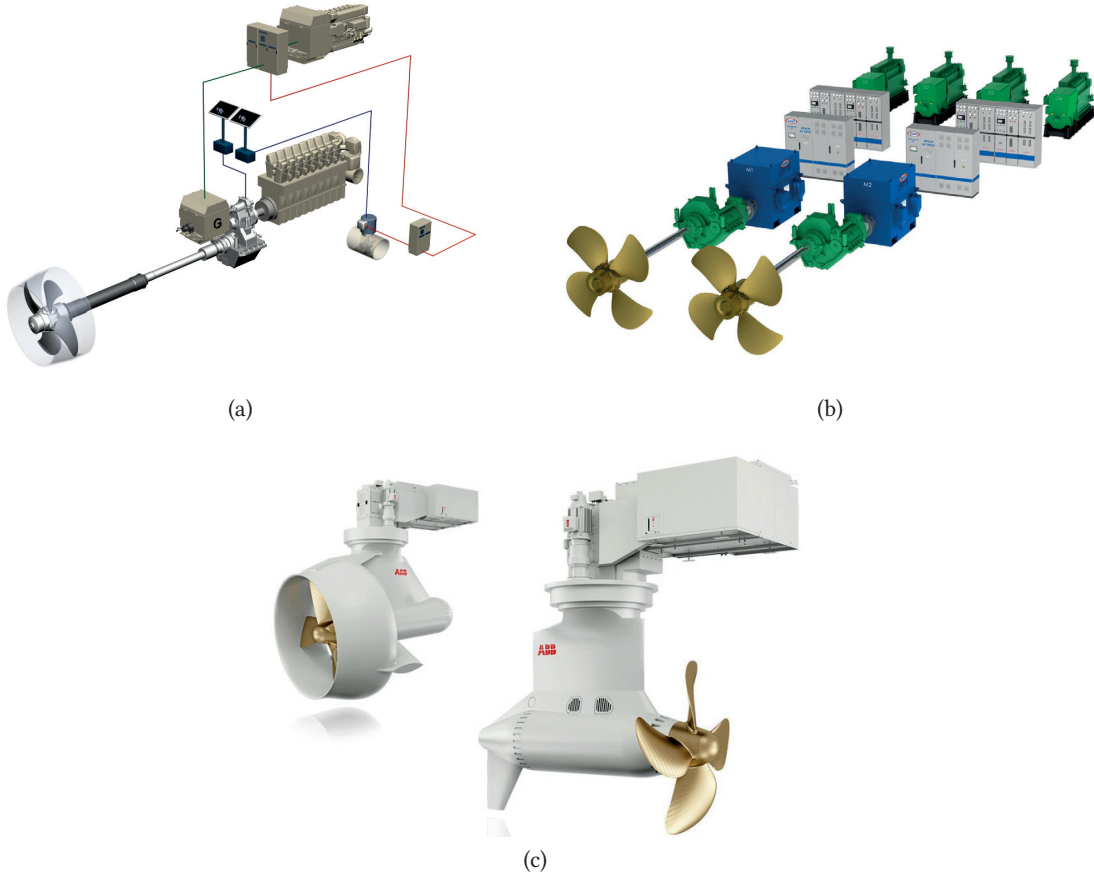


**Figure 1.1** (a) Diesel propulsion of ships with main engine driving the propeller through a drive shaft [10]. (b) Diesel electric propulsion of ships with diesel-generator set providing power to the VSD driving the motor interfaced with a propeller through a drive shaft [11]. (c) Examples of podded propulsion (AZIPOD ABB), which remove requirement of the drive shafts [12].

are still being widely used and offered for propulsion application [8] and use shaft generators for on-board electricity [9].

Over time, the evolution of various electrical technologies, e.g., improved electrical machinery and availability of high power electronics, led to the development of VSDs driving high efficiency motors. Thus in the late 1980's, electrical propulsion systems started slowly to make a comeback in the ship propulsion, with the introduction of electrical propulsion in RMS Queen Elizabeth 2 [6]. Introduction of podded propulsor also made electric propulsion more attractive, as shown in **Fig. 1.1(c)**. Its unique construction guaranteed more space in the ship, as the motor is located outside the ship in a pod. Furthermore, its ability to rotate about its axis provided high maneuverability for large ships.

### 1.2.2 Ship On-Board MVAC Power Distribution Network

As electrical propulsion became popular, the on-board PDN was revamped and MVAC PDN was introduced to handle the high power requirements of the propulsion system and, in some cases, non-propulsion loads as well. This system has a diesel generator connected to an electrical generator

**Table 1.1** Voltage levels for different power levels for MVAC PDNs [13].

| Voltage Class | Power Level |
|---------------|-------------|
| 11 kV         | > 20 MW     |
| 6.6 kV        | 4 - 20 MW   |
| 690 V         | < 4 MW      |
| 400/230 V     | hotel loads |

that then supplies a switchboard distributing electrical power to the MV VSD interfaced to the motor, responsible for propelling the ship. A typical MVAC distribution scheme is shown in **Fig. 1.1(b)** and distribution voltage levels for different loads are given in **Table 1.1**.

A lot of development work, in this field, has been done especially with commercial ships. The promising future it presents has attracted in particular military installations from around the world [7]. The move towards electric ship propulsion provides the opportunity to build ships that are efficient in fuel use and have wide operational range. On the other hand, it also provides flexibility to the ship designers for integrating high power non-propulsion loads. The advantage of the fuel economy arises from the fact that prime movers are mechanically decoupled from the propulsion system. Also, the generator's frequency is no more related to the speed of the motor due to the insertion of the power converter [6], [14]. This is equally valid for both ac (state-of-the art) and dc (emerging trend) PDNs.

### 1.2.3 Ship On-Board DC Power Distribution Network

MVAC PDNs require the generator's frequency to be adjusted (kept constant) for the distribution ac frequency, e.g., 50/60 Hz, irrespective of the loading conditions. This is where the dc PDNs offer improvements on the generation side, since due to the rectification of the generator ac voltage, actual

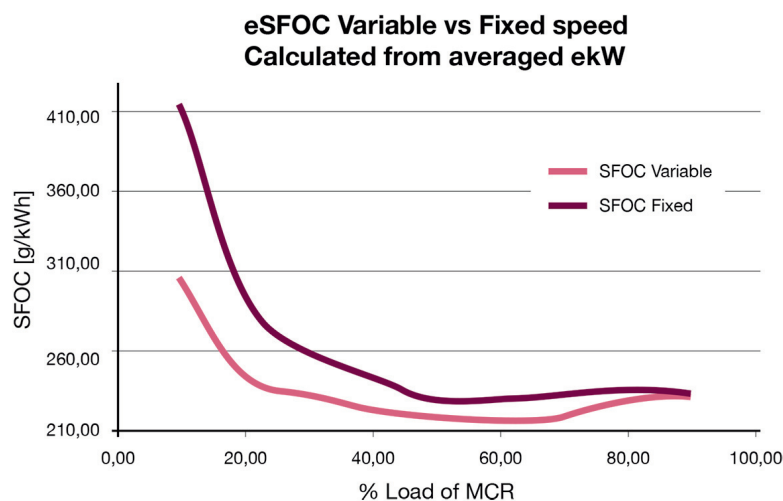


**Figure 1.2** Specific fuel oil consumption (SFOC) at fixed and variable speed operations for different loading conditions [15]. The fuel savings are clear at low loading condition.



operating speed can be adjusted to the demand. This flexibility not only improves the efficiency on the generation side, but also requires changes in the PDN of the ship. Improvement in specific fuel oil consumptions for variable speed operation of diesel generators for a platform support vessel with dynamic positioning (DP) is shown in **Fig. 1.2**. High-speed generators can also be connected to the dc distribution system through a power converter. This allows reducing the size of the machine, as smaller generators with higher rotational speed, smaller torque and higher power density can replace the bulky 50/60 Hz generators [16]. This also leads to the removal of the bulky VCTs and reducing the footprint of the installed equipment and providing flexibility in the design of the ship. The main benefits of dc PDNs are summarized below [17], [18]:

- Efficient operation of the system and fuel savings.
- Smaller footprint of installed equipment and space saving.
- Lower installation and operation costs.
- Reduced maintenance of engines.
- Reduced green house gas emissions.
- Reduction in noise and vibration.
- Simpler interface with energy storage.

Considering the possible benefits of the dc PDN, IEEE and IEC have made efforts to streamline the existing and define new standards that are related to building power electronic equipment for ship applications. A detailed list of all the standards applicable to the dc distribution and development of power electronic equipment is given in [19]. IEEE standards which are directly related to ship power electronic equipment and power system are:

- *IEEE Std. 1662-2008 “Guide for the Design and Application of Power Electronics (PE) in Electrical Power Systems on Ships”.*
- *IEEE Std. 1709-2010 “Recommended Practice for 1 to 35 kV Medium Voltage DC Power Systems on Ships”.*

*IEEE Std. 1709-2010* defines the MVDC system on ship [20]. It considers that all electrical sources and loads are connected to each other through a MVDC bus and power electronic equipment. This approach allows connecting different generation, storage and loads. It also defines the functional blocks of the power system that are shown in **Fig. 1.3**. A brief description of the different elements of **Fig. 1.3** is presented below:

- *Power Generation*: primary power source which converts fuel to electrical power.
- *Shore Power Interface*: converts power from shore source to on-board MVDC.
- *Pulse Load*: draws large amount of power from the system sporadically.
- *Energy Storage*: supplies power to the system when required and also draws power from the system to recharge.
- *Propulsion*: primary load of the ship that provides propulsion. It may provide power during crash stop.

- *Ship Service*: consists of power converters that provide power to different load centers.
- *Dedicated High Power Load*: draws power of 1 MW or more.
- *MVDC Bus*: connects different loads, isolates and interrupts power supply when there is a fault.

This standard also defines the possible voltage levels, given in Table 1.2, that can be considered in the new dc PDN.

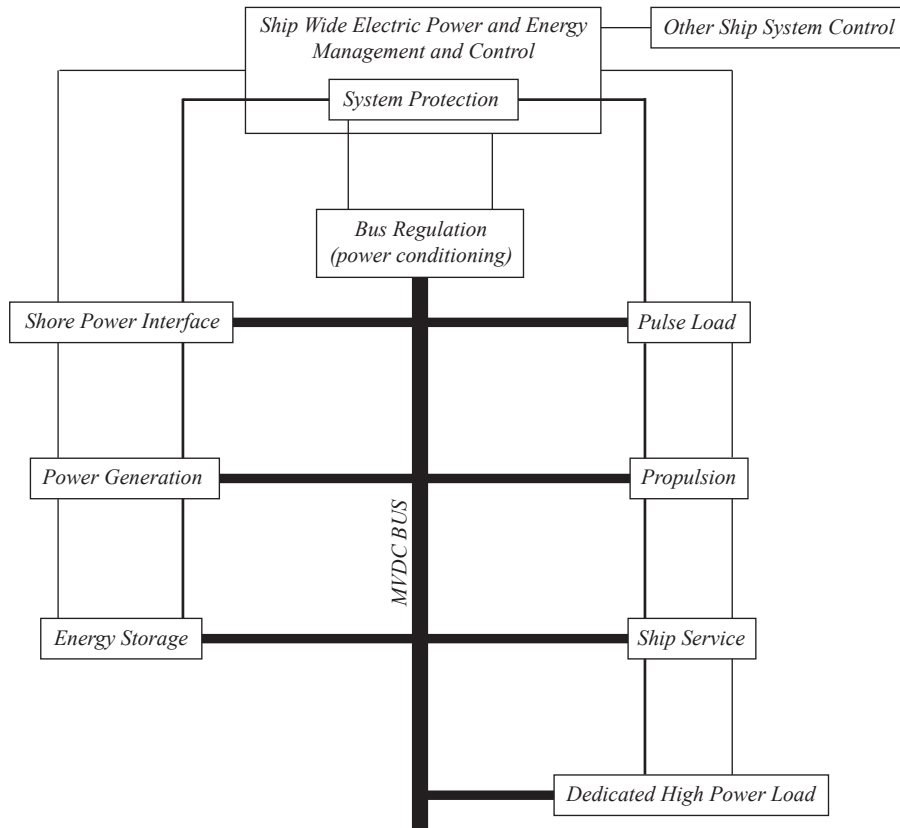


**Figure 1.3** MVDC functional block diagram from [20].

**Table 1.2** Voltage classes for ship dc PDN [20].

|                              | MVDC Class<br>kV | Nominal MVDC<br>kV | Maximum MVDC<br>kV |
|------------------------------|------------------|--------------------|--------------------|
| <b>Established Classes</b>   | 1.5              | 1.5 ( $\pm 0.75$ ) | 2 ( $\pm 1$ )      |
|                              | 3                | 3 ( $\pm 1.5$ )    | 5 ( $\pm 2.5$ )    |
| <b>Future Design Classes</b> | 6                | 6 ( $\pm 3$ )      | 10 ( $\pm 5$ )     |
|                              | 12               | 12 ( $\pm 6$ )     | 16 ( $\pm 8$ )     |
|                              | 18               | 18 ( $\pm 9$ )     | 22 ( $\pm 11$ )    |
|                              | 24               | 24 ( $\pm 12$ )    | 28 ( $\pm 14$ )    |
|                              | 30               | 30 ( $\pm 15$ )    | 34 ( $\pm 17$ )    |

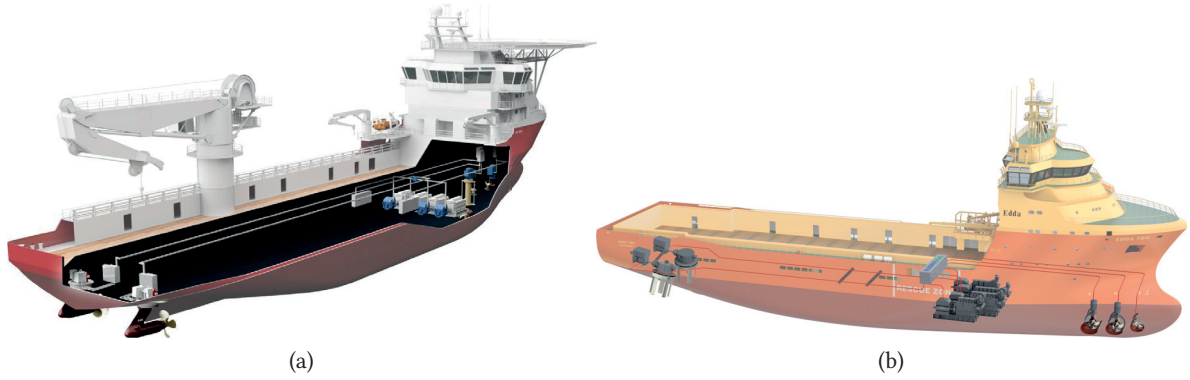


**Figure 1.4** (a) LVDC PDN implemented in *Dina Star* by ABB [17]. (b) *BlueDrive PlusC* system developed by Siemens [18].

### 1.3 Ship On-Board LVDC Power Distribution Network

In addition to the earlier discussed initiatives by IEEE and IEC, especially for MVDC PDNs, different manufacturers, e.g., ABB, Siemens, and Rolls Royce, have retrofitted or introduced low voltage dc (LVDC) PDNs in ships [17], [18], [21]. These PDNs highlight the benefits of dc PDNs in ships and are developed utilizing the available low voltage (LV) power electronic technologies, e.g., rectifiers, inverters, LVDC breakers, battery storage, etc., while, removing the ac switchboards and VCTs [17]. Furthermore fuses, isolators and power electronic switches, in rectifiers, are used to isolate faults and block fault currents[17], [18].

A 1 kV LVDC PDN, developed by ABB for power levels upto 20 MW, is implemented in a multi-purpose platform support vessel named *Dina Star*. This pilot project has shown that the system is 20% more efficient and the installed equipment has upto 30% less weight and smaller footprint compared to an equivalent ac distribution network [17]. Additionally, in this PDN the converters are spatially close to their respective sources and loads, e.g., rectifiers are located close to the generators. The layout of this system is shown in **Fig. 1.4(a)**. Similar systems are developed by *Rolls-Royce* for ferries, where some systems completely run on batteries [21].

*BlueDrive PlusC* system, developed by *Siemens*, is slightly different from the others as it is a ‘fully integrated power distribution’ [18]. This system has all the switchboards, rectifiers and inverters concentrated in one place and ac cables are used to connect generators, machines and other loads to the *BlueDrive PlusC* system. As a result of the variable operation of the generators in this system, the green house gases (GHGs) are reduced by 25%, while the NOx emissions are lowered by 83%. The layout of this system is shown in **Fig. 1.4(b)**. A summary of commercial LVDC PDNs is provided in Table 1.3.

### 1.4 Ship On-Board MVDC Power Distribution Network

In larger vessels, e.g., liquefied natural gas (LNG) tankers, drill ships, cargo ships etc., the power requirement is higher than 20 MW and can reach as high as 100 MW. For these applications LVDC PDNs would be required to handle very large currents, which would not be technically feasible due

**Table 1.3** LVDC PDNs developed by different manufacturers and their applications.

| LVDC PDN Manufacturer | Distribution Voltage | Power Plant      | Application   | Ship  |
|-----------------------|----------------------|------------------|---|---|
| <i>ABB</i>            | 1 kV<br>-            | Diesel & Battery | Platform Support<br>Cable-laying<br>Ferry   | Dina Star<br>NKT Nikita<br>-  |
| <i>Siemens</i>        | 1 kV<br>-            | Diesel & Battery | Platform Support<br>Offshore Construction<br>Offshore Support<br>Service Operation<br>Ferry | Edda Ferd<br>MV Sourthern Tide<br>Edda Freya<br>Esvagt Faraday<br>Normand Maximus<br>Esvagt Froude<br>Esvagt Njord<br>Windea La Cour<br>- |
| <i>Rolls-Royce</i>    | -                    | Diesel & Battery | Ferry   | -   |

to thermal, insulation and mechanical limits of the LV equipment. Therefore, higher voltage level dc PDNs are needed to exploit benefits of dc PDNs, and this opens opportunities to explore and develop MVDC PDNs. As these PDNs are expected to handle higher power, as replacements for the MVAC PDNs, there are number of challenges they face. These challenges include lack of standalone MVDC technologies, e.g., rectifiers and inverters, MVDC breakers, commercial MVDC cables, active and passive filters, etc., and also no commercial MVDC PDNs exist.

For technical and commercial feasibility of the MVDC PDNs, the utilization of present commercial technology is desired. Considering the present semiconductor technology, the bandwidths of the commercially available MV power electronic equipment are lower compared to the LV power electronic equipment. Additionally, as no commercial MVDC PDNs exist, this implies lack of system level studies. These studies are required to explore the different dynamic challenges arising from the limits and capabilities of the present MV power electronic technologies that must be understood to ensure uninterrupted operation. Additionally, the impact of different equipment on the system stability must be explored, which eventually leads to defining design guidelines for the MVDC PDNs.

#### 1.4.1 Objectives of the Thesis

In view of the above discussion, few of the technical issues pertaining to the implementation and the stability of the MVDC PDNs with present commercial technology are discussed in this thesis. The following points are analyzed in particular:

- Possible MVDC PDNs for LNG tanker and drill ship, considering the present technologies, and the opportunities and challenges of implementing an MVDC PDN.
- Design of high quality MVDC supplies conforming to the expectation of fuel efficiency, energy density, to overcome lack of dc breaker, and their fault tolerances.

- Investigation and definition of stability regions of two-port and multi-port MVDC PDNs, considering the impact of bandwidths of the present MV converters and passive elements of the network, e.g., filter capacitors and distribution cables.

#### 1.4.2 Contributions of the Thesis

The main contributions of the thesis are:

- The possible evolution of the ship on-board PDN, from the existing MVAC to MVDC PDN, is analyzed by examining real world cases and two possible MVDC PDN architectures are discussed in details considering the present commercial technologies.
- The source - load interactions, in the future MVDC PDN, are analyzed considering different commercial rectifier technologies and variations in generator frequencies, filtering effort for both rectifiers and inverters, distribution lengths and system loading.
- Multi-terminal MVDC PDNs are modeled and analyzed using multiple input multiple output (MIMO) modeling techniques, which overcome single input single output (SISO) analysis drawbacks and provides a reliable method to map interactions among various sources and loads.

### 1.5 Outline of the Thesis

The thesis is organized in two parts and contains eight chapters.

The first part provides a critical discussion on the shift towards MVDC PDN from MVAC PDN, considering marine applications, and then analyzes the available technologies. Here, high quality MVDC supplies are also proposed:

- In *Chapter 2*, a discussion is provided on the commercially available and emerging new technologies for prime movers, generators, rectifiers, filters, MVDC cables, inverters and motors that can be employed later on in the MVDC PDNs.
- *Chapter 3* describes, in detail, MVAC PDNs for two large ships namely *LNG tanker* and *drill ship* and proposes possible MVDC PDNs for these cases, considering their functions and operational requirements.
- High quality MVDC supplies are proposed and designed in *Chapter 4* for different power levels and distribution voltage for marine MVDC PDNs. Additionally, as dc breakers are not readily available, these supplies are evaluated for their fault handling capabilities.

The second part presents an analysis on the system stability of the MVDC PDNs taking into account the commercially available technologies:

- *Chapter 5* introduces the dynamic stability assessment tool and small signal modeling of different source and load converters. Impedance modeling is used to represent the dynamic behavior of diode rectifier, thyristor rectifier, active rectifiers and inverter drives. This takes into account the behavior of the control strategies employed for these power electronic converters. The

impact of variations of passive elements e.g., filter capacitors and cable lengths, in a two-port network, and the dynamic interactions between the different source converters and load are analyzed using Nyquist Criteria. The findings are verified with time-domain simulations carried out in PLECS®.

- This analysis is extended to modular multilevel converter (MMC) based rectifier in *Chapter 6*. Here again the impact of the control and the passive elements (considering variations in them) are analyzed for their influence on system stability.
- Multi-port MVDC PDNs are modeled and analyzed in *Chapter 7*. State space modeling is presented for different possible MVDC architectures. The impact of the variations of the passive elements is analyzed by mapping closed-loop pole movements and unstable system configurations are highlighted. The findings are verified with time-domain simulations carried out in PLECS®.
- *Chapter 8* provides the summary of the findings, contributions of this thesis and the future work to be carried out.

## 1.6 List of Publications

The publications resulting directly from the *PhD Thesis* are:

### Journal

1. **U. Javaid**, F. D. Freijedo, D. Dujic and W. van der Merwe, "Dynamic Assessment of Source-Load Interactions in Marine MVDC Distribution," IEEE Transactions on Industrial Electronics, vol. 64, no. 6, pp. 4372-4381, June 2017.
2. **U. Javaid**, F. D. Freijedo, D. Dujic and W. van der Merwe, "MVDC Supply Technologies for Marine Electrical Distribution Systems," CPSS Transactions on Power Electronics and Applications, 2018.

### Conferences

1. **U. Javaid**, D. Dujic and W. van der Merwe, "MVDC Marine Electrical Distribution: Are we ready?," 41st Annual Conference of the IEEE Industrial Electronics Society (IECON), Yokohama, 2015, pp. 823-828.
2. **U. Javaid**, A. Christe, F. D. Freijedo and D. Dujic, "Interactions between Bandwidth Limited CPLs and MMC Based MVDC Supply," IEEE Energy Conversion Congress and Exposition (ECCE), Cincinnati, OH, 2017, pp. 2679-2685.
3. F. D. Freijedo, **U. Javaid** and D. Dujic, "Conformal Mapping of Impedance Stability Models for System-Level Dynamics Assessments," 19th International Symposium POWER ELECTRONICS (Ee), Novi Sad, 2017.

4. **U. Javaid**, F. D. Freijedo, D. Dujic and W. van der Merwe, "Marine MVDC Multi-Phase Multi-Pulse Supply," 43rd Annual Conference of the IEEE Industrial Electronics Society (IECON), Beijing, 2017, pp. 6807-6812.

### **Others**

1. **U. Javaid** and D. Dujic, "Arbitrary Order Generalized State Space Average Modeling of Switching Converters," IEEE Energy Conversion Congress and Exposition (ECCE), Montreal, QC, 2015, pp. 6399-6406.





# 2

## Technologies - Marine On-Board Power Distribution Networks

*In this chapter, a review is provided of the technologies commercially available and proposed in the literature. These technologies are expected to be part of the generation, distribution and loads of the future ship on-board MVDC PDNs.*

### 2.1 Introduction

The previous chapter highlighted the interest in a possible migration to the MVDC PDN for large vessels. It is expected that a realistic MVDC PDN will be conceived by borrowing the knowledge base of the state-of-the-art MVAC and LVDC PDNs, and the different technologies used to implement these systems. Additionally, it is expected that the development of new technologies, e.g., high power dc-dc converters and new protection-coordination strategies will also be required. In order to understand the opportunities and challenges of the MVDC PDN, this chapter describes possible technologies that are either commercially available or proposed in the literature. It should be noted that, in this thesis, the primary focus is on the propulsion loads, as they make up almost 80% of the installed loads. Furthermore, the auxiliary loads, e.g., hotel loads, pumps and so on that usually make up only 20% of the load, are not expected to go through any radical change and are not addressed in this study.

A notional MVAC PDN is shown in **Fig. 2.1(a)**. This system shows a fixed speed PM driving a fixed speed generator through a gearbox. The gearbox (with approximately 70% efficiency [22]) is necessary, in some instances, where the speed of the PM and the generator are not the same and the ac frequency must be maintained at 50/60 Hz. The distribution system is connected to the VSD through a low frequency (LF) VCT that supplies power to the VSD at appropriate voltage levels. The evolution of the

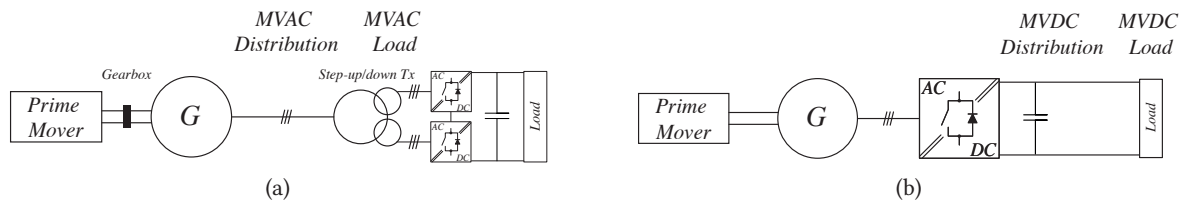


**Figure 2.1** (a) Simplified notional MVAC distribution with gearbox interfacing prime mover (PM) and generator, and multi-secondary VCT connected to the propulsion VSD. (b) Simplified notional MVDC distribution without gearbox and VCT.

notional MVAC PDN into an MVDC PDN is shown in **Fig. 2.1(b)**, where the gearbox can be omitted as variable or high speed generation is permitted, to provide efficient fuel consumption, and additionally, the VCT can also be removed to provide flexibility and space in the overall system design. To explore the possibilities for application of the different equipment, from MVAC PDNs, in the main power chain of the MVDC PDN, three groups can be defined:

- *Power Generation System*: includes the PMs, generators, transformers and rectifiers.
- *Distribution System*: includes the filters and distribution medium, e.g., bus bars and cables.
- *Propulsion Loads*: includes the inverter drives and motors<sup>1</sup>.

The description of the different equipment and their possible application in the future MVDC PDN is analyzed below.

## 2.2 Power Generation System

The power generation system is the prime source that feeds the propulsion loads in the PDN<sup>2</sup>. In the conventional MVAC PDN, this system's goal is to produce ac power at a fixed frequency, but with the MVDC PDN, the conventional settings of this system can be changed, as each generator would have a rectifier and consequently generator synchronization would not be required. Therefore, variable or high speed generation can be introduced that would improve the fuel efficiency. The main equipment in this group, considering existing MVAC and future MVDC PDNs are:

- Prime Movers: convert chemical energy to mechanical energy.
- Generators: convert mechanical energy to electrical energy.
- Voltage Coordination Transformers: voltage coordination for different loads and galvanic isolation.
- Rectifiers: ac to dc conversion for the MVDC PDNs.

### 2.2.1 Prime Movers

In most of the marine applications, internal combustion engines (ICEs) are used and are usually run on heavy fuel oil (HFO). In case gas is available as a cheaper alternative, gas turbines (GTs), smaller steam turbines or combined cycle turbines are also found, especially, in high speed vessels and LNG tankers [13]. These different engines are inherently very inefficient (40% for constant speed operations) and burn large quantities of expensive fuel. Over the years, efforts are being made to make them more efficient and reduce the GHGs emitted by them [23]. LVDC PDNs, discussed earlier, have shown that the upto 20% fuel savings can be achieved by variable operation of the PMs, which also reduces the GHGs [17], [18]. Additionally, to achieve fuel efficiency in MVAC PDNs in ships, dynamic ac (DAC)<sup>3</sup> has been introduced which has improved fuel efficiency upto 6% in the MVAC PDNs [24]. Apart from

---

<sup>1</sup>Many different high power loads, e.g., pumps, drill drives, etc. can be considered, but here the focus is limited to propulsion drives and motors.

<sup>2</sup>Auxiliary generation units are not discussed here.

<sup>3</sup>ac frequency is varied between 48 - 60 Hz for low and high loading.

**Table 2.1** Specifications of ICEs and GTs for marine applications.

| PM        | Manufacturer | Power                  | Efficiency | Speed                      | Fuel Type  | Ref        |
|-----------|--------------|------------------------|------------|----------------------------|------------|------------|
| ICE       | Wärtsilä     | 0.92 - 11.2 MW         | 42 - 52%   | 600 - 1000 rpm             | Liquid/Gas | [26], [27] |
|           | MAN          | 0.45 - 12 MW           | 48 - 55%   | 720 - 1800 rpm             | Liquid/Gas | [28], [29] |
|           | GE           | 1.3 - 4.7 MW           | ≈50%       | 900 - 1050 rpm             | Liquid/Gas | [30]       |
|           | Rolls Royce  | 3.6 - 9.6 MW           | 44 - 48.5% | 720/750 rpm                | Liquid/Gas | [31]       |
| GT        | GE           | 4.5 - 42 MW            | ≈40%       | 3.6 - 7 krpm               | Gas        | [32]       |
|           | Rolls Royce  | 3 - 40 MW              | ≈40%       | 3.3 - 15 krpm              | Gas        | [33]       |
| ICE<br>GT | Literature   | 1 - 10 MW<br>3 - 40 MW | ≈40%       | 720/750 rpm<br>3 - 15 krpm | Liquid/Gas | [13]       |

fuel savings and positive environmental impact, MVDC PDNs also provide an opportunity to increase the energy density and reduce footprint of the PMs by allowing usage of the GTs<sup>4</sup> as the principle PMs [25]. Different possible PM technologies that can be adopted for MVDC PDNs are discussed below and a summary of them is provided in Table 2.1.

#### 2.2.1.1 Internal Combustion Engines

The state-of-the-art MVAC PDNs largely employ ICEs, which usually run in medium speed (400 - 1000 rpm) to high speed range (1000 rpm and above) [34]. The availability of these PMs is of high interest as they are main power source, therefore, they are highly reliable with sophisticated diagnostics and short repair times [13]. These ICEs are primarily run on liquid fuel, e.g., HFO or marine diesel oil, but can also be run on gas for applications like LNG tankers, where boil-off gas from LNG tanks can be used. Different efforts are being made by the manufacturers to improve the efficiency of the ICEs. The optimum fuel consumption of a medium speed ICE for 85% loading is around 200 g/kWh, however, when operated in variable speed mode, i.e., 50% to 100% of their rated speed, the fuel consumption goes down to 70 g/kWh [35], [36]. Additionally, to reduce the GHGs, due to environmental concerns, International Maritime Organization (IMO) has introduced Tier II and Tier III emission reduction programs and, therefore, more and more ICEs with dual fuel capability are being utilized [28]. Low to mid-speed ICEs usually have a big footprint, but from Table 2.1, it can be seen that medium speed ICEs have the highest efficiency and with variable speed operation in MVDC PDNs also provide an opportunity to improve their fuel consumption. A typical ICE is shown in Fig. 2.2(a).

#### 2.2.1.2 Gas Turbines

The compact size of GTs has seen them being deployed in military applications, and are also becoming popular choice for auxiliary power generators [13]. In an MVDC PDN setting, the GTs are an excellent candidate to replace ICEs, as the main PMs, because they are reliable and compact, and would ensure energy density in the future ship MVDC PDN. However, they are less efficient (≈40%) compared to medium speed ICEs, as can be observed from Table 2.1 and are expensive to run [25], [37]. Despite

<sup>4</sup>GTs are mostly used for auxiliary generation in large vessels [13].

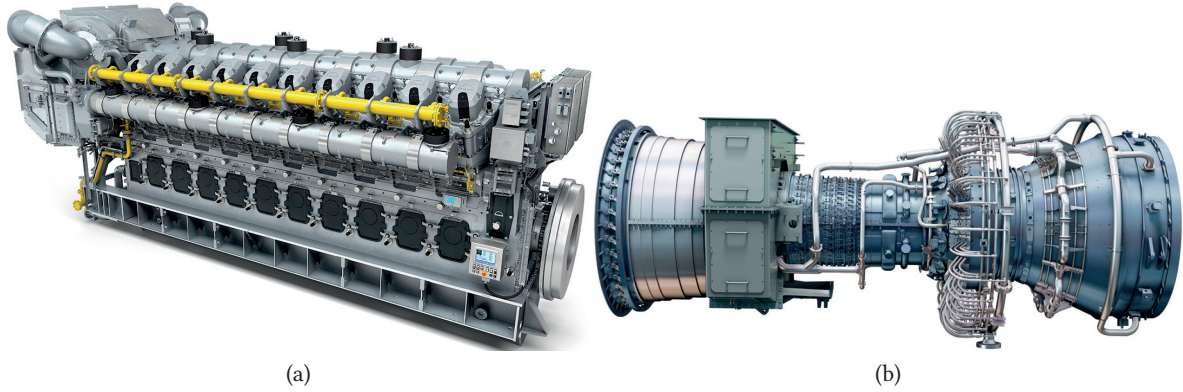


**Figure 2.2** (a) Typical ICE used in marine applications [28]. (b) GT for marine applications [32].

these disadvantages, the GTs can play a major role in the future MVDC PDNs when deployed to operate in a large speed range, e.g., an ideal utilization of the GTs is possible when connected to high speed generators, operating between 50 - 1k Hz for different loading conditions. In such circumstances, GTs will ensure energy density, reliability and flexibility of the MVDC PDN. Table 2.1 provides the summary of a few commercial offerings of GTs for marine applications. A typical GT for marine applications is shown in Fig. 2.2(b).

### 2.2.2 Generators

The second part, of the power generation system in the ship on-board PDNs, are the electrical machines that are operated as generators. In the MVAC PDNs, these generators are coupled, either directly or through a gearbox, to the PM shafts to produce constant frequency ac voltages (50/60 Hz). For medium speed ICEs, the generators are operated at 720/750 rpm and in case of high speed ICEs, they are operated at 1500/1800 rpm to produce 50/60 Hz ac frequency. Similar to the variable operation of the PMs, in the future MVDC PDNs, the generators are also expected to operate at variable speeds, therefore, discarding the need to synchronize different generators. This provides freedom to select machines other than standard synchronous machines (SMs), e.g., high speed permanent magnet synchronous machines (PMSMs), which can be directly coupled to high speed ICEs or GTs and this can lead to complete discarding of the gearbox. Additionally, multi-phase machines, previously only used for propulsion application on ship, can also be considered as generators, as they not only increase the energy density of the system, but also allow connection of multi-pulse rectifiers that are essential in producing high quality MVDC supplies<sup>5</sup>. This aspect is explored in detail in Chapter 4. Summary and key features of a few selected generators are given in Table 2.2.

#### 2.2.2.1 Synchronous Generators

In the state-of-the-art MVAC PDNs, SMs are mostly used as generators [13]. The frequency of the sinusoidal voltage induced in these generators depends on the number of poles of the machine and is also proportional to the speed of rotation. Usually the generators used for 60 Hz have ten poles

<sup>5</sup>In MVAC PDNs multi-secondary VCTs are used to connect to the rectifiers of the VSDs to produce high-quality dc-link voltages.

and a speed of 720 rpm, whereas, 50 Hz generators have a speed of 750 rpm with eight poles. Other options in use are two, four and six poles with 3600 rpm, 1800 rpm and 1200 rpm, respectively, for 60 Hz generation, and 3000 rpm, 1500 rpm and 1000 rpm, respectively, for 50 Hz generation. Furthermore, brushless excitation is utilized, in marine systems, to reduce the overall maintenance time and associated downtime, and to improve reliability of the generators [13].

Automatic voltage regulators (AVRs), with feed-forward stator current, control the excitation current of the field windings to maintain the terminal voltage of the generators. In steady state operations, the voltage regulation is limited to  $\pm 2.5\%$  of the nominal voltage, while, voltage transients are limited to  $-15\%$  or  $+20\%$  of the nominal generator voltage. As multiple generators are usually connected in parallel in the MVAC PDNs, the oscillations in the generator voltage due to load sharing among the generators or load changes are damped by the damper windings [13]. An example of a SM for marine application is shown in Fig. 2.3(a).

#### 2.2.2.2 Permanent Magnet Synchronous Generators

The current applications of PMSMs are mostly as turbo compressors in oil and gas industries [40], but are now also readily employed in wind turbines [39]. As MVDC PDNs provide freedom in selecting different generators for the electricity production, PMSMs are one of the leading contenders to be connected to the high speed ICEs or the GTs as ultra-high speed generators, and can easily be operated at 8000 rpm and above [41], [42]. The high speed of PMSMs is possible due to the presence of permanent magnets in place of field winding, unlike conventional SMs, and also results in a higher efficiency of the PMSMs [43]. However, there are certain shortcomings of using PMSMs, as generators, because of the lack of extended operational experience with this technology and, hence, the realization of their full potential is difficult. A few commercially available PMSMs are listed in Table 2.2 and shown in Fig. 2.3(b).

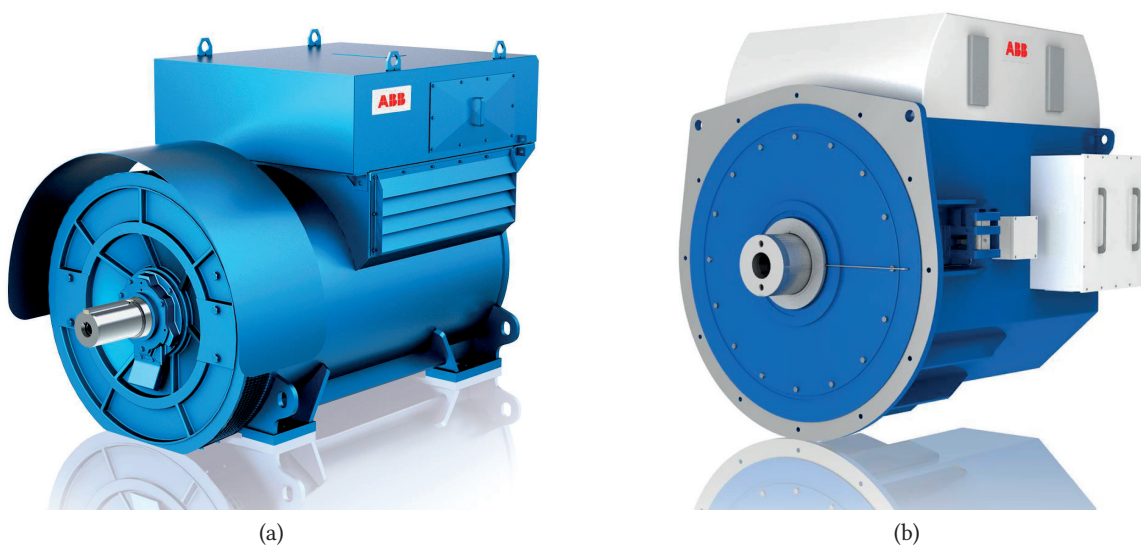


**Figure 2.3** (a) SM for marine applications [38]. (b) Commercially available PMSM [39].



**Table 2.2** Specifications of generators for marine applications.

| Generator | Manufacturer | Power        | Voltage       | Speed           | Ref  |
|-----------|--------------|--------------|---------------|-----------------|------|
| SM        | ABB          | 1 - 50 MVA   | 1 - 15 kV     | 500 - 1800 rpm  | [38] |
|           | Siemens      | 0.38 - 20 MW | 0.4 - 13.8 kV | 500 - 1800 rpm  | [45] |
|           | GE           | 2.5 - 45 MW  | 0.4 - 15 kV   | 300 - 1200 rpm  | [46] |
| PMSM      | ABB          | 1.5 - 7.9 MW | -             | 1000 - 1800 rpm | [39] |
|           | Siemens      | 1 - 5 MW     | -             | -               | [47] |

### 2.2.2.3 Multi-Phase Generators

The utilization of multi-phase machines (generators) has been under discussion since 1970's [44], this covers both SMs and PMSMs. Commercial multi-phase SMs and PMSMs are available and used for propulsion as they offer redundancy. An example of these machines will be seen in **Fig. 3.2**. In state-of-the-art MVAC PDNs, 3-phase generation is preferred because it provides the best compromise for energy density and also the equipment required to operate the system efficiently. Multi-phase machines, while increasing the energy density of the system, make the system more complicated, i.e., higher requirement of cabling, protection equipment and so on, which may also lead to complexity of operation and maintenance. The potential application of them, as generators, for the MVDC PDNs is proposed in [14]. Additionally, their use as possible generators allows connection of multi-pulse rectifiers (discussed in detail in *chapter 4*).

### 2.2.3 Transformers

The distribution voltage, in the MVAC PDNs, are chosen depending on the power requirements of the system, e.g., 11 kV distribution voltage is recommended for installed power greater than 20 MW, similarly, 6.6 kV for installed power range of 4 - 20 MW, etc. (Table 1.1) [13], [48]. Higher voltages are used for higher installed powers to reduce the thermal and the mechanical stresses on the distribution system. High power loads, e.g., propulsion VSDs are usually rated for 3.3 kV, and in order to service them LF VCTs (example shown in **Fig. 2.4(a)**) are required. These transformers not only provide voltage coordination for the VSDs and the other large group of LVAC loads, but also galvanic isolation. However, they are bulky, heavy and occupy significant space in the already constrained area in the ship. They usually have oil as cooling and insulation medium which, in case of fault, can be a fire hazard, or cause for other environmental concerns especially if there is an oil spill. Besides these issues, VCTs are instrumental in producing high quality dc voltages for propulsion inverters, as they have multiple phase-shifted secondaries that can be interfaced to multi-pulse rectifiers. These transformers also help in limiting fault currents and improving the power quality indices, e.g., reduction in distortion in currents and voltages that would otherwise have a negative impact on the marine generators. IEC standards are also available for design of the marine transformers depending on their functionality [49].

In the future MVDC PDNs, LF VCTs are expected to be removed, but the use of the multi-pulse rectifiers is necessary to achieve a high quality MVDC supply. This, as discussed earlier, can be achieved by utilization of the multi-phase generators, which are not the exact replacement technology.



**Figure 2.4** LF VCT for marine applications [50].

#### 2.2.4 Rectifiers

In the MVAC PDNs, rectifiers are only the input converter of the high power VSDs<sup>6</sup>, shown in **Fig. 2.5**, but in the future MVDC PDNs they are set to take a more central role as they are pivotal to supply dc power to the various loads. As regeneration is not of high importance in the ship on-board MVAC PDNs, so most of these rectifiers are multi-pulse diode rectifier units (DRUs) connected to multi-secondary transformers [51]. The rectifiers will now be directly interfaced with generators, where they will convert ac voltage to dc voltage and also determine quality of the MVDC supply. Another feature of this direct interfacing of generators and rectifiers is the lack of synchronization requirement of the generators, which will, as discussed earlier, lead to better fuel efficiency and higher energy density. In the future MVDC PDNs, different rectifier topologies such as diode, thyristor, active (classical 2-level/multi-level topologies) or MMC can be considered, based on the different benefits they bring at the system level.

##### 2.2.4.1 Diode Rectifier Unit

The DRUs are the simplest and cheapest of the different rectifier topologies because they are constructed with passive devices and lack the ability to regulate dc-side voltage or ac-side currents. To control the dc-side voltage, they rely on the AVR of the synchronous generator that is usually slow, with a bandwidth of around 1 Hz. The schematic of the DRU, with a capacitive filter, is shown in **Fig. 2.6(a)**. For the different power levels, they are arranged in 12, 18 or 24-pulse series or parallel configurations and interfaced with appropriately sized LF VCTs having 2, 3 or 4 secondaries. Additionally, the DRUs are also being employed in the LVDC PDNs [18]. The DRUs, due to their preference in the marine VSDs, present an easy adaptation from MVAC PDNs to MVDC PDNs, especially, when multi-phase generators are used.

<sup>6</sup>VSDs are usually in a back-to-back configuration, with capacitive filters in the middle.

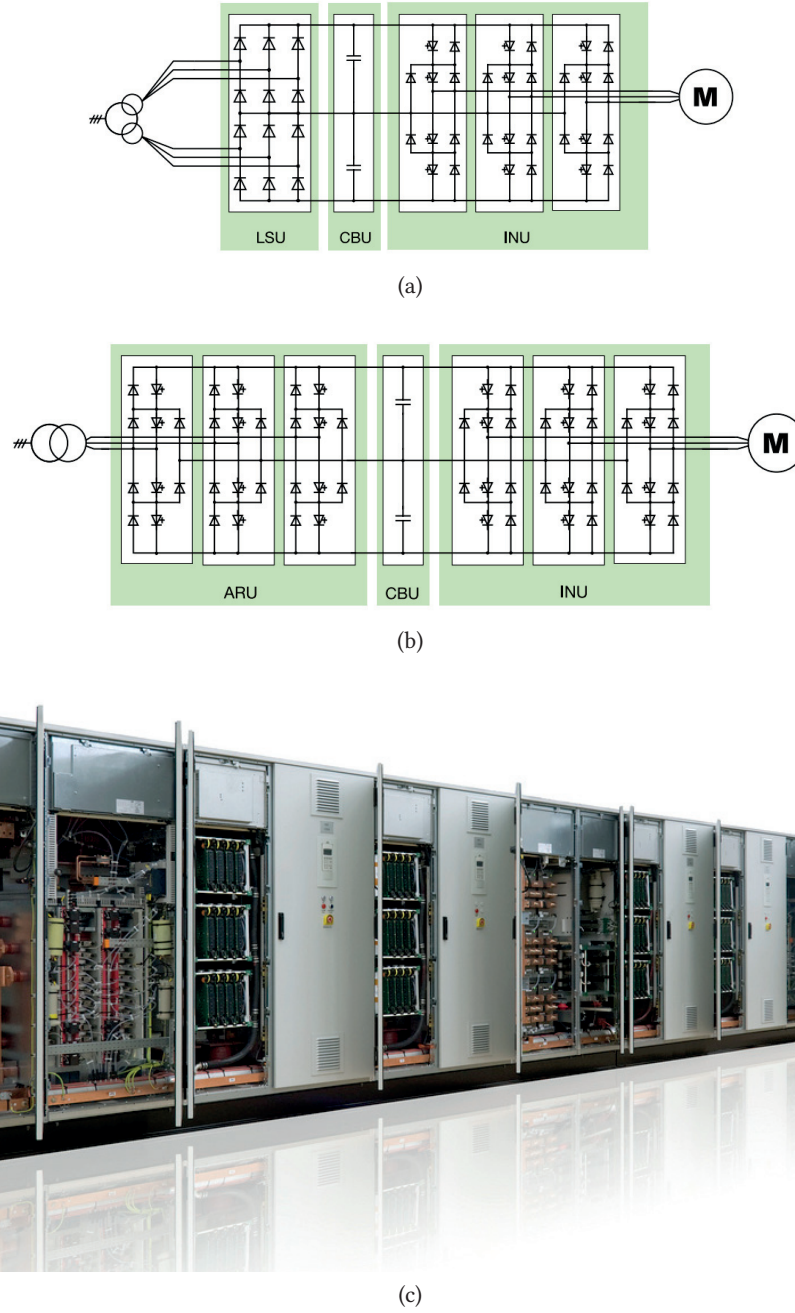


**Figure 2.5** Schematics of ACS6000 MV Drive from ABB [5]. (a) with 12-pulse DRU. (b) with 6-pulse active rectifier unit (ARU). (c) An actual ACS6000 MV drive from ABB used for on-shore industrial application.

#### 2.2.4.2 Thyristor Rectifier Unit

The thyristor rectifier units (TRUs) are widely used in high voltage dc (HVDC) applications [52], but they are not part of most of the commercial high power VSD offerings. However, compared to DRUs, TRUs have a more complicated construction but provide a certain level of controllability, in a narrow range, of the dc-side voltage and can also minimize fault currents [53]. These properties of TRUs



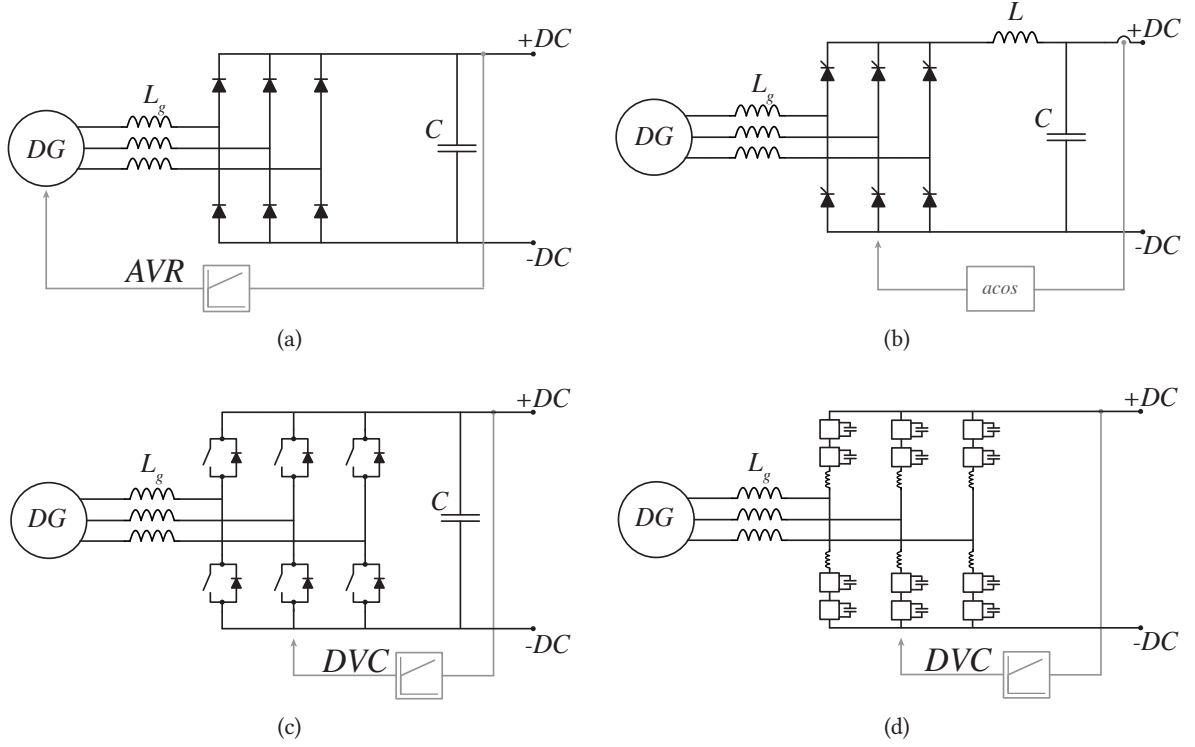


**Figure 2.6** Different rectifiers to be considered for the MVDC PDNs. (a) Diode rectifier. (b) Thyristor rectifier. (c) Classic 2-level active rectifier. (d) MMC as rectifier.

are being utilized for marine LVDC PDNs and also make them a possible choice for the future ship on-board MVDC PDN [35], [53]. The schematic of a TRU with an  $LC$  filter is shown in **Fig. 2.6(b)**. Their control is based on the well known inverse cosine control, which controls the firing angle to achieve desired voltages for the dc-side. The bandwidth of this control is usually within a range of 1 - 10 Hz [52]. The application of TRUs as MVDC supply converters, in ship on-board MVDC PDNs, requires further investigation, establishment of merits for their use in place of DRUs and commercial availability.

#### 2.2.4.3 Active Rectifier Unit

The third type of commercially available rectifiers are ARUs (classical 2-level/multi-level topologies). Simplified schematic of an ARU with a capacitive filter is shown in **Fig. 2.6(c)**. The ARUs are fully controlled four-quadrant converters, which have very good dynamic performance as they can tightly regulate the dc-side voltage, and, at the same time, control the ac-side currents to reduce ac-side harmonics. The commercially available ARUs have different topologies, e.g., classic 2-level voltage source converter (VSC) and multi-level like 3-L neutral point clamped converter (NPC), 3-L active neutral point clamped converter (ANPC), 4-L flying capacitor converter (FC) and 9-L cascaded h-bridge converter (CHB). The most widely used topology, in MV applications among these, is the 3-L NPC [54]. The control of these rectifiers has a cascaded structure, with inner current loop and outer voltage loop, which is usually fast and only limited by the device switching frequency and sampling frequency. A

reasonable bandwidth of rectifiers switching at 1 kHz is around 100 Hz.

Compared to both DRUs and TRUs, the ARUs are relatively expensive and their ability as a four-quadrant converter, is of limited use in the marine MVDC PDNs, as no regeneration is possible to the generators. Additionally, in the event of a dc-side fault, ARU cannot limit the fault current and are always dependent on external means to protect them and the system [55]. ARUs are useful, in the case, when high dynamic performance and quality is of the utmost importance, otherwise their application is difficult to justify.

#### 2.2.4.4 Modular Multilevel Converter

Another popular active rectifier topology is the MMC and is shown in **Fig. 2.6(d)**. The MMCs are used mostly in the HVDC applications, but recently have generated a lot interest for MVDC applications due to their higher efficiency (low switching frequency), modularity, voltage scalability and their inherent structure (sub-modules) also reduces filtering requirement [56]–[59]. MMCs are being used for shaft generator applications and as drive inverters by Siemens [60]. Additionally, MMCs with bipolar sub-modules can limit dc-side fault currents. Their possible usage as rectifiers in the marine MVDC PDNs has been proposed in [61]. MMCs are also highly complicated to control as they require multiple control structures, e.g., voltage balancing controls, circulating current control, voltage control etc., have a bigger footprint than other rectifiers, are much more expensive to deploy and maintain and scalability for multi-phase generators is also very complex.

### 2.3 Distribution System

The distribution system, as the name suggests, distributes/carries the power from the source to the loads. In an MVAC PDN, it consists of different switchboards and MVAC cables. In the simplest definition, the MVDC PDN would be distributed high power multi-motor VSDs, therefore, the distribution system here, primarily, would consist of:

- Filters: passive and active filters.
- Electrical distribution: bus bars and cables.

#### 2.3.1 Filters

A centralized dc-link capacitor bank is used in the commercial VSDs, which decouples the rectifier and the inverter, as shown in **Fig. 2.5(a)**. In the MVDC PDN, it is expected that the centralized capacitor bank will be distributed across the PDN, i.e., each converter will have a reduced size filter located close to itself. The type and size of passive filter employed in the system depends on the converter type, e.g., DRU and ARU require only a capacitive filter at their output, while, a TRU requires an LC filter [52]. However, in case of an MMC, each sub-module has a capacitor and the converter does not require any external filter. The inverter drives will also require small capacitive filters at their inputs.

Series active dc filters, albeit not present in the VSDs, are being proposed for voltage support and harmonic elimination [62], [63]. These filters are shown to lower the ripple in the distribution to

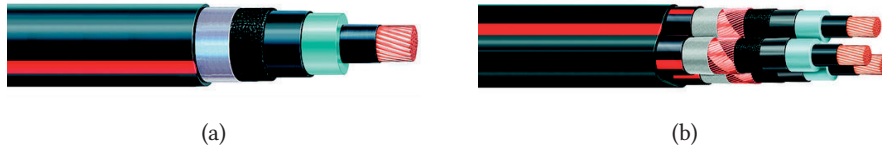


**Figure 2.7** Commercially available XPLE 12 kV MVAC cables [65]. (a) 1-pole MV cable. (b) 3-pole MV cable.

acceptable levels for the MVDC PDNs with TRUs as source converters. Additionally, isolated high power dc-dc converters based on MMCs with energy storage elements, are being considered to provide active filtering in the MVDC PDNs [64].

### 2.3.2 Cables

Both bus bars and cables can be used as distribution medium for the MVDC PDNs, but it is expected that similar to the MVAC PDNs, cables will be employed for bulk power distribution, while, bus bars will primarily be used within the different converters and equipment. Standardized MVAC cables (single-pole or three-pole) for different distribution voltages are commercially available, as shown in **Fig. 2.7**. However, standardized MVDC cables are not available and, therefore, the MVAC cables are expected to be employed initially for distribution in the MVDC PDNs. The cables in the MVAC PDNs suffer from skin and proximity effect, which are caused by the changing magnetic field of the ac current and result in the non-uniform distribution of the ac current [1]. In case of skin effect, the current density is higher at the surface of the conductor compared to the center due to the higher reactance at the center, whereas, the interaction of the magnetic fields of two closely located conductors, causes the current density to shift to the near or far edge of the conductors, depending on the direction of the ac current. Both these effects result in reduced current carrying capacity of the cables.

In the MVDC PDNs, these effects are not expected due to unidirectional nature of the dc current and the cables are expected to be fully utilized for their current carrying capability, which might lead to lower cabling requirement in the system. Additionally, in the large vessel on-board MVDC PDNs, the maximum distribution distances are expected to be around 300 m.

## 2.4 Propulsion Loads

The third group, of the main power chain of the ship on-board PDN, is the propulsion load. In the state-of-the-art MVAC PDN, this consists of the high power propulsion VSD (**Fig. 2.5**) and high power machines, operating as motors **Fig. 2.8**. These drive the propeller/thruster through a shaft or, in some new vessels, podded propulsors/thrusters, where machine is located within the propeller/thruster (**Fig. 1.1(c)**, this arrangement removes the need of drive shafts and rudders). Different manufactures are offering them such as *Azipods* from ABB and *Azimuthing Podded Propulsors* from Rolls-Royce [8], [12]. In the MVDC PDNs, the VSD will exist as a standalone inverter drive, i.e., an inverter connected to a motor.



**Figure 2.8** Commercially available propulsion motors [68]. (a) IM. (b) SM.

### 2.4.1 Inverters

The commercially available VSDs employ different inverter topologies, like the ARUs, and can be classic 2-level VSC or multi-level like 3-L NPC, 3-L ANPC, 4-L FC, 9-L CHB and most recently MMC [58], [66]. To ensure high performance in the commercial VSDs, usually vector control techniques, e.g., field-oriented control (FOC) and direct torque control (DTC), are used to drive the motors. Considering the present semiconductor technology and the large amount of power handled by the VSD inverters, the losses are minimized in the inverters by using lower switching frequencies. These switching frequencies, limited by thermal constraints, can be as low as 150 Hz for inverters with integrated-gate commutated-thyristors (IGCTs) [67].

### 2.4.2 Motors

The propulsion motors, responsible for producing propulsion in ships, are the main load of the ship on-board PDN and can reach up to 80% of the installed capacity. Depending on the size and function of the ship, the commercial motor units can be rated from 3 - 13.8 kV and 3 - 22 MW [12], [68]. In the lower power range, i.e., lower than 5 MW, induction machines (IMs) are utilized, whereas, most of the applications requiring more than 5 MW units employ SMs [13]. PMSMs are gaining more and more popularity and are becoming the most common machine in the podded propulsors/thrusters. The podded propulsors used in cruise ships and ferries are rated as high as 22 MW. The higher power machines, in some cases, are multi-phase machines. These machines are supplied by different VSDs to achieve redundancy.

## 2.5 Energy Storage Technologies and High Power dc-dc Converters

In addition to the present technologies, the future MVDC PDN allows integration of new technologies that can further increase the system efficiency, reduce the GHGs and the footprint of the installed equipment, while providing more flexibility in the system design. The two main technologies that can play a role in the main power chain of the MVDC PDNs are: (i) energy storage (ES) and (ii)

high power dc-dc converters. ES technologies, e.g., batteries, fuel cells, super capacitors, etc. can be connected to the main power chain and provide a possibility to regenerate power in the marine PDNs and use it whenever required. In addition to this, there are a number of benefits that can be extracted from the ES technologies [69]:

- *Spinning Reserve*: the ES can step-in, in case any of the generators goes offline due to any reason. This role can also be implemented locally for any sub-system to improve its availability in the total ship operation.
- *Peak Shaving*: in this role, ES can supply peak loads and as a result the generators operate in an optimal manner, which not only improves fuel efficiency but also reduces the GHGs.
- *Improved Dynamic Performance*: as a consequence of using the ES for peak shaving, the dynamic performance of the system is improved, as ES can service the loads much faster than the ICEs.
- *Optimal Generation Scheduling*: an optimal generation scheduling can be devised, which ensures that the generators are all the time operating at the most optimal loading.
- *Zero Emission Operation*: additionally, sufficiently sized ES can ensure that the ship does not require its various ICEs to operate when it enters harbor. This functionality can also be exploited during ICE maintenance.

High-power step-down dc-dc converters are important for the future MVDC PDN to enable the complete range of benefits expected from it, as they provide an interface between MVDC PDNs and LVDC PDNs in the system, but they are not commercially available. Different possible dc-dc converter technologies, e.g., dual active bridge and LLC resonant converters (input-series output-parallel, input-parallel output-series) have been proposed over the years to achieve this. Additionally, these converters can be used for interfacing the ES technologies to the MVDC PDN, e.g., a bi-directional three-port resonant converter topology is proposed in [70], which not only interfaces MVDC PDNs with LVDC PDNs, but also allows connection with ES.

## 2.6 Summary

In this chapter, a critical review of the commercially available technologies, for MVAC PDNs, and proposed technologies, for future MVDC PDNs, is presented. As the early adopters of MVDC PDNs are expected to heavily borrow from the state-of-the-art MVAC PDNs, most of these technologies will be utilized in the future MVDC PDNs. The configurations in which these technologies will be part of the MVDC PDNs will require a shuffle in the equipment layouts and additional functionality from them, e.g., the highest impact will be on the VSDs as they will now be effectively spread across the complete system. The subsystems, such as rectifiers, filters and inverters of the VSDs, will now have an impact across the whole PDN, in contrast to the earlier configuration, when they were galvanically isolated from the PDN by the LF VCTs. Additionally, the expected removal of LF VCTs arises questions in regards to the possible MVDC supply configurations, as it opens up both challenges and opportunities. In the next chapter, two real world cases are critically analyzed for a migration from MVAC PDN to MVDC PDN.



# 3

## Case Studies - Ship On-Board MVDC Power Distribution Networks

*In this chapter, two different high power vessels are presented and their state-of-the-art MVAC PDNs are discussed. The evolution of their respective MVAC PDNs into MVDC PDNs is also presented considering the requirements and functions of the vessels. This discussion highlights the challenges and opportunities in the implementation of MVDC PDNs.*

### 3.1 Introduction

Different works can be found in the literature that are addressing the different aspects of the ship on-board MVDC PDNs. As more and more power electronic systems will become standard equipment in ships, an analysis of the paradigm shift these will cause in the design process of the power systems for different vessels is presented in [71], [72]. Furthermore, in [73] a comparison of passive and active rectifiers to produce dc distribution voltages is presented, considering the degree of control they provide for the dc-link voltage. Marine systems are expected to have short cables (for large vessels upto 200 - 300 m) connecting different equipment together and to ensure a continuous service, a selective and highly reliable protection system is required. Therefore, a coordinated strategy including power converters and low voltage protection devices is proposed in [74]. Average modeling of the generators, rectifiers, propulsion units and so on is presented in [75], [76]. These models play an important role in the system stability studies. The system stability is pivotal for secure, continuous and uninterrupted operation of the PDN and implications of a large number of power converters are discussed in [77]. Additionally, in [78], efficiency of different equipment in a generalized MVDC PDN, for marine applications, is calculated and steps are put forth to optimize the overall efficiency of the MVDC PDN.

Even though, the literature describes different aspects and advancements in the understanding of the MVDC PDNs in ships, this move comes with its challenges. As highlighted in the previous chapter, these challenges include the need for improvements in the existing and the development of new technologies for diesel engines, gas turbines, generators, rectifiers, inverters, motors, protection equipment, high power dc-dc converters, active and passive filters, energy storage, and MVDC cables to enable MVDC PDN. In this chapter, a discussion on the state-of-the-art MVAC PDNs and a critical analysis of the future MVDC PDN, in large vessels, is provided considering two real world examples. These two cases are:

- LNG tanker - transport vessel





**Figure 3.1** Example of [79]: (a) LNG tanker. (b) Drill ship.

- Drill ship - exploration vessel

Typical ships for these two cases are shown in **Fig. 3.1**, and help in better understanding of the requirements to replace the existing systems and a proper identification of the technology gaps.

### 3.1.1 MVAC PDN - LNG Tanker

The simplified single line diagram of an existing LNG tanker, with an MVAC PDN, is shown in **Fig. 3.2**. This system has four generators with a combined capacity of 42 MW and each generator produces an output voltage of 6.6 kV. Additionally, the MVAC distribution voltage is 6.6 kV, directly set by the generators, and the ac frequency is 60 Hz. The four generators are divided into two groups of two generators (8.4 MW + 12.6 MW) each, which are then connected to each of the two main switchboards (MSB 1 and MSB 2). These switchboards then supply the power to the different loads in the system. Additionally, each of these main switchboards has a short circuit handling capacity of 31.5 kA. In order to ensure continuous operation, in case there is a loss of any of the generators, the main switchboards are interconnected through the ac bus-tie X.

As the entire MVAC PDN is made redundant, therefore, it is sufficient to consider only half of it for a functional description. From the perspective of MSB 1, three different groups of loads are connected to it. The first and the largest of these loads is the propulsion VSD, which is supplying an 11.1 MW, 3 kV, 6-phase motor (with two neutrals) that is in turn driving a fixed pitch propeller connected to it through a gearbox. As the voltage of the motor is lower than the distribution voltage, two multi-secondary line frequency transformers, rated at 6.4 MW, are used for voltage coordination. The output of these transformers is connected to two 12-pulse rectifiers, which results in 24-pulse rectification and proper voltage level at the input of the inverter stage of the VSD. The complete VSD is made redundant to ensure operation, even at the loss of any of the inverter units, albeit at reduced power.

The second group of loads, directly supplied by MSB 1, comprises of a step-down line frequency transformer rated at 2.8 MW and 6.6kV/450 V (supplying hotel loads), a bow thruster rated at 2.5 MW, and two motors rated at 0.46 MW each. The total power rating of this group is 6.22 MW. The last group of loads is connected to MSB 1 through another switch board SB 1. This group has a step-down



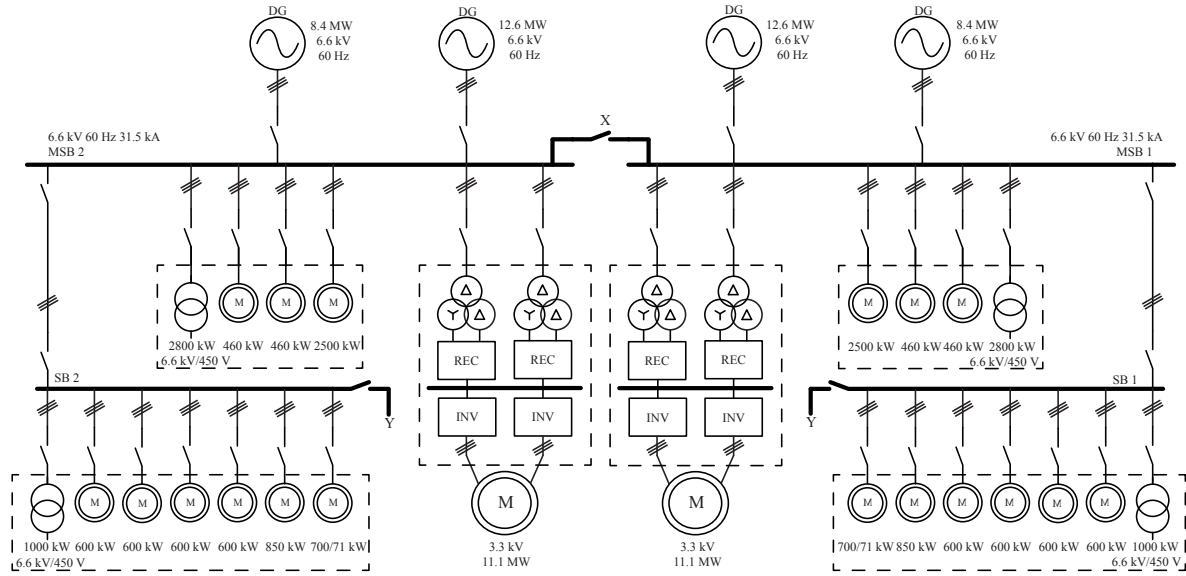


**Figure 3.2** Simplified single-line diagram of a MVAC PDN of a LNG tanker. Redundancy concept allows for interconnections between different switchboards using ac bus-ties X and Y.

transformer rated at 1 MW and 6.6k/450 V, and a group of 6 motors with a total power of 3.95 MW. Therefore, the total power rating of this group is 4.95 MW. These motors, in this group, are usually driving pumps and the lack of need for the frequency converters for these pumps results in very simple and reliable implementation of the system, despite its non-optimal efficiency and problems with inrush (starting) currents. Another interconnecting ac bus-tie Y is present to allow connection between SB 1 and SB 2, in case there is a loss of MSB 1. This allows continuous service of loads connected at SB 1. Similar is valid for MSB 2 and SB 2 as identical system is present on the left hand side of the **Fig. 3.2**.

### 3.1.1.1 Load Profile - LNG Tanker

LNG tankers mostly spend their time on traveling between ports. 90% of this time is in the open waters, while the remaining 10% is spent on crossing different transit canals, loading and unloading LNG and other low speed or stationary tasks. During transit, the LNG tanker operates at 80% of its installed capacity where its propulsion system is the bulk load. However, some of the direct-to-line motors are also used as pumps and compressors to maintain the liquefied state of the natural gas and remove the boil off gas. Once the LNG tanker enters the harbor the propulsion is turned off and only the direct-to-line motors and hotel hotels are supplied, until it is back in the open water. Furthermore, in cases where it must make up for the lost time, due to traffic or any other delays, LNG tanker might be required to operate at 90% of the installed power capacity.

### 3.1.2 MVAC PDN - Drill Ship

The simplified single line diagram of a drill ship, with an MVAC PDN, is shown in **Fig. 3.3**. This network consists of three identical sub-systems interconnected to ensure redundancy and **Fig. 3.3**

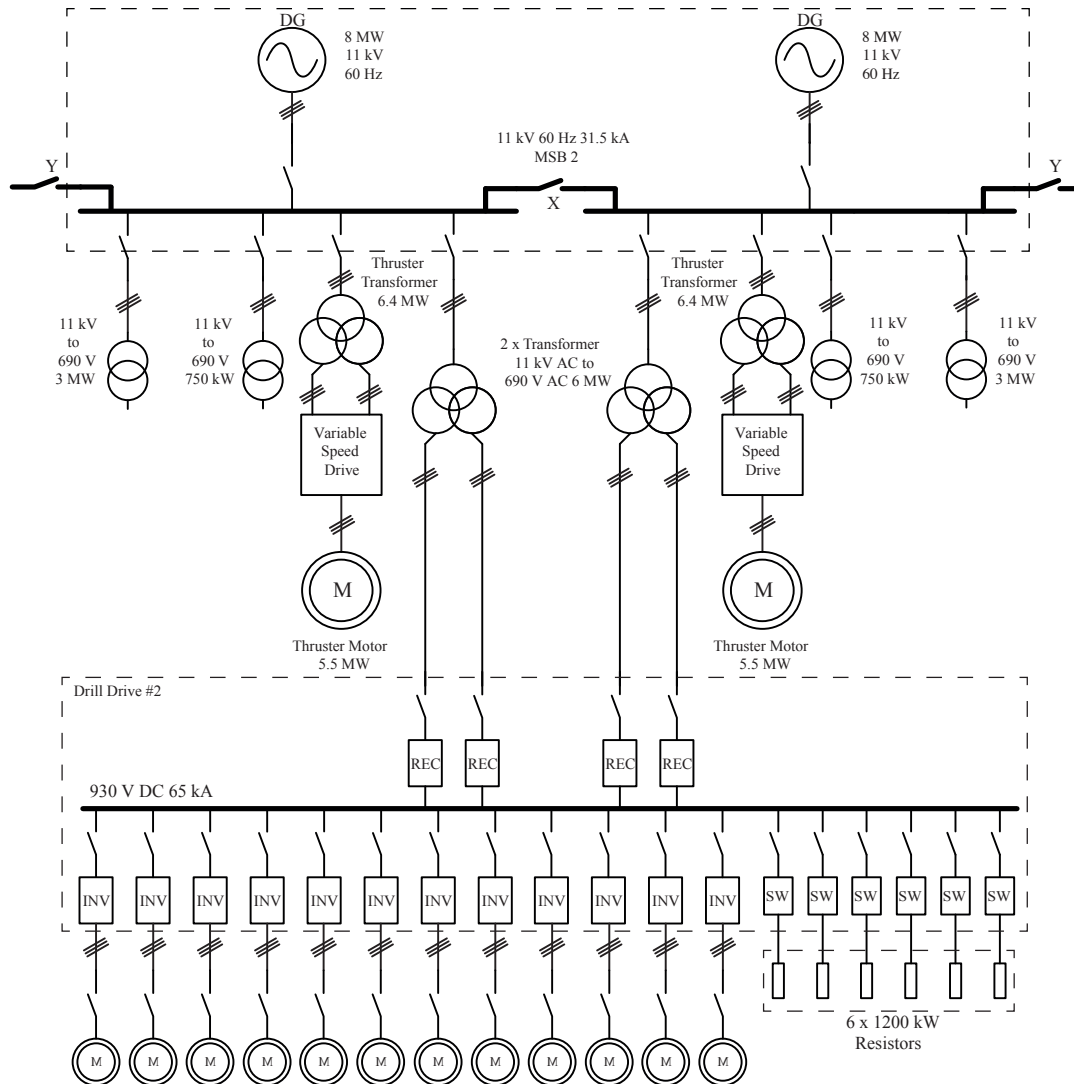


**Figure 3.3** Simplified single-line diagram of 1/3 of the MVAC PDN of a drill ship. Redundancy concept allows for interconnections between different switchboards using switches Y. It can be observed that a specialized drive is employed for driving the different LV pumps and drill motors.

only shows 1/3 of the complete network i.e., switchboard (MSB 2) and all the loads connected to it, and this is sufficient for the functional description of the system. The interconnection switches Y are used to connect to the remaining two main switchboards namely MSB 1 and MSB 3. This system has six generators with combined capacity of 48 MW and each generator produces an output voltage of 11 kV. Additionally, the distribution voltage is also 11 kV, which is directly maintained by the generators, and an ac frequency of 60 Hz.

As shown in **Fig. 3.3**, the main switchboard (MSB 2) has two of the six generators (8 MW + 8 MW) connected to it, which service the loads connected to it and a short circuit handling capacity of 31.5 kA. Internally MSB 2 has another interconnection ac bus-tie X interconnecting the two sub-switchboards to maintain redundancy, in case of loss of any of the generator. The loads connected to

MSB 2 can be classified in three groups. The first group consists of the drill drive that is connected to the MSB 2 through two step-down transformers rated at 6 MW each and 11k/690 V. These two transformers in turn are connected to each of the sub-switchboards of MSB 2. On the drill drive side, these transformers are supplying a pair of rectifiers that results in a 12-pulse rectification. The LVDC bus, of the drill drive, is maintained at 930 V and has a short circuit capacity of 65 kA. 12 inverters are connected to the bus, which control the operation of the drill motors. Additionally, as no regeneration is possible, a group of 6 braking resistors, each rated at 1.2 MW, is also connected to the LVDC bus to dissipate the braking energy. The total drill drive load, connected to MSB 2, is 12 MW.

The second group of loads are the two thruster drives connected to the two sub-switchboards of MSB 2 through two step-down transformers rated at 6.4 MW each. Each of these thruster drives is driving a 5.5 MW thruster motor, thus making the total thruster load as 11 MW. The third group of loads consists of four step-down transformers with two of them rated at 3 MW, 11k/690 V each and the other two at 0.75 MW, 11k/690 V each. Thus total power requirement of hotel loads is 7.5 MW. Identical loads are connected to MSB 1 and MSB 3.

The drill drive is one of the largest loads in this system. In order to implement a full MVDC PDN in the drill ship will require reconfiguration of the drill drive and also development of high power dc-dc converters to step-down the MV distribution voltage to proper LV levels. Therefore, full MVDC might not be the solution for a drill ship considering the presently available technology.

#### 3.1.2.1 Load Profile - Drill Ship

The thrusters of the drill ship are used for dual purpose, firstly they work as propellers when the ship is in transit from the port to a drilling location. In this case, the loading reaches upto 15% of the installed capacity. Secondly, once at the drilling location, they ensure that the ship stays at the given GPS coordinates, in the sea, for the complete drilling duration. This is achieved by DP<sup>1</sup> of the ship. During drilling phase, the drill drives are the main load for calm sea conditions, however, the loading of the ship might reach 85% of the installed capacity for rough sea conditions as the thrusters try to maintain the position of the vessel [80].

### 3.2 Architectures - MVDC Power Distribution Network

As highlighted earlier, MVDC PDNs have considerable advantages over the existing MVAC PDNs such as improved fuel and system efficiency, reduction in the operation costs and the footprint of the installed equipment, and so on. Subsequently, the generators are expected not to be synchronized with each other and, with appropriate voltage class of generators, main loads (e.g., propulsion motors) and distribution, the low frequency transformers would also not be required. This is not a trivial problem to solve. Nonetheless, significant modifications will be required in the existing equipment and development of new equipment to enable and accommodate dc power transfer.

For MVDC PDNs, a proper dc protection-coordination system is required that can handle high power and work for the voltage levels indicated in Table 1.2. All the components involved in the power

<sup>1</sup>Computer controlled system to maintain a ship's position taking constant inputs from different sensors and GPS satellites.

chain are expected to protect themselves against high voltages and currents [20], therefore, making the protection-coordination systems complex as these components are also expected to prevent the fault from propagating to nearby components and ensure uninterrupted operation of the system. In short, the protection-coordination systems in the MVDC PDNs are expected to detect the faults in a very short time in the range of 1 - 10 ms, take action to localize and isolate them and reconfigure the PDN for maximum availability and reliability of the system. However, the suitable protection equipment, for expected MVDC distribution voltage levels, is clearly not available. Additionally, LV loads (ac or dc), serviced earlier by dedicated low frequency transformers, need special step-down converters to power them. Despite considerable research effort, high power dc-dc converters are still not commercially available, including the so called power electronic transformer [81].

A significant research and development effort is required to make MVDC PDNs a reality, yet the MVDC principles laid down in [20] may not be applicable to all ships. This is explored in the subsequent subsections, where potential architectural evolution towards MVDC PDN is explored for an LNG tanker and a drill ship.

### **3.2.1 LNG Tanker - Possible PDNs**

The implementation of MVDC PDN in an LNG tanker has been analyzed considering two possible MVDC architectures:

- *Hybrid MVAC/MVDC PDN*: largely preserving the MVAC distribution, while introducing the MVDC distribution for large propulsion loads.
- *Full MVDC PDN*: completely overhauling the distribution network with new equipment.

#### **3.2.1.1 Hybrid MVAC/MVDC Power Distribution Network**

In view of the large number of loads without any power electronic converters and served directly from the MVAC PDN, a hybrid MVAC/MVDC PDN is proposed that is shown in **Fig. 3.4**. This architecture largely preserves the MVAC PDN, i.e., the diesel-generator sets operate at 60 Hz ac frequency and supply ac power to all the direct-to-line motors (e.g., different pumps and bow thrusters) and the step-down line frequency transformers that serve the low voltage hotel loads. The drawback of this configuration is that diesel-generator sets are operated at a constant frequency to maintain the ac frequency, the generators are synchronized to the distribution and no fuel savings compared to the MVAC PDN is possible.

Nonetheless, the bulky line frequency transformers, at the input of the propulsion VSDs, can be removed by the introduction of a dedicated MVDC PDN. This can be achieved by re-purposing and redesigning (to withstand the double of the original voltages) of the rectifiers of the VSDs. The rectification of the MVAC voltage determines the dc-side voltage. As the multi-winding transformers are removed, only 6-pulse rectification is possible that will result in low quality MVDC supply (high ripple factor on the dc-side [52]). Considering passive rectification of the 6.6 kV ac voltage, around 10 kV dc voltage is achieved. The rectification can also be done by active rectifiers, which can regulate the dc voltage and also provide a possibility to regenerate. In the marine systems, usually regeneration is not a possibility and for rare occasions (e.g., crash stop), which might require braking, braking

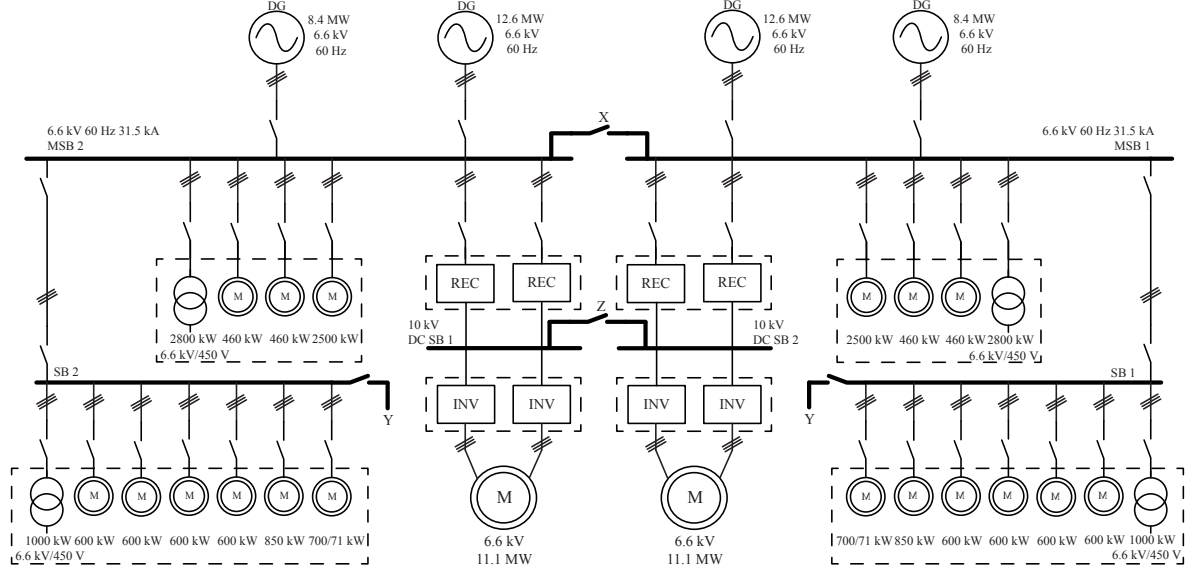


**Figure 3.4** Single-line diagram of the proposed hybrid MVAC/MVDC PDN for an LNG tanker. The voltage ratings of the rectifiers, inverters and propulsion motors are double compared to those shown in Fig. 3.2.

choppers are used. The inverters of the propulsion VSDs are now directly fed from the MVDC distribution, as shown in Fig. 3.4. Just like the rectifiers, the inverters and the propulsion motors are expected to withstand and operate under higher voltages, double in this case. This would mean the input voltage of inverters is now 10 kV, whereas originally it was 5 kV, while the motor is rated at 6 kV instead of 3 kV. This will lead to replacement of the existing motors with new higher voltage rated motors.

Although this implies major redesign in the whole propulsion chain, it provides opportunities to spatially optimize the ship architecture as rectifiers and inverters can be placed close to their respective sources and loads. Additionally, new equipment can be installed for different dedicated ship operations. With all the expected changes in the propulsion chain, redundancy is still preserved in the system and another layer is added through MVDC PDN by the possibility to interconnect DC SB 1 and DC SB 2 through dc bus-tie Z. This can help in bypassing a faulty rectifier.

### 3.2.1.2 Full MVDC Power Distribution Network

The second possibility is the complete implementation of the MVDC PDN concept, as shown in Fig. 3.5. In order to establish a ship wide MVDC distribution, dedicated rectifiers (passive or active) for each diesel-generator set are proposed. This will ensure that the generators can be operated at different speeds, corresponding to the system loading, and eventually result in an efficient operation and fuel savings. Furthermore, the distribution voltage is dependent on the generator voltage class and the corresponding rectifiers, which in this case is around 10 kV. As all the generators are 3-phase, only 6-pulse rectification is possible which does not produce high quality dc supplies [82]. This can be overcome by utilizing multi-phase multi-pulse supplies to produce high quality dc distribution (detailed discussion in Chapter 4). As a distributed MVDC architecture is proposed, dc voltage is available on dedicated switchboards and all the power electronic converters are located in close

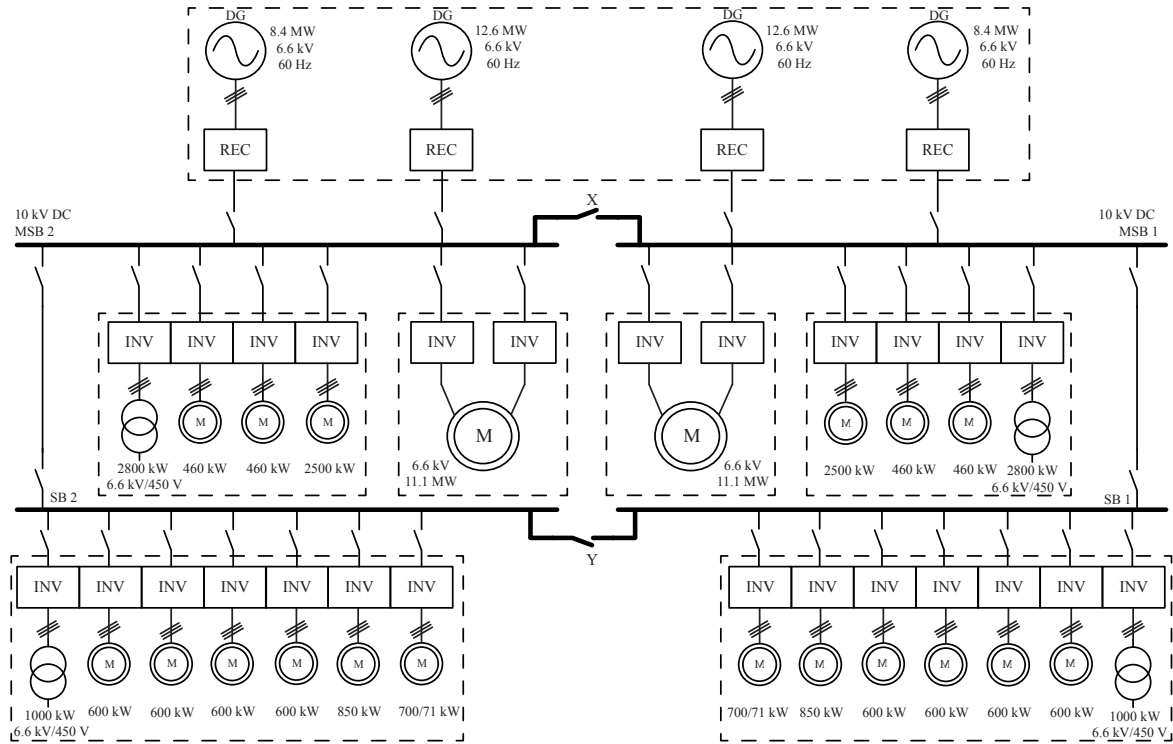


**Figure 3.5** Single-line diagram of proposed full MVDC PDN for a LNG tanker.

vicinity of their respective sources/loads. For example, propulsion inverters are connected to MSB 1 and MSB 2, respectively, and located close to the propulsion motors.

As pointed out earlier, there are a large number of direct-to-line motors in the system and in order to supply power to them through the MVDC PDN, a large number of inverters are required as shown in **Fig. 3.5**. For this solution to be simple and cost effective, the inverters must have sufficient ratings to supply them and a high output voltage quality (e.g., a sine filter at the output, required only for motors designed for direct grid operation). This would help operate these motors similar to the MVAC distribution. On one hand, this greatly increases the system costs, but on the other hand provides controllability and improves system efficiency. For the low voltage ac loads, in the system, dedicated inverters and step-down transformers are considered to generate 450 V. Another possible choice is to consider a combination of a step-down dc-dc converter and inverter to supply these loads. A proper solution is only possible by developing new or adapting existing technologies, e.g., using a medium frequency transformers in dc-dc converter can be considered for attaining proper voltage and galvanic isolation. System redundancy is maintained through dc bus-ties X and Y, similar to the original system.

A new protection coordination concept for MVDC PDN is required to handle faults in the system. The converters, in this system, may also play a role in limiting the fault current but this is highly dependent on the type of converter. Additionally, due to the lack of commercialized MVDC breaker technology for expected distribution voltages, given in Table 1.2, a proper assessment and research and development is still required in this area.

### 3.2.2 Drill Ship - Possible Architectures

As special loads are present in drill ship, only a hybrid MVAC/MVDC PDN is considered for the drill ship.

#### 3.2.2.1 Hybrid MVAC/MVDC Power Distribution Network

The application of drill ship requires installation of highly specialized equipment, e.g., drill drives, which are the biggest load in this case. These specially designed loads do not provide much flexibility when conceiving a new distribution architecture. Additionally, as no high power dc-dc converters are commercially available, interconnection between MVDC and LVDC PDNs cannot be easily realized.

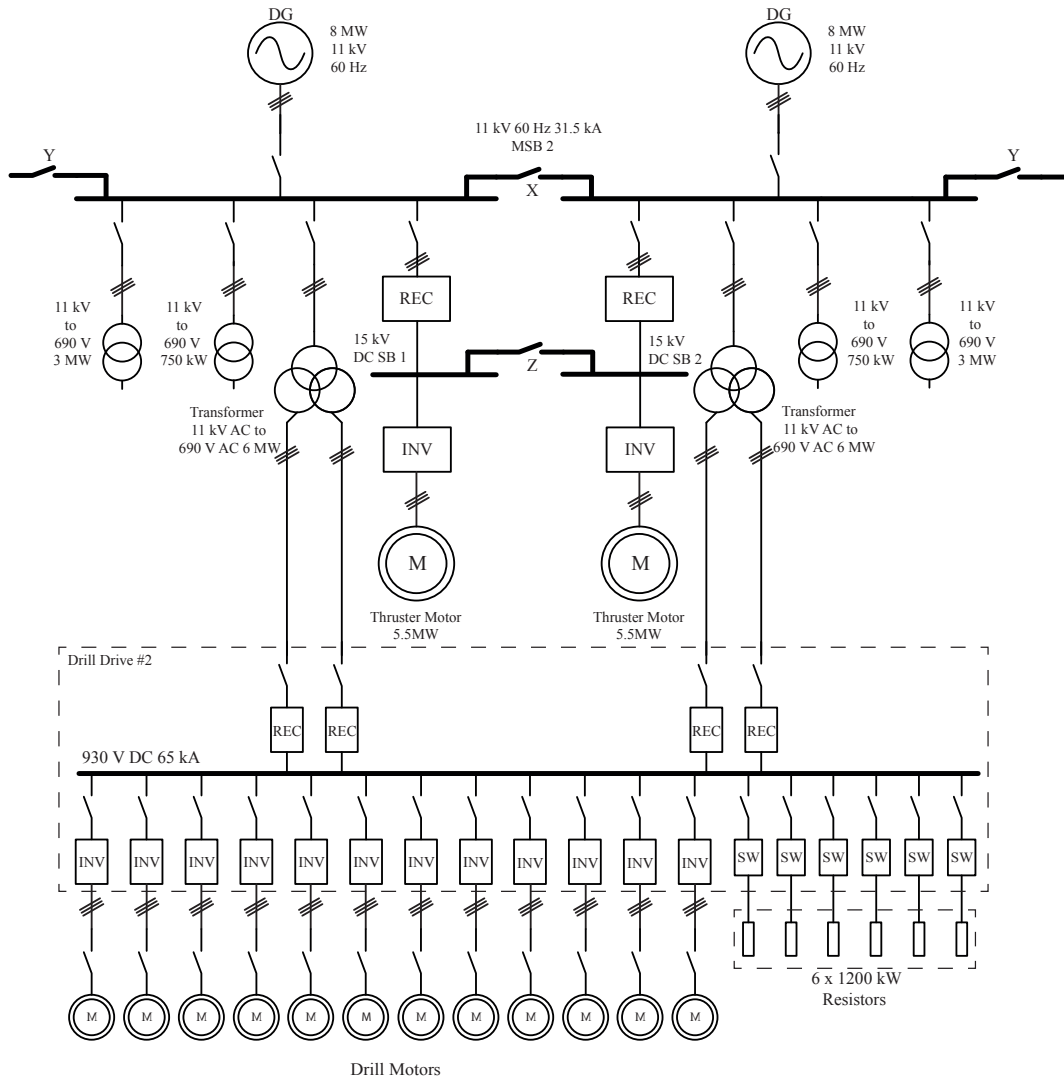


**Figure 3.6** Single-line diagram of the proposed hybrid MVAC/MVDC PDN for the drill ship. Propulsion inverters and propulsion motors voltage ratings are equal to the distribution voltage.



Therefore, only a hybrid MVAC/MVDC architecture is proposed for the drill ship, as illustrated in **Fig. 3.6**. Here only 1/3 of the proposed architecture is shown, as the other systems are identical to this one to maintain redundancy. This architecture preserves the existing MVAC PDN to supply the drill drives and the hotel loads through step-down transformers, at the same time, the MVDC PDN is introduced for the thruster drives. The redundancy is maintained with ac bus-ties X and Y, similar to the existing system, while dc bus-tie Z is introduced to add redundancy in the MVDC PDN.

The MVDC PDN is provided by means of dedicated rectifiers connected to the MVAC main switchboards, leading to a dc distribution voltage of around 15 kV. The bulky transformers for the thruster drives are removed in this scenario. As the MVAC distribution is 3-phase, therefore, only 6-pulse rectifiers can be used. Additionally, active rectifiers can be used for regeneration as there are other loads connected to the MVAC distribution, but as they are usually expensive their utilization needs to be justified for this apparent benefit. As the thruster inverters and motors are connected directly to the new MVDC distribution, they must match in voltage ratings. The drawback of this PDN, as discussed for LNG tanker, is that the generators are still required to be synchronized and, thus, fuel efficiency can not be achieved. However, the bulky thruster transformers can be removed and provide more space for other installations.

### 3.3 Summary

From the critical discussion and proposal of the different MVDC architectures for the real world cases studied, it is clear that despite the advantages of MVDC PDN, the transformation from MVAC to MVDC is not straightforward and a few critical technologies are also not available. Evidently, the absence of technologies in different parts of the system is a hurdle in the implementation of MVDC PDN. A short summary is provided in Table 3.1 and Table 3.2, as an overview of the possible benefits and challenges of these architectures. It can be seen that hybrid MVAC/MVDC PDNs are less invasive and help remove the LF VCTs, but do not provide any fuel savings. However, the full MVDC PDNs provide all the expected benefits of the dc PDNs, but require development of new technologies, e.g., dc-dc converters, protection-coordination for MVDC PDNs, and so on.

On a more general level, MVDC PDN does not require constant ac frequency, and opens up opportunities to utilize variable and high speed generators with active rectifiers. The filtering effort, at the output of the rectifiers, will need to be designed by considering the system loading profiles and energy management requirement of the ship. Moreover, unlike the standardized MVAC cables, cable technology for MVDC applications are not standardized or available. In the MVDC PDN, the load inverters and the corresponding motors require higher voltage rating for operating at higher dc

**Table 3.1** Potential benefits and challenges of a hybrid MVAC/MVDC PDN.

| Potential Benefits                              | Challenges   |
|---|--|
| Less invasive ship architecture modification    | Fixed speed prime movers and generators              |
| Removal of bulky propulsion drives transformers | Inefficient use of direct-to-line motors (as before) |
| Possibility to re-generate from MVDC to MVAC    | Two different protection schemes (ac and dc)         |
| Possibility to exchange energy between drives   | Non-availability of high power dc-dc converters      |
| AC protection is already available              | Voltage coordination in not flexible MVDC, MVAC      |



**Table 3.2** Potential benefits and challenges of a full MVDC PDN.

| Potential Benefits                              | Challenges                                      |
|---|---|
| High speed prime movers and generators          | No commercial rectifiers for MVDC               |
| Removal of bulky propulsion drives transformers | Lack of MVDC protection devices                 |
| Possibility to re-generate from MVDC            | Two different protection schemes (ac and dc)    |
| Possibility to exchange energy between drives   | Non-availability of high power dc-dc converters |
| Ability to integrate energy storage into MVDC   | Voltage coordination                            |

voltages, as recommended in Table 1.2. Most of the commercially available drive inverters are rated for a dc-link under 10 kV, hence, developmental work is required for distribution voltages above 10 kV. The propulsion/thruster motors are usually induction motors for their rugged design and low maintenance requirements. Additionally, permanent magnet synchronous motors (PMSM) and wound rotor synchronous machine (WRSM) are also increasingly being used due to their higher efficiency and better dynamic performance. However, these motors are expected to match the distribution voltage, e.g., 6.6 kV motor is required for a 10 kV MVDC distribution.

As LF VCTs are expected to be removed, a direct adoption of the standard 3-phase generators, from MVAC PDN, cannot produce high quality dc voltages. Therefore, in order to produce high quality dc-side voltages, generators with more than 3-phases (e.g., 6, 9, 12, ...-phase) are more advantageous. These generators will allow interface of multi-pulse rectifiers (e.g., 12, 18, 24, ... -pulse) that can produce high quality dc supply by utilizing passive rectifiers, also reduce per-phase currents and improve redundancy in the system. Additionally in MVAC PDNs due to the presence of the VCTs, the distribution voltage does not always define the voltage classes of the generators or loads (motors) and they can be selected independently. Whereas, in MVDC PDNs, the generators, motors and distribution equipment have to be of the same voltage class. A possible solution to these challenges is proposed with multi-phase multi-pulse rectifiers in *Chapter 4*.

A higher penetration of the power electronic equipment is expected in the MVDC PDN and the systems dynamics and protection-coordination strategies will change compared to the existing MVAC PDN. Therefore, system design studies targeting these issues are required before conceiving an MVDC PDN. In this thesis, a study of the system stability considering the impact of passive elements and converter dynamics is carried out (*Chapter 5, 6 and 7*) to ensure uninterrupted and reliable operation of the system, whereas, the discussion on protection-coordination strategies is out of scope of the thesis.



# 4

## Multi-Phase Multi-Pulse Power Supplies for MVDC Power Distribution Networks

*In this chapter, multi-phase multi-pulse supply configurations are explored to achieve high quality power supplies for the MVDC power distribution networks. These configurations bring simplicity, reliability and fault tolerant behavior with sufficient dynamic performance. A proper design also ensures reliable fault current (thermal) withstand capabilities.*

### 4.1 Introduction

The discussions and analyses, in the previous chapters, have highlighted the advantages and opportunities available within the framework of MVDC PDNs. Most of these advantages, e.g., fuel efficiency, energy density, lower operational costs and lower equipment footprint, revolve around the technologies and operational strategies of the power generation systems that will be deployed in the MVDC PDNs. These power generation systems are expected to supply distribution systems with different distribution voltage levels (5 - 35 kV [20]), depending on the power requirement of a particular MVDC PDN. Additionally, these supplies can be operated with different operation modes of the prime movers, e.g., fixed speed or variable speed, which can achieve varying degree of fuel efficiency.

Apart from the expected fuel efficiency, the MVDC PDNs are also required to have a fault tolerant behavior. To overcome the technological gap due to the non-availability of commercial dc breakers, a number of ways of blocking or limiting the fault current, in short time scale, i.e., 4 - 10 ms and considering source-side converters, have been presented [53], [83]–[85]. In [83], [84], interruption of the fault currents with different hybrid circuits is proposed, but these topologies usually end up making the system inefficient [53]. Additionally, fault current isolating topologies for ARUs are presented in [85], while the controllability of TRUs is exploited in [53], and current fold back principle is proposed to limit fault currents in a few milliseconds. In the recently established LVDC PDNs for ships, a number of strategies are used to overcome fault currents due to different faults and, at the same time, ensure high availability of different equipment. These strategies are: special LVDC fault tolerant bus-ties, power electronic converters with fault blocking capability, higher short circuit current capacity of power electronic converters, generators with high sub-transient reactance, generator excitation removal, fuses, isolator switcher and so on [17], [18].

A standard solution considering state-of-the-art MVAC PDN technology with 3-phase generators implies a 6-pulse supply, which has certain drawbacks discussed in the next section. These drawbacks can be overcome by a multi-phase, multi-pulse supply, which is discussed and analyzed in this chapter.

## 4.2 MVDC Supply - 3-phase, 6-pulse

For a 3-phase supply configuration, depending on the voltage class, different options can be considered for the prime movers, generator types, ac and dc voltage levels, operating frequencies, as well as type and control of the supply-side converter. A standard MVAC system supply with ICEs and synchronous generators, with frequency and AVR control, supplies VSDs through multi-secondary LF VCTs, which are then interfaced to DRUs arranged in multi-pulse configuration to generate dc-link voltage. A similar arrangement can be employed for MVDC supply by removing both the VCTs and the multi-pulse DRU configurations. Additionally, GTs and high speed SMs or PMSMs can be used to produce 3-phase supplies, but would require fast recovery diodes in place of standard recovery diodes.

A major shortcoming of the 3-phase supply emerges as the voltage and power levels are increased. As LF VCTs are set to be removed, the voltage classes of voltage of the generators and the load must be similar, e.g., 11 kV generator requires a 11 kV propulsion motor or vice versa. Additionally, for increased voltage levels more devices will be connected in series, which will increase the complexity of the auxiliary circuits, like voltage balancing circuits and snubbers. The power quality of the 6-pulse rectifiers also is quite low [86]. Equipment level redundancy would be impossible and only the present system level redundancy would be allowed. Another challenge is to achieve equipment level redundancy and voltage scalability, therefore, multi-phase, multi-pulse supplies are explored in the next section.

## 4.3 MVDC Supply - $N \times 3$ -phase, $N \times 6$ -pulse

As discussed earlier, to produce high-quality dc-link voltages in VSDs, multi-secondary LF VCTs are employed that are connected to the multi-pulse rectifiers. To achieve similar benefits in the MVDC PDNs, generators with multiples of 3-phase windings feeding multiple 6-pulse rectifiers are attractive solutions for MVDC supplies. Multi-pulse rectifiers provide a high quality dc supply, e.g., 12-pulse rectifiers have a better dc-side power quality because of the low ripple factor (1%) [82], which is much lower compared to the recommended 5% in [20]. While different rectifier topologies have been discussed in *chapter 2*, DRUs are chosen to achieve the high quality MVDC supply because:

- They are already the preferred rectifier in the VSDs used in the marine applications, which has led to accumulation of considerable operational experience and design knowledge.
- The benefits of employing TRUs, in place of DRUs, are not substantial, except for the cases where fault current limiting capability is highly desired. Additionally, TRUs can be operated at  $\alpha = 0^\circ$  to operate as DRUs and their control is only employed in case of faults, but still TRUs are expected to be more expensive than the DRUs.
- As no regeneration takes place in the marine systems, the four-quadrant and highly controllable ARUs (classic 2-L, multi-level or MMCs) are likely too complex and expensive for these applications.

In the commercial VSDs, multiple units of 6-pulse DRUs are arranged in series and parallel configurations to achieve 12, 18, 24-pulse DRUs for different voltages and power levels [51]. This is possible due to the presence of multi-secondary VCTs. In MVDC PDNs multi-phase generators could partially take

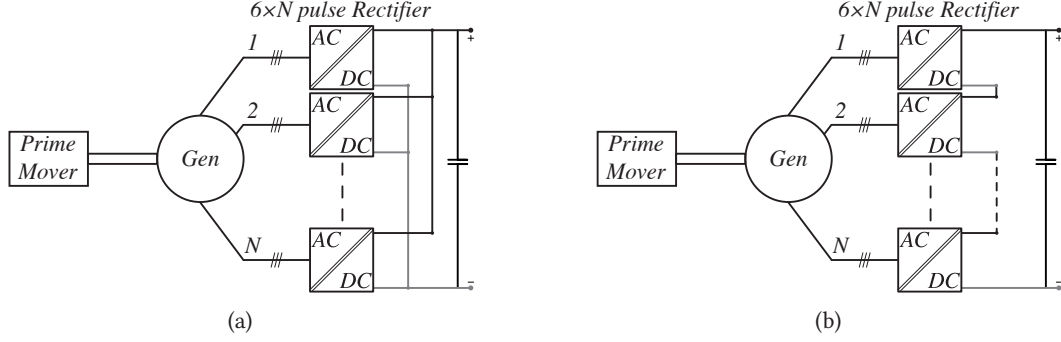


**Figure 4.1**  $N \times 3$ -phase system configuration. (a) Parallel connection of rectifiers. (b) Series connection of rectifiers.

this role and allow series and parallel arrangement of DRUs. Additionally, the multi-phase generators can provide a fault tolerant supply in event of generator or rectifier fault, remove harmonics lower than  $6 \times N$  of the fundamental frequency ( $N$  = number of DRUs in multi-pulse configuration), and also improve energy density.

Considering DRUs based multi-phase multi-pulse MVDC supplies, a number of advantages are expected from them, which are:

- A simple construction to achieve high quality supply, with possibility to use 6, 9, 12, ...-phase generators.
- Additional redundancy, i.e., equipment level, and fault tolerance.
- Freedom to choose voltage classes of generators and motors.
- Efficient usage of present semiconductor technology.

Possible arrangements of this supply configuration are shown in **Fig. 4.1**, and discussion on their advantages and challenges is presented hereafter.

#### 4.3.1 Multi-Pulse - Parallel Connection

Multi-pulse rectifier, achieved by parallel connection of several rectifiers, is shown in **Fig. 4.1(a)**. In this arrangement, each winding set of the generator has its own neutral terminal and is rated to the full voltage of the ac-side, i.e., to produce a 5 kV dc-side voltage, each winding set is rated to 3.7 kV ac. If the MVDC distribution voltage is 10 kV, then ac voltage is 7.4 kV and so is the rating of each winding set. However, as the load is supplied by each winding set, so the total load current is divided among the different winding sets, i.e.:

$$I_{N,ac/dc} = I_{rated,ac/dc}/N \quad (4.1)$$

Here  $N$  is the number of 3-phase winding sets of the generator. In similar fashion to the generator winding sets, each of the 6-pulse rectifier, in the parallel arrangement, is rated to withstand the full dc-side distribution voltage (e.g., 5 kV, 10 kV, ...) and supplies  $1/N$  of the rated load current. Additionally, based on the distribution voltage level and the voltage class of the selected semiconductors (4.5 kV,

6 kV), series connection of several devices may be required which will lead to higher number of auxiliary circuits, i.e., snubbers, and static and dynamic voltage balancing circuits.

The parallel connection of rectifiers, although it provides high quality MVDC supply, but, like 3-phase supplies, does not provide flexibility in choosing the voltage classes of generators and motors. This is true under the assumption that propulsion motors and other pumps are supplied by MVDC PDN through a dedicated inverter. In spite of this, in case of a fault due to a 3-phase winding set or a rectifier, a de-rated system operation is still possible in which only essential loads are supplied, whereas, the non-essential loads are disconnected. In short, the multi-pulse parallel rectifiers can be selected to achieve fault tolerance in the ship on-board MVDC PDNs, wherever this functionality is of the highest importance.

#### 4.3.2 Multi-Pulse - Series Connection

The second type of multi-pulse rectifiers, under consideration, are achieved by the series connection of 6-pulse rectifier units, as shown in **Fig. 4.1(b)**. The voltage ratings of the generator winding sets and rectifiers, in this case, are:

$$V_{N,ac/dc} = V_{rated,ac/dc}/N \quad (4.2)$$

Here, similar to multi-pulse parallel rectifiers,  $N$  is the number of winding sets of generator that is also the number of series connected rectifiers. Additionally, the full load current is supplied by each winding set and each rectifier must be rated to withstand the full load current. Among the advantages, of the series connection, is the lower voltage class requirement of the semiconductor devices. As the voltage stress is shared among the different rectifiers, fewer devices are expected to be connected in series that leads to fewer auxiliary circuits, e.g., snubbers and voltage balancing circuits and thus a

**Table 4.1**  $N \times 3$ -phase,  $N \times 6$ -pulse level MVDC supply design.

| PM  | Generator     |                  | Rectifier          |       |
|---|---------------|------------------|--------------------|-------|
|   | No. of Phases | Voltage          | Config             | MVDC  |
| Any   | 6             | 2×3×3.7 kV       | DRU,12-p,P         | 5 kV  |
|   |               | 2×3×1.85 kV      | DRU,12-p,S         |       |
|   | 9             | 3×3×3.7 kV       | DRU,18-p,P         |       |
|   |               | 3×3×1.23 kV      | DRU,18-p,S         |       |
|   | 12            | 4×3×3.7 kV       | DRU,24-p,P         |       |
|   |               | 4×3×925 V        | DRU,24-p,S         |       |
|   | 15            | 5×3×3.7 kV       | DRU,36-p,P         |       |
|   |               | 5×3×740 V        | DRU,36-p,S         |       |
| Higher phase numbers and voltages affect rectifier arrangements |               | Similar to above | Parallel or Series | 10 kV |
|   |               |                  |                    | 15 kV |
|   |               |                  |                    | 20 kV |
|   |               |                  |                    | 25 kV |
|   |               |                  |                    | 30 kV |
|   |               |                  |                    | 35 kV |

**Table 4.2** DRU sub-module parameters considered in this study.

| Module Parameters              |   |
|--------------------------------|---|
| Rated Power ( $P_n$ )          | 9 MW  |
| Rated DC Voltage ( $V_{dc}$ )  | 5 kV  |
| Rated AC Voltage ( $V_{ac}$ )  | 3.7 kV  |
| Rated Frequency ( $f_n$ )      | 50 Hz   |
| Generator Inductance ( $L_g$ ) | $0.1 \times \frac{V_{dc}^2}{2\pi f_n S_n}$ mH |
| Cable Parameters               |   |
| Cable Inductance ( $L_c$ )     | 0.347 mH/km                                   |
| Cable Resistance ( $R_c$ )     | 0.089 $\Omega$ /km                            |
| Cable Capacitance ( $C_c$ )    | 0.307 $\mu$ F/km                              |

simpler construction of the rectifier sub-module. An additional advantage, of such rectifiers, is the flexibility they provide in choosing the voltage class of the generators and the corresponding loads (propulsion motors and pumps etc.), i.e., with proper series connection of the rectifiers, generators of lower voltage class can supply propulsion motors with higher voltage class. However, the multi-pulse series rectifiers do not provide redundancy in case of faults (generator or rectifier) and will results in loss of generation. Even bypassing the faulty rectifier module will only allow reduced MVDC distribution voltage, which is of little practical applicability.

A summary of the different MVDC PDN voltages and the required ac voltage classes of the multi-phase generators for both parallel and series connection of rectifiers is given in Table 4.1. It can be seen that various combinations provide flexibility for the ship designers to optimize the overall system and achieve voltage coordination among generators and motors.

## 4.4 Multi-Phase Multi-Pulse MVDC Supply

As discussed earlier, the power generation system consists of the PMs, generators and rectifiers for the MVDC PDNs, and each one of these plays a role to achieve the expected benefits of MVDC PDNs. In the previous section, two possible MVDC supply configurations are discussed, from which N×3-phase, N×6-pulse supply configuration is proposed as a possible high quality MVDC supply. Before starting an analysis on practical MVDC supplies, it is worth mentioning that to utilize present semiconductor technology (diodes optimized for 50/60 Hz operation) and remove gear box, medium speed ICEs (720/750 rpm, 48% efficiency, operated in DAC) are considered as PMs driving SMs for this case.

### 4.4.1 Design of DRU Sub-module

As an example, a DRU sub-module is designed that will later be used for different supplies. The ratings and the electrical parameters of this example system, around the DRU sub-module, are given in Table 4.2. The DRU sub-module is designed using ABB diodes, with blocking voltage rating of 6 kV [87]. The required blocking voltage of the device branch of the DRU is given by:

$$V_{RSM} = \sqrt{2}V_{S,rms} \times k \quad (4.3)$$

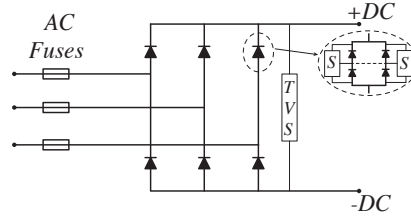


**Figure 4.2** DRU sub-module with snubbers (S) and transient voltage suppression (TVS) circuits.

Here  $V_{RSM}$  is the absolute maximum rating of the diode,  $V_{S,rms}$  is the rms value of the ac voltage and  $k$  is the safety factor normally considered as 2.2 [88]. A 3.7 kV  $V_{S,rms}$  implies that the blocking voltage required is 11.5 kV, which results in the series connection of two devices (with auxiliary circuits). Furthermore, two more devices are connected in parallel to ensure that the DRU sub-module can withstand high fault currents and this will be further elaborated with respect to  $Pt$ . In short, four (2+2) devices are connected per branch of the DRU sub-module. Schematics of the DRU sub-module are given in **Fig. 4.2**. It should be noted that the two devices connected in parallel must have minimal discrepancies in the  $v_f$  and  $r_t$ , to ensure approximately even sharing of current between the devices. The parameters of the selected diode and losses and efficiency of the DRU sub-module are given in **Table 4.3**.

In addition to the electrical characteristics of the DRU sub-module, the thermal behavior is also of interest. During the normal operation of the rectifier, losses are incurred at each diode and its junction temperature  $T_j$  should not exceed the maximum junction temperature  $T_{j,max}$  specified in the data sheet of the device. For the selected diode,  $T_{j,max} = 150^\circ\text{C}$  [87]. The  $T_j$  of the diode can be calculated, for any loading level, by knowing the heat sink temperature and the calculation of the temperature difference between the junction and the heat sink, which is given by:

$$\Delta T_{JH} = P_{loss} \times (R_{th,jc} + R_{th,ch}) \quad (4.4)$$

Here  $R_{th,jc}$  and  $R_{th,ch}$  are the thermal resistance from the junction to the case and the case to the heat sink, respectively. Considering the losses per device, given in **Table 4.3**, and  $R_{th,jc} = 42\text{ K/kW}$  and  $R_{th,ch} = 8\text{ K/kW}$  from the data sheet [87], the corresponding  $\Delta T_{JH} = 37^\circ\text{C}$ . For a heat sink temperature of  $80^\circ\text{C}$ , the resulting  $T_j = 117^\circ\text{C}$  for each diode, which is less than the maximum allowable limit of  $T_{j,max} = 150^\circ\text{C}$ . Hence, the DRU sub-module has sufficient thermal ratings to operate at full load.

**Table 4.3** Design of 9 MW 6-pulse DRU sub-module.

| Device              |            | Parameters                 | 6-Pulse Rectifier Module             |
|---------------------|------------|----------------------------|--------------------------------------|
| <i>Manufacturer</i> | ABB        | $V_{RRM}$ (V)              | 2625 @ 4 devices connected in series |
| <i>Model</i>        | 5SDDo6D600 | $I_{d,avg}$ (A)            | 300                                  |
| $V_{RRM}$ (V)       | 6000       | $I_{d,peak}$ (A)           | 910                                  |
| $I_{f,avg}$ (A)     | 662        | $I_{d,rms}$ (A)            | 520                                  |
| $I_{f,rms}$ (A)     | 1040       | <i>No. of devices</i>      | 24                                   |
| $I_{FSM}$ (A)       | 10500      | <i>Loss per device</i> (W) | 740                                  |
| $v_f$ (V)           | 1.066      | <i>Total loss</i> (W)      | 17700                                |
| $r_t$ (mΩ)          | 0.778      | <i>Efficiency</i>          | 99.5%                                |



Two cases are presented here that utilize the above designed DRU sub-module.

#### 4.4.2 Case 1: 18 MW, 5 kV, 12-Pulse Parallel Rectifier

In the first case, a 6-phase ( $2 \times 3$ -phase) SM is considered connected to two of the DRU sub-modules to make a 12-pulse parallel rectifier, as shown in Fig. 4.3(a). Here each of the generator winding set is rated at 9 MW and 3.7 kV ac, respectively. This voltage rating of the generator defines the insulation requirements of the generator. The resultant MVDC supply not only provides a high quality 5 kV distribution voltage, but also redundancy and fault tolerance in the PDN. In case of a fault of generator or rectifier, such as failure of one of the winding sets or DRU sub-module, the MVDC PDN can still operate in de-rated mode (all non-essentials are disconnected) and with a lower quality supply (as only 6-pulse rectification is available). The capacitive filter at the output of the rectifier is designed in accordance to the procedure laid forth in [82]. The ac-side input voltage and current, and dc-side voltage and current of each of the DRU sub-module are given in Fig. 4.4(a), Fig. 4.4(c) and Fig. 4.4(e), whereas, dc-side voltage and current for the complete rectifier system supplying a 18 MW load are shown in Fig. 4.5(a). The load is varied from 25% to 100% at 2.5 s and then dropped to 75% at 5 s. The only control working is the AVR of the generator which corrects the voltage.

#### 4.4.3 Case 2: 27 MW, 15 kV, 18-Pulse Series Rectifier

In the second case, a 9-phase ( $3 \times 3$ -phase) SM is considered connected to three of the DRU sub-modules to make a 18-pulse series rectifier, as shown in Fig. 4.3(b). Similar to the first case, each of the winding sets of the rectifier are rated at 9 MW and 3.7 kV ac, respectively. This configuration leads to a high quality 15 kV MVDC supply, which provides flexibility in selecting the voltage classes of the generators and the propulsion motors, e.g., in this configuration, an 11 kV propulsion motor can be supplied by the 3.7 kV generator. However, in case of any faults for generator winding sets or DRU modules, the complete supply chain is required to be taken offline to be repaired and only then it is available for load service. The ac-side input voltage and current, and dc-side voltage and current of each of the DRU sub-module are given in Fig. 4.4(b), Fig. 4.4(d) and Fig. 4.4(f), whereas, dc-side voltage and current for the complete rectifier system supplying a 27 MW load are shown in Fig. 4.5(b). The load

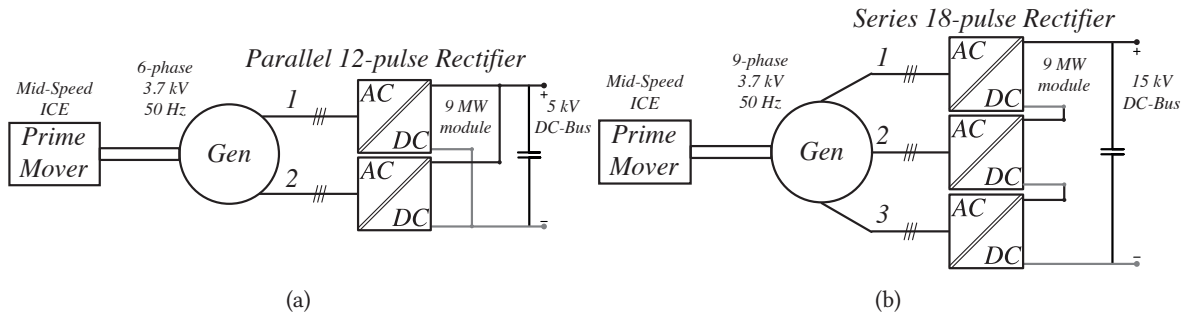


**Figure 4.3** Proposed multi-phase multi-pulse configuration. (a) Case 1: 18 MW, 5 kV, 12-pulse parallel rectifier based dc supply with 18 mF filter. (b) Case 2: 27 MW, 15 kV, 18-pulse series rectifier based dc supply with 27 mF filter.

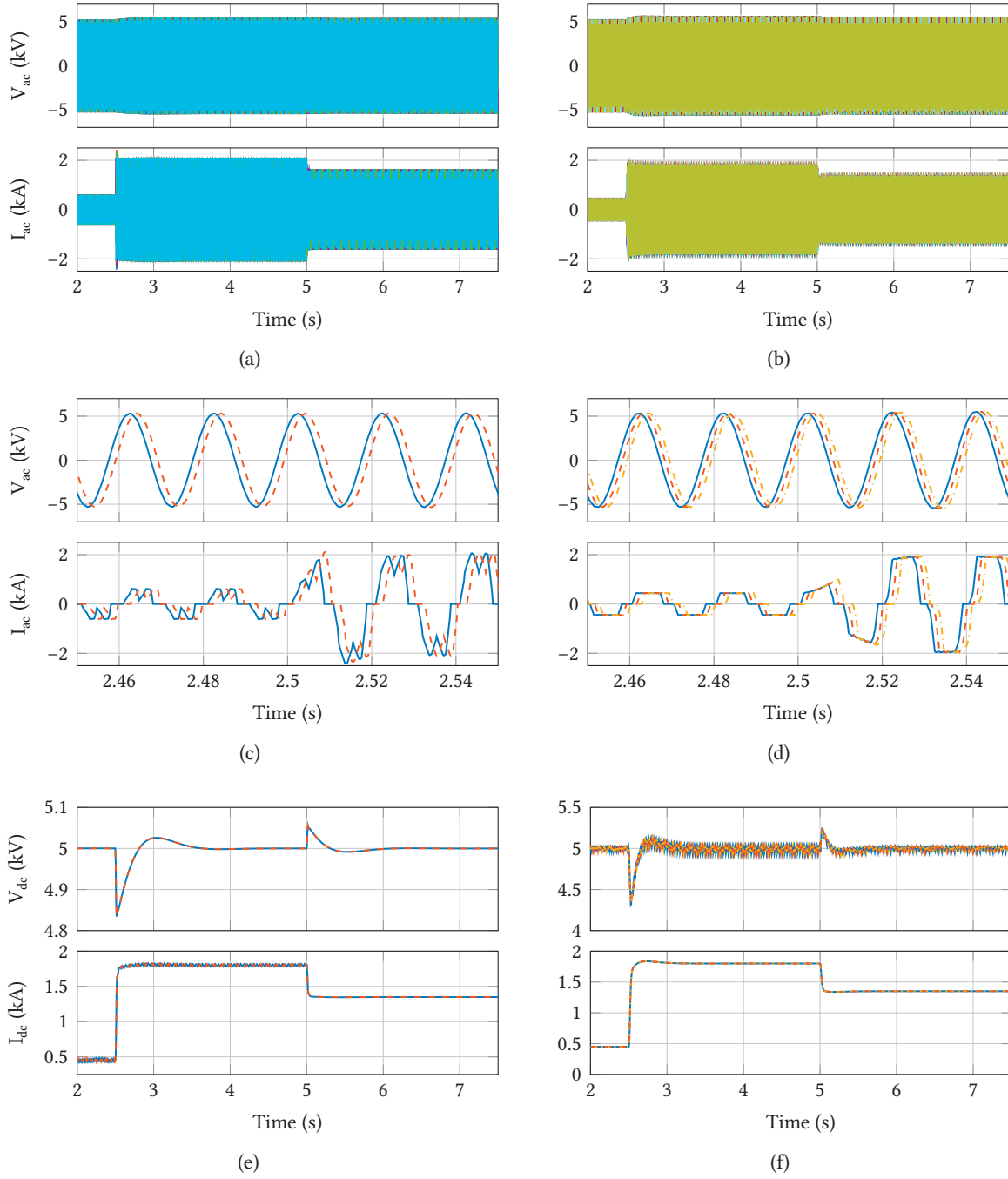


**Figure 4.4** The ac and dc-side voltage and current waveforms for DRU sub-modules for Case 1 and Case 2. (a) and (b) AC voltage and current for Case 1 and Case 2, respectively, highlighting envelope of the voltages and currents. (c) and (d) Zoom in of the load change from 25% to 100% at 2.5 s for Case 1 and Case 2, respectively (— solid for phase A of the 1<sup>st</sup> winding set, — dashed for phase A of the 2<sup>nd</sup> winding set and — dash-dotted for phase A of the 3<sup>rd</sup> winding set). (e) and (f) DC voltages and currents for Case 1 and Case 2, respectively (— solid for 1<sup>st</sup> sub-module, — dashed for 2<sup>nd</sup> sub-module and — dash-dotted for 3<sup>rd</sup> sub-module).

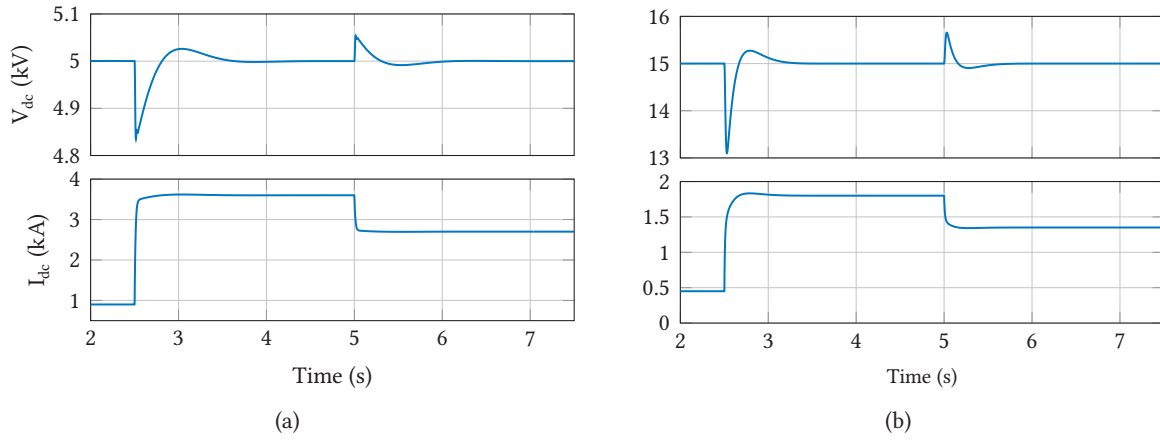


**Figure 4.5** Time domain simulations for (a) Case 1. (b) Case 2.

is varied from 25% to 100% at 2.5 s and then dropped to 75% at 5 s. The only control working is the AVR of the generator which corrects the voltage.

#### 4.4.4 Fault Withstand Capabilities

In any complex PDN, faults are unavoidable circumstances that can happen at any time and all the equipment in the PDN is required to be properly characterized for adequate fault withstand capabilities. In the state-of-the-art MVAC PDNs, all the equipment in the power chain, e.g., generators, transformers, cables, and so on, are characterized to withstand the initial fault current surge, i.e., 10 - 15 times the rated current. The ac circuit breakers only operate after 0.5 s, when the fault current is 3 - 5 times the rated current [13]. In the future MVDC PDNs, power electronic equipment will make the back bone of the power chain, but it usually has a lower over-current capability compared to the other equipment (used in MVAC PDNs). Thus they are the bottlenecks of the system short circuit current capabilities and it is of high importance, for the system designer, to know the surge current and thermal capabilities of these power electronic equipment to devise an effective protection-coordination strategy.

In line with the description of LVDC PDN fault handling presented earlier [18], the multi-phase generators, of the two MVDC supplies discussed above, are considered to have excitation removal systems that can reduce the short circuit currents in case of faults. The reduction in fault current, due to excitation removal, is very slow in comparison to the dynamics of faults, i.e., excitation time constants are usually in the order of seconds, while the fault currents rise in a matter of milliseconds [18]. Furthermore, to test the fault handling capability of the proposed rectifiers for a pole-to-pole dc fault, two scenarios are also defined. Both scenarios consider that the excitation removal system acts in 2 ms and the excitation time constant is 5 s:

- Generator with rated  $X''_g$ .
- Generator with  $1.5 \times \text{rated } X''_g$ .

The two scenarios, defined above, test the impact of the excitation removal and variations in the  $X''_g$  of the multi-phase generators on the fault energy and the resulting implications on the fault

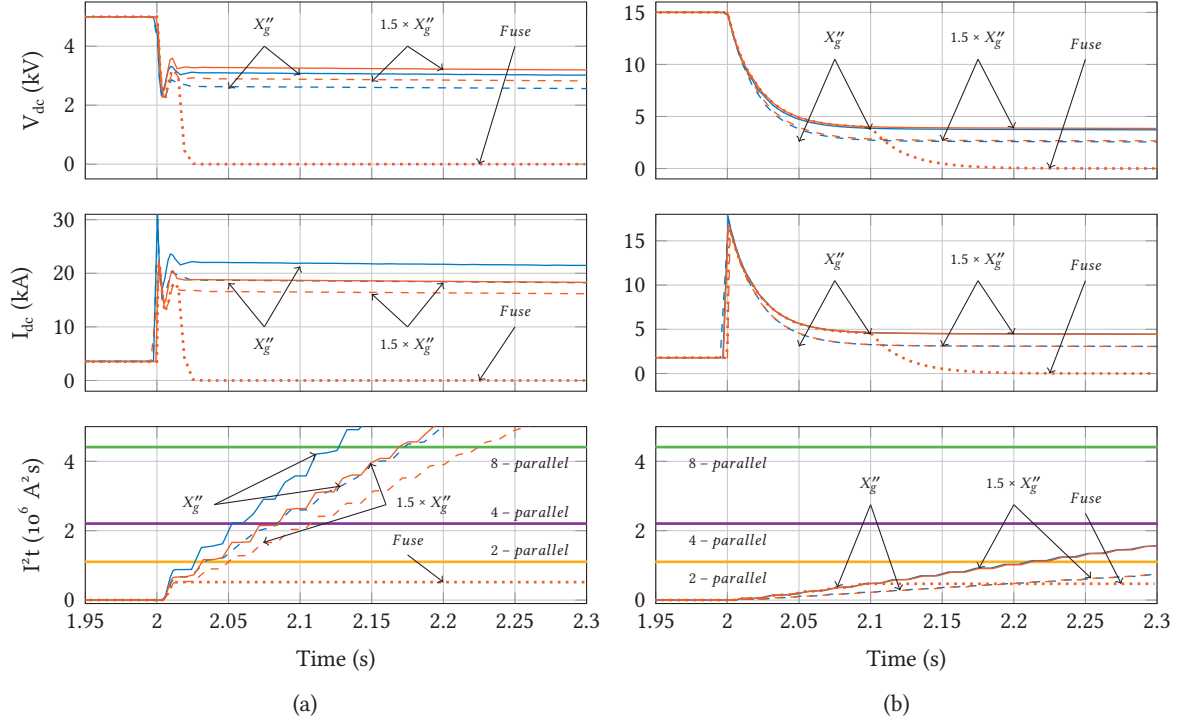


**Figure 4.6** Simulation results for dc-side pole-to-pole fault at 2 s. Considering (i) —  $\text{Rated } X''_g$ , (ii) —  $1.5 \times \text{Rated } X''_g$  with two different points for fault: at 10 m ( $L_c = 7 \mu\text{H}$ ) (solid line) and at 200 m ( $L_c = 0.14 \text{ mH}$ ) (dashed line) from the source and (iii) —  $1.5 \times \text{Rated } X''_g$  with ac-side fuses (dotted line). A comparison of fault  $I^2t$  with allowed  $I^2t$  of — 2, — 4 and — 8 parallel devices conducting. (a) Case 1. (b) Case 2.

withstand capabilities of the multi-pulse rectifiers. Another two sub-scenarios can also be introduced that analyze the impact of variation of the distribution lengths (i.e., point of fault occurrence in the PDN) on the fault energy. Considering all these variations, the 12-pulse parallel and 18-pulse series rectifiers are simulated for a fault at 2 s with a 10% fault impedance, and the corresponding dc-side voltages, currents and fault energies ( $I^2t$ ) are shown in **Fig. 4.6**. It can be observed, for both cases, that the higher  $X''_g$  reduces the fault current, but does not impact the peak or the initial surge current that is ten times the rated current. However, if the fault occurs farther from the rectifier, the impact of the distribution cable is significant and not only it reduces the initial surge current, but also the average fault current is reduced. This is due to the higher inductance and resistance in the fault path.

The surge currents for the 12-pulse parallel rectifier, for different scenarios, reach up to 31 kA as shown in **Fig. 4.6(a)**. Due to the intrinsic nature of this case, the surge current is shared among both DRU sub-modules. However, for the 18-pulse series rectifiers, for different scenarios, the initial surge of 17.6 kA as shown in **Fig. 4.6(b)**, flows through all of its sub-modules. The device selected to construct the DRU sub-module has a surge current  $I_{\text{FSM}}$  of 10.5 kA for a 10 ms half-sine pulse, as given in **Table 4.3**. As discussed earlier, parallel connection of two devices is used in constructing the sub-module, therefore, theoretically each of them can withstand the initial fault current of 21 kA for a 10 ms half-sine pulse<sup>1</sup>. In both cases, the initial fault surge current pulses of 15.5 kA and 17.6 kA (10 ms half-sine pulse) are below the surge current capability of the DRU sub-modules. Therefore,

<sup>1</sup>Due to some manufacturing differences, this might not be the actual case and the real  $I_{\text{FSM}}$  might be lower.

both these rectifiers are sufficiently sized to handle initial fault currents.

A comparison of the fault energies, for different system variations discussed above, with the thermal withstand ( $I^2t$ ) of different number of diodes connected in parallel is shown in the bottom plots of **Fig. 4.6**, for both cases. From **Fig. 4.6(a)**, it can be observed that the fault energy rises very quickly, i.e., it exceeds the combined  $I^2t$  capacity of two diodes connected in parallel in 25 ms. Even for the higher  $X''_g$  and  $L_c = 0.14$  mH, the  $I^2t$  capacity of two diodes connected in parallel is surpassed in 50 ms. Another insight from **Fig. 4.6(a)** is that an even higher number of parallel connected diodes (eight diodes) is not enough to withstand the fault energy and external means of protecting the rectifier must be employed. The fault energy rises rather slow for *Case 2*, compared to *Case 1*, as can be observed from **Fig. 4.6(b)**. Even though the fault energy rises slowly, it still surpasses the  $I^2t$  of 2 diode in parallel in  $\approx 200$  ms. Complementary to the *Case 1*, external means must be employed to protect this rectifier. This is necessary because connection of several diodes in parallel might not be sufficient or practically feasible, and the reduction in fault current, from removal of excitation, is only possible after several seconds which is too long for the rectifiers to withstand the fault energy.

As MVDC breakers are not available to clear faults, a rather inexpensive way to protect these rectifiers would be to consider fast fuses (able to melt in a few milliseconds) on the ac-side of the rectifiers, which will limit the fault current and the resultant energy through the diodes. For both high and low fault currents, the fuses must act fast enough to protect the rectifiers in *Case 1* and *Case 2*, respectively. In *Case 1*, for rated  $X''_g$  and  $L_c = 7 \mu\text{H}$ , the average fault current is 21.5 kA, whereas, for  $1.5 \times \text{rated } X''_g$  and  $L_c = 0.14$  mH, the average fault current is 16.6 kA. For both scenarios, the fault current is high and the fuses must melt with a few milliseconds to provide effective protection. In *Case 2*, the average fault currents for rated  $X''_g$  and  $1.5 \times \text{rated } X''_g$ , irrespective of  $L_c$ , are 5 kA and 3 kA, respectively. For both these scenarios, the average fault current is very close to the full load rated current of 1.8 kA, therefore, in this case the fuses must be able to melt fast enough to clear the fault currents.

In summary, the fuses selected for protecting these rectifiers must withstand the rated current and voltage, for normal operations, but must melt fast enough to remove fault currents and the associated fault energy  $I^2t$ , i.e.,  $I^2t_{\text{fuse}} < I^2t_{\text{diode}}$ . The impact of fuses on currents and voltages, for both cases, can be seen in **Fig. 4.6**. As this is a special application, a possible series and parallel connection of fuses (with no more than 10% mismatch among fuses) is expected to properly protect the rectifiers and special sourcing might be required from the manufactures [89], [90].

## 4.5 Summary

In this chapter, possible MVDC supply configurations are discussed and multi-phase multi-pulse configuration is chosen as it ensures high quality MVDC supply. The two possible arrangements of the multi-phase multi-pulse configuration are the parallel and series connection of rectifiers. Multi-pulse parallel rectifiers increase the redundancy and fault tolerance of the system, while the multi-pulse series rectifiers brings flexibility in selection of voltage classes of generators and motors in the system. In short, multi-phase multi-pulse supplies are simple and provide degrees of freedom to design appropriate supply depending on the application.

The concept of multi-phase multi-pulse supplies is explored further by presentation of two possible MVDC supplies. To ensure fuel efficiency, while utilizing present semiconductor technology, medium

speed ICEs (operated in DAC mode) are considered as the prime movers that are driving multi-phase SMs. The first MVDC supply considers a  $2\times 3$ -phase generator interfaced with a 12-pulse parallel rectifier for a 18 MW, 5 kV MVDC PDN, while, the second MVDC supply considers a  $3\times 3$ -phase generator interfaced with a 18-pulse series rectifier for a 27 MW, 15 kV MVDC PDN. A DRU sub-module is designed for these multi-pulse rectifiers, which can withstand the thermal load of the normal operation and also the initial fault currents for dc-side faults. However, if the faults are not cleared within milliseconds, the diodes in the rectifiers will fail, due to high fault energy, and will need to be replaced. Fast fuses, placed on the ac-side, can be used to protect these rectifiers and stop the fault currents from propagating in the PDN.

The selection of either multi-pulse parallel or series rectifiers depends on the system designers, the requirements and the function of the vessels and the availability of appropriate equipment.

# 5

## Source - Load Interactions in the MVDC Power Distribution Network

*This chapter presents the dynamic stability assessment methodology and also the small signal modeling of the different source and load converters. Impedance modeling is used to represent the dynamic behavior of the rectifiers and the inverter drives, taking into account their control strategies. The impact of variations of the passive elements, e.g., filter capacitors and cable lengths, in a two-port network, and the dynamic interactions between the different source converters and load are analyzed using Nyquist Criterion. Main findings are verified by the time-domain simulations.*

### 5.1 Introduction

As discussed in the introduction, the thesis has two parts. The first part of the thesis looked into a range of topics related to the physical equipment to be deployed in the MVDC PDNs for the ship on-board PDNs. It was seen that in order to achieve a full MVDC PDN, new technologies for voltage coordination and protection need to be developed; however, in the beginning the present commercial technologies are also expected to be deployed. Therefore, the role of these technologies, applicable in the main power chain, has been critically analyzed. The different opportunities and challenges arising from the evolution of the ship on-board PDN are also highlighted by presenting two real-world examples, namely LNG Tanker and Drill Ship. Additionally, high quality MVDC supplies for the marine MVDC PDNs, utilizing the readily accessible technologies, are presented and their thermal and fault behaviors are analyzed.

The second part of the thesis looks into the stability of the MVDC PDN. As discussed in *Chapter 2*, most of the present technologies are expected to be used in the future MVDC PDNs. Therefore, a study covering the impact of the dynamic behavior of the power electronic converters on the stability of the future MVDC PDN is required. The load converters, i.e., motor drives in the MVDC PDN, tightly regulate the speed of the machines and, consequently, their input power. This leads to a constant power load (CPL) behavior at the input terminals of the loads, which implies that any increase/decrease in the terminal voltage will result in decrease/increase in the current that leads to negative incremental impedance  $dv/di < 0$ . The negative impedance characteristics of the CPLs cause the stability challenges [91]. Over the years, efforts have been made to discuss and propose possible solutions for the stability related issues [77], [92]–[99]. In these studies, the dc-side dynamics of the power electronic converters have been modeled as impedances in [92]–[94]. It can be seen from these works that small signal modeling is sufficient to linearize the power electronic systems. Moreover, to assess the relative stability of the dc PDN, impedance stability criteria can be applied by using Nyquist



plots or Bode diagrams [92]–[94]. In [95], this approach is extended to multi-terminal dc PDNs. Apart from the assessment of the dc PDN stability, different control strategies for the dc distribution voltage, e.g., linearization via state feedback (LSF), backstepping, linear quadratic gaussian (LQG) and synergetic control, have been proposed and compared for an MVDC PDN with buck converters connected to CPLs [77], [96]–[99]. Much of the literature targets the CPL behavior of the loads and addresses the issues arising from it but, in [73], a comparison is presented between passive and active rectifiers based on their response times and voltage control capabilities, when supplying pulsed loads.

In this chapter, firstly a discussion is provided on few of the stability criteria presented in literature for stability analysis. Secondly, a stability assessment is carried out for a possible MVDC PDN for a large vessel considering available industrial technologies and realistic operating conditions. To analyze the dynamic interactions between the different source and load converters, the behavior of these converters is modeled as impedances and admittances at selected operating points for determining the potential unstable conditions, which can adversely impact the MVDC PDN design and operation [20], [93], [94]. The dynamic assessment presented here looks into the contributions of the generator inductances, dc-bus capacitors, cable effects and source and load control strategies. This will provide thorough understanding of the behavior of these elements and their influence on the dynamics of the future MVDC PDN. Additionally, design figures of merit from Nyquist plots are also shown, which highlight relevant stability information that can be used for designing the future MVDC PDN.

## 5.2 Overview of Stability Criteria

In this section, a brief discussion is provided on few of the different stability criteria proposed for analyzing dc PDNs. To describe these criteria, an example is shown in **Fig. 5.1**, where two independent stable systems can be interconnected to build a new system. It can be assumed that these two systems are stable and have gains (transfer functions) defined as:

$$\begin{aligned} T_A(s) &= \frac{V_{out,A}(s)}{I_{in,A}(s)} \\ T_B(s) &= \frac{I_{out,B}(s)}{V_{in,B}(s)} \end{aligned} \quad (5.1)$$

Furthermore, from the interconnection point of view, the output and input characteristics of these two systems are represented as  $Z_{out,A}(s)$  and  $Y_{in,B}(s)$ , respectively in reference to **Fig. 5.1**. The

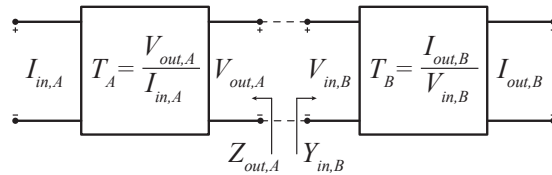


**Figure 5.1** Block representation of interconnection of two independent systems. These two systems are obtained using small signal modeling techniques.



interconnection of these two systems yields a new gain which can be defined as:

$$\begin{aligned} T_{AB}(s) &= \frac{I_{out,B}(s)}{I_{in,A}(s)} = T_A(s)T_B(s) \frac{Y_{in,B}^{-1}(s)}{Y_{in,B}^{-1}(s) + Z_{out,A}(s)} \\ &= T_A(s)T_B(s) \frac{1}{1 + Z_{out,A}(s)Y_{in,B}(s)} \end{aligned} \quad (5.2)$$

From (5.2), it can be seen that the product of  $Z_{out,A}(s)Y_{in,B}(s)$ , also called the *minor loop gain*, can be used to determine the system stability as  $T_A$  and  $T_B$  are already stable. A necessary and sufficient condition can be specified by the application of Nyquist Criterion on the product  $Z_{out,A}(s)Y_{in,B}(s)$ , i.e., the system is stable if and only if the Nyquist contour of  $Z_{out,A}(s)Y_{in,B}(s)$  does not encircle the critical point of  $(-1,0)$  [93]. Additionally, this ratio also maps the dynamic interactions of these two independent systems.

Considering the above described concept, over time different stability criteria have been proposed to determine the stability of the system. In these criteria the characteristic functions  $Z_{out,A}(s)$  and  $Y_{in,B}(s)$  are considered as impedance and admittance, respectively. Most notable among these criteria are: (i) *Middlebrook criterion*, (ii) *gain margin and phase margin (GM/PM) criterion*, (iii) *opposing argument criterion* and (iv) *energy source analysis consortium (ESAC) criterion*. A graphical summary of the stability boundaries specified by these criteria is shown in **Fig. 5.2**.

### Middlebrook Criterion

The oldest proposed stability criterion aimed to determine the stability of a closed-loop controlled switching converter with an input filter [93], [100]. This criterion not only addresses the system stability, but also helps in determining the design rules to ensure system stability. The stability condition of this criterion can be expressed as:

$$\|Z_{out,A}(s)Y_{in,B}(s)\| \ll 1 \quad (5.3)$$

(5.3) imposes a sufficient condition of small gain on the *minor loop gain*, which ensures there is never an encirclement of the critical point  $(-1,0)$ . This can also be observed from **Fig. 5.2** where an arbitrary

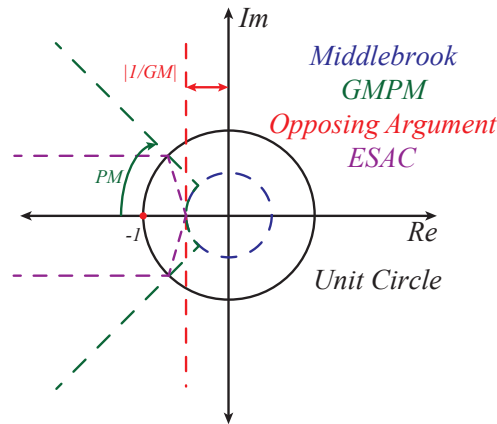


**Figure 5.2** Different stability criteria and their boundaries.

small gain boundary is defined as a **blue dashed circle**. As the criterion only considers the magnitude of the *minor loop gain*, it is very simple to apply on different practical systems, however, it imposes very conservative constraints on the design parameters and this may result in large component values [93], which might not be practically feasible.

### GMPM Criterion

To counter the conservativeness of the Middlebrook criterion, another criterion was proposed in [101] and shown in **Fig. 5.2** as **green dashed arc and lines**. This criterion is called *gain margin and phase margin* because it defines limits for both gain and phase of the *minor loop gain* to ensure stability of an interconnected system. The two limits are mathematically expressed as:

$$\|Z_{out,A}(s)Y_{in,B}(s)\| \leq \frac{1}{GM} \text{ and } |\angle Z_{out,A}(s) + \angle Y_{in,B}(s)| \leq 180^\circ - PM \quad (5.4)$$

Here the magnitude and phase angle of both  $Z_{out,A}$  and  $Y_{in,B}$  must be known. The limit on gain margin is specified as 6 dB (0.5 for polar plots) and all the *minor loop gains* below this limit have no constraints on the phase margin, but for any *minor loop gain* above this limit, it must have a phase margin of  $60^\circ$ . These limits are defined based on good design practice. The GMPM criterion is employed, in [93], to design load impedances to ensure system stability.

### Opposing Argument Criterion

In order to apply the GMPM criterion to systems with multiple loads, efforts were made to use individual load admittances rather than to lump all the admittances in  $Y_{in,B}$ . This led to the proposal of scaling each load admittance according to its participation in the total load consumption [102]. In some cases, it was shown that this technique may fail when the loads are not proportional to each other [93]. A solution of this problem was provided in terms of *opposing argument criterion* in [103], where a new stability limit is defined as  $-1/GM$  (shown in **Fig. 5.2** as **vertical dashed red line**). This limit defines the forbidden region and also ensures that there is no encirclement of the critical point  $(-1,0)$ .

For the systems with  $n$  multiple loads, admittance of each load can be defined as  $Y_{in,B}^i$ . The limit on each resultant *minor loop gain* is given as [103]:

$$\Re(Z_{out,A}(s)Y_{in,B}^i(s)) \leq -\frac{1}{GM} \frac{P_{in}^i}{P_{total}} \quad (5.5)$$

Here  $i = 1, 2, \dots, n$ , the limit  $-1/GM$  is scaled with respect to its participation in the total load consumption given by  $P_{in}^i/P_{total}$ . Similar to GMPM, there is no limit on the phase of the *minor loop gain* if the condition given in (5.5) is fulfilled, otherwise the phase must be equal to:

$$\phi^i = \arcsin\left(\frac{1}{GM} Z_{out,A}(s)Y_{in,B}^i(s) \frac{P_{in}^i}{P_{total}}\right) \quad (5.6)$$

Here again, it is important to know the magnitude and phase angle of  $Z_{out,A}$  and each  $Y_{in,B}^i$ .

### ESAC Criterion

The ESAC criterion, proposed in [94], is similar to both GMPM criterion and *opposing argument criterion* as it can impose the required stability limits on the different subsystems, but these limits are less conservative compared to the former two criteria [93]. This can also be observed from **Fig. 5.2**, as the boundary is defined by **purple dashed line** and the forbidden area within this boundary is the least compared to all the others. Additionally, most of the stability criteria define a sufficient condition for system stability and this condition may be fulfilled or violated for different grouping of the components in the systems. However, the ESAC criterion also tries to make the stability assessment independent of the grouping of the components, as each component is modeled independently, and different demonstrative examples can be found in [94]. Another advantage of ESAC is the possibility to construct stability regions for component variations. Despite these advantages, the ESAC criterion is numerically very complex and requires a specially built toolbox to utilize for any stability related studies [104].

### 5.3 Small Signal Modeling of the MVDC PDN

From the discussion in *Chapter 3*, it was seen that marine PDNs are physically concentrated and isolated networks, which are tailored to the functionality of the vessel. **Fig. 5.3** illustrates a simplified MVDC PDN for a large vessel, with power requirements reaching several MWs. In this PDN, there are four diesel generator sets connected to their individual rectifiers, each rectifier having its own filter and disconnector, that are supplying an MVDC PDN. The PDN is supplying four inverter drives also having their individual disconnector and input filter. As the marine PDNs are expected to be

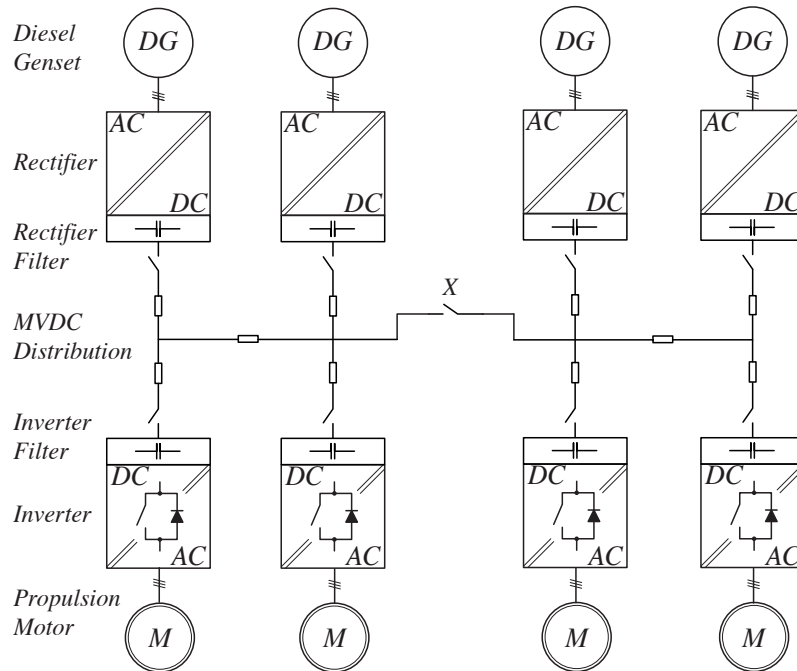


**Figure 5.3** Simplified ship on-board MVDC PDN.

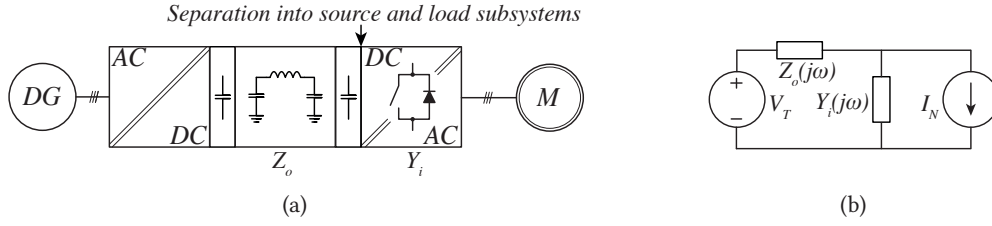


**Figure 5.4** (a) Two-port MVDC PDN (SISO system). The system is partitioned at the arrow in accordance with stability definition and the conditions for measuring impedance/admittance [92], [100]. (b) Linearized equivalent model of a two-port MVDC PDN for the stability analysis.

redundant, switch  $X$  is present to interconnect them in case of failure of the MVDC supplies on either side.

As mentioned earlier, an analysis is carried out regarding the dynamic interactions of the source and load subsystems and their dependency on the generator and filter inductances, the filter capacitors, the source side converter control strategies and the cable inductances and capacitances on the possible resonances in the system and their implications on the system stability. In order to utilize impedance stability criteria, the complex PDN of **Fig. 5.3** can be simplified by using basic linear properties, e.g., superposition principle and considering similar loading cycles for both the sources and loads [93], [94]. The simplified PDN, with equivalent sources and loads, is shown in **Fig. 5.4(a)**. Generalized figures of merit can be extracted from this simplified two-port PDN for different sources and loads.

The two-port PDN, shown in **Fig. 5.4(a)**, can be further grouped into two different subsystems, i.e., generator, rectifier, filter, distribution cable (represented as equivalent  $\pi$  - section model), input capacitor as source, while inverter and motor as load. This partition point is also illustrated in **Fig. 5.4(a)**. The linearized representation of **Fig. 5.4(a)** is shown in **Fig. 5.4(b)** [92], [94], [100], which is consistent with the description of *section 5.2* and **Fig. 5.1**. The source side characteristics are modeled as Thevenin equivalent impedance because it supports the distribution voltage, whereas, the

**Table 5.1** System parameters used for this study and parameter variations and their impact on inductances in the system.

| System Parameters        |                                       | Induction Motor Ratings        |                           | Cable Parameters            |                    |
|--------------------------|---------------------------------------|--------------------------------|---------------------------|-----------------------------|--------------------|
| Rated Apparent Power     | 7 MVA                                 | Rated Power                    | 6.5 MW                    | Cable Inductance            | 0.347 mH/km        |
| Rated Direct Voltage     | 5 kV                                  | Rated Voltage                  | 3.05 kV                   | Cable Resistance            | 0.089 $\Omega$ /km |
| Rated Frequency          | 50 Hz                                 | Rated Current                  | 1.4 kA                    | Cable Capacitance           | 0.307 $\mu$ F/km   |
| Phase Reactor Inductance | $0.1 \frac{V_{dc,n}^2}{2\pi f_g S_n}$ | Rated Frequency                | 19 Hz                     |                             |                    |
| Phase Reactor Resistance | 3 m $\Omega$                          | Rated Speed                    | 376 rpm                   |                             |                    |
| Switching Frequency      | 250 Hz                                | Power Factor                   | 0.92                      |                             |                    |
| Parametric Variations    |                                       | Impact on different quantities |                           |                             |                    |
| Generator Frequency      | 50 Hz - 100 Hz                        | $L_{cable}$                    | 6.94 $\mu$ H @ 10 m       | 0.694 mH @ 1 km             |                    |
| System Load              | 25% - 100%                            | $L_g$                          | 1.137 mH @ 50 Hz          | 0.568 mH @ 100 Hz           |                    |
| Rectifier Filter         | 1 mF - 10 mF                          | $L_f$ (Valid only for TRU)     |                           |                             |                    |
| Cable Length             | 10 m - 1 km                           | @ 50 Hz                        | 1.53 mH, $C_{rec} = 1$ mF | 0.115 mH, $C_{rec} = 10$ mF |                    |
| Inverter Filter          | 1 mF - 10 mF                          | @ 100 Hz                       | 0.25 mH, $C_{rec} = 1$ mF | 0.044 mH, $C_{rec} = 10$ mF |                    |

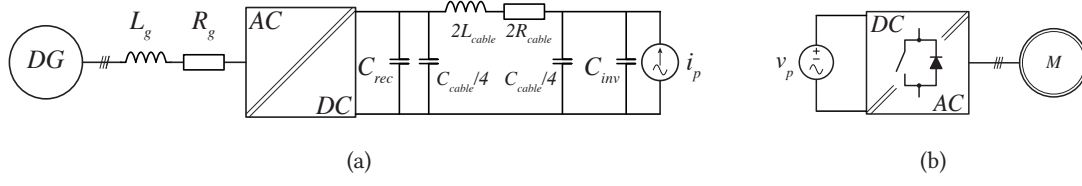


**Figure 5.5** (a) Source impedance measurement arrangement. (b) Load admittance measurement arrangement.

load side is modeled as a Norton equivalent admittance because a constant current (proportional to power) is being injected into the load. The Norton equivalent admittance covers the CPL behavior of the inverter drives. The source voltage  $V_T$ , the load current  $I_N$ , the output impedance of the source  $Z_o$  and the input load admittance  $Y_i$  must all be stable, i.e., there poles must be in left half plane (LHP). The *minor loop gain* of system shown in **Fig. 5.4(b)** is:

$$H_{mlg}(j\omega) = Z_o(j\omega)Y_i(j\omega) \quad (5.7)$$

Here  $s$  is substituted with  $j\omega$ . This is later used for constructing the Nyquist trajectories to assess the stability of the system under consideration. The parameters considered for this study are given in Table 5.1.

## 5.4 Source/Load Impedance/Admittance Measurement

To utilize (5.7) for dynamic assessment of the MVDC PDN shown in **Fig. 5.4(a)**, the source and load subsystems must be represented as impedances and admittances. In this study, three different source side converters, e.g., DRU, TRU and ARU are considered for their interactions with inverter drives for variations in the generator frequencies, filter sizes, distribution cable lengths and the different loading conditions. The range of variations in these system elements is listed in Table 5.1. In order to measure the impedances and admittances of the source and load subsystems, current and voltage perturbations, as multitone signals, are injected at the terminals and the resulting voltages and currents are measured and are illustrated in **Fig. 5.5**. The ratios of the measured quantities and the injected perturbations give the impedances and admittances, respectively. The injected perturbations are within a frequency window of 0.1 - 10k Hz, which is considered to be sufficient to capture all the expected resonances due to control or passive elements in the PDN.

### 5.4.1 Load Admittance - Propulsion Drive

The load under consideration is the inverter drive which is feeding, in this chapter, an induction motor. The parameters of the induction motor considered here are given in Table 5.1. The high performance drive is using FOC for controlling the machine speed and torque. The schematics of an indirect FOC are shown in **Fig. 5.6**. The inner current control is carried in  $dq$ -frame and the PI controllers are tuned using *magnitude optimum*, while the speed control is tuned using *symmetric optimum*. The PI controller parameters for both current and speed control are given in Table 5.2.

The load admittance is measured for two operating points, i.e., full load, which implies 100% of the rated speed and rated torque, and light load, which implies 100% of the rated speed and 25% rated

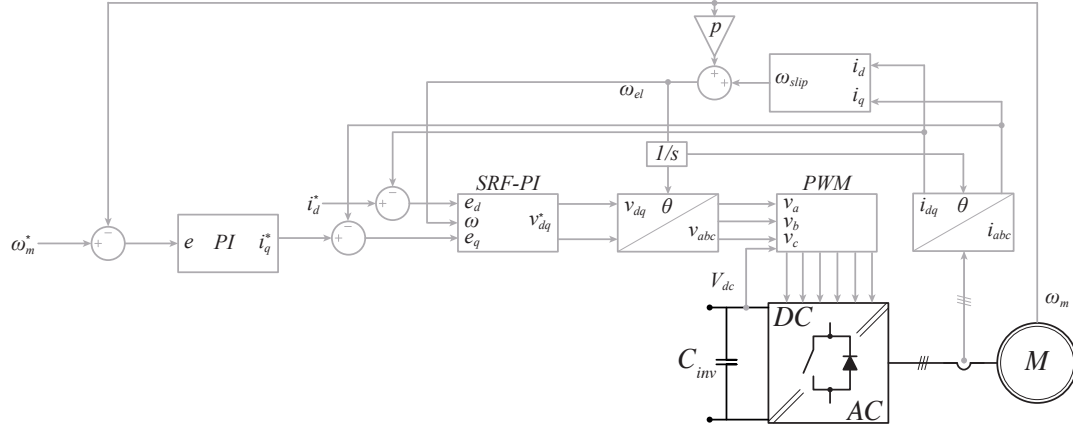


Figure 5.6 Vector controlled of inverter drive.

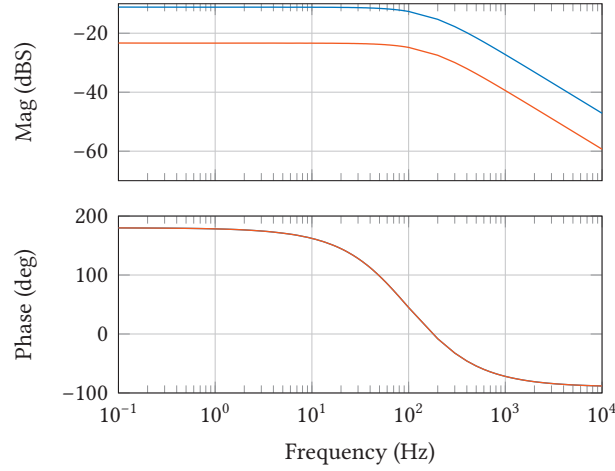


Figure 5.7 Load admittance in a frequency window of 0.1 - 10k Hz for — 100% load and — 25% load.

torque, and it is shown in **Fig. 5.7**. These admittances display a CPL behavior upto the current control bandwidth of 100 Hz and then become inductive showing the internal motor characteristics. The low current control bandwidth shows the limitations on the switching frequency of the MV inverters.

#### 5.4.2 Source Impedance - Diode Rectifier Unit

DRU is the first rectifier under consideration and its schematics and AVR control scheme are given in **Fig. 5.8**. The dc-link voltage is maintained using the AVR of the generator. The PI controller corrects the terminal voltage of the generator in accordance to the feedback from the terminals of the DRU. The response time of the control loop is dependent on the time constant  $T_f$  of the generator field winding. The PI parameters are given in Table 5.2. The output of the DRU is filtered by a capacitive filter  $C_{rec}$ . The impedances of the DRU are measured for different parametric variations listed in Table 5.1 and are shown in **Fig. 5.9**. As the AVR control bandwidth is in the range of 1 s, all the resonances are caused by the inductances and capacitances present in the circuit. The low frequency resonance, shaded blue in **Fig. 5.9**, is caused by the ac-side generator inductance and the filter capacitors at the

**Table 5.2** Control parameters for source and load subsystems.

|                 |   |                 |   |              |           |              |            |
|-----------------|---|-----------------|---|--------------|-----------|--------------|------------|
| $K_{ps,FOC}$    | 437500 kgm <sup>2</sup> /s <sup>2</sup> | $K_{is,FOC}$    | 13671875 kgm <sup>2</sup> /s <sup>3</sup> | $K_{pi,FOC}$ | 0.338 V/A | $K_{ii,FOC}$ | 3.456 Vs/A |
| $K_{p,DRU}$     | 1 A/V                                   | $K_{i,DRU}$     | 10 As/V                                   | $K_{p,TRU}$  | 0.05 A/V  | $K_{i,TRU}$  | 10 As/V    |
| $K_{pv,ARU}$    | 0.044 A/V                               | $K_{iv,ARU}$    | 0.967 As/V                                | $K_{pi,ARU}$ | 0.5 V/A   | $K_{ii,ARU}$ | 4e-4 Vs/A  |
| $K_{p,pll,ARU}$ | 0.044 /V                                | $K_{i,pll,ARU}$ | 987 s/V                                   |              |           |              |            |

output of the rectifier and the input of the inverter drive. The cable inductance does not have an impact, as it is quite small and is only playing a role at higher frequencies. The natural resonance frequency can be calculated by:

$$f_{LC} = \frac{1}{2\pi\sqrt{2L_g C_1}} \quad (5.8)$$

Here  $C_1 = C_{rec} + C_{inv}$ . It must be noted that  $C_{cable}$  is neglected as its value is very low in comparison to  $C_{rec}$  or  $C_{inv}$ . The calculation of natural resonance frequency with (5.8) is only valid for the cases when  $L_g \ll L_{cable}$ . In cases where  $L_g \approx L_{cable}$ , the impact of  $L_{cable}$  on the low frequency resonance cannot be neglected and the determination of the low frequency resonance is no longer straight forward. The second resonance occurs at higher frequency and is shaded red in **Fig. 5.9**. This resonance is caused by the cable inductance and the filter capacitances on the rectifier and inverter sides, whereas, the much larger generator inductance can be considered as open circuit in this case. The high frequency

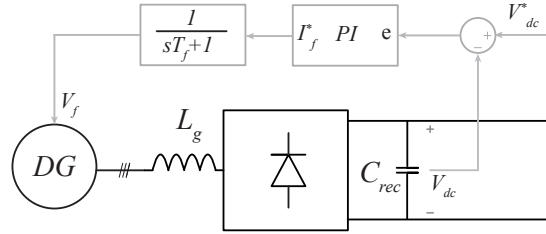


**Figure 5.8** Schematics of DRU and AVR control scheme to maintain dc-link voltage with  $T_f (\approx 1 \text{ s})$  being the time constant of the generator's field winding.

**Table 5.3** Natural resonance frequencies for DRU using (5.8) and (5.9).

| System Configurations     |                           |      | $f_g = 50 \text{ Hz}$ |           | $f_g = 100 \text{ Hz}$ |           |
|---------------------------|---------------------------|------|-----------------------|-----------|------------------------|-----------|
|                           |                           |      | $f_{LC}$              | $f_{CLC}$ | $f_{LC}$               | $f_{CLC}$ |
| $C_{rec} = 1 \text{ mF}$  | $C_{inv} = 1 \text{ mF}$  | 10 m | 75 Hz                 | 2701 Hz   | 106 Hz                 | 2701 Hz   |
| $C_{rec} = 1 \text{ mF}$  | $C_{inv} = 10 \text{ mF}$ | 10 m | 32 Hz                 | 2003 Hz   | 45 Hz                  | 2003 Hz   |
| $C_{rec} = 10 \text{ mF}$ | $C_{inv} = 1 \text{ mF}$  | 10 m | 32 Hz                 | 2003 Hz   | 45 Hz                  | 2003 Hz   |
| $C_{rec} = 10 \text{ mF}$ | $C_{inv} = 10 \text{ mF}$ | 10 m | 24 Hz                 | 854.5 Hz  | 34 Hz                  | 854.5 Hz  |
| $C_{rec} = 1 \text{ mF}$  | $C_{inv} = 1 \text{ mF}$  | 1 km | 75 Hz                 | 270.1 Hz  | 106 Hz                 | 270.1 Hz  |
| $C_{rec} = 1 \text{ mF}$  | $C_{inv} = 10 \text{ mF}$ | 1 km | 32 Hz                 | 200.3 Hz  | 45 Hz                  | 200.3 Hz  |
| $C_{rec} = 10 \text{ mF}$ | $C_{inv} = 1 \text{ mF}$  | 1 km | 32 Hz                 | 200.3 Hz  | 45 Hz                  | 200.3 Hz  |
| $C_{rec} = 10 \text{ mF}$ | $C_{inv} = 10 \text{ mF}$ | 1 km | 24 Hz                 | 85.4 Hz   | 34 Hz                  | 85.4 Hz   |

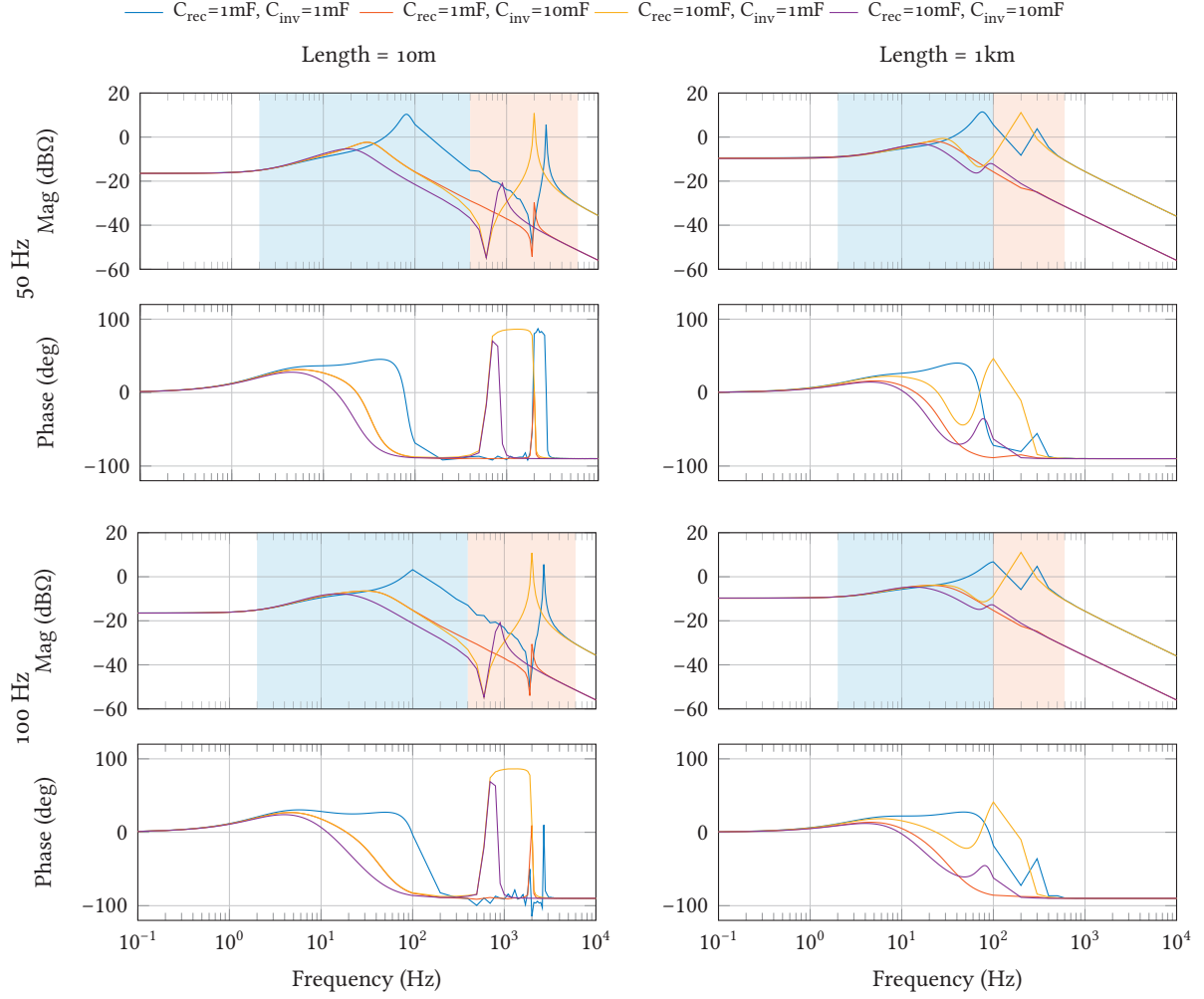


**Figure 5.9** DRU impedances in a frequency window of 0.1 - 10k Hz for different filtering efforts. The low frequency resonances, caused by the generator inductance and filter capacitors, are shaded blue. Whereas, the high frequency resonances, caused by cable inductance and filter capacitors, are shaded red.

resonance is given as:

$$f_{CLC} = \frac{1}{2\pi} \sqrt{\frac{1}{L_{cable}} \left( \frac{1}{C_{rec}} + \frac{1}{C_{inv}} \right)} \quad (5.9)$$

As the value of  $L_g$  changes with variations in generator frequency, it impacts the frequency at which the low frequency resonance occurs. Additionally, changes in the distribution cable length cause the cable inductance to have a higher or lower value resulting in a shift of the high frequency resonances towards lower or higher frequencies. These changes in the values  $L_g$  and  $L_{cable}$  are illustrated in Fig. 5.9 and Table 5.1. The natural resonance frequencies for the parametric variations of Table 5.1 for the DRU case are given in Table 5.3.



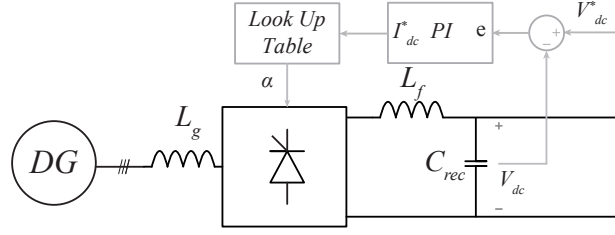


**Figure 5.10** Schematics of TRU and modified inverse cosine control scheme to maintain dc-link voltage.

### 5.4.3 Source Impedance - Thyristor Rectifier Unit

The second case under consideration here is TRU, with the schematics given in **Fig. 5.10**. As discussed earlier, TRUs can be controlled using the thyristor firing angle  $\alpha$ , and this ability can be used to maintain the voltage of the dc distribution. Here a modified inverse cosine control strategy ([52]) is employed that takes voltage feedback from the filter capacitor and produces reference for dc-side current, which then produces the required firing angle  $\alpha$  to maintain the dc-side voltage. The schematics of this control are also given in **Fig. 5.10** and the PI parameters in Table 5.2. Due to higher ripple and switching harmonics, an LC filter is used at the output of the TRU. The inductance, in the LC filter, can be calculated for a constant cut-off frequency and is calculated as:

$$L_f = \frac{V_{ripple}}{12\pi f_g I_{DCmin}} \quad (5.10)$$

Here  $V_{ripple}$  is the ripple voltage and  $I_{DCmin}$  is the minimum current dc current (10% of rated current) in the load. The TRU impedances, for the parametric variations listed in Table 5.1, are shown in **Fig. 5.11**. Different values of  $L_f$  are also given in Table 5.1 for the variations in  $f_g$  and  $C_{rec}$ . The TRU control has a very small bandwidth and is acting at very low frequencies, i.e., upto 2 Hz. All the resonances, similar to DRU case, are caused by the inductances and capacitances in the system, and can be observed from **Fig. 5.11**. The low frequency resonance is now also affected by  $L_f$ , therefore, (5.8) can now be updated to show the impact of  $L_f$ . The new expression is:

$$f_{LC} = \frac{1}{2\pi\sqrt{L_1 C_1}} \quad (5.11)$$

Here  $L_1 = 2L_g + L_f$  and  $C_1 = C_{rec} + C_{inv}$ . The higher frequency resonance, similar to DRU case, is due to the cable inductances and rectifier and inverter capacitances and is determined using (5.9).

### 5.4.4 Source Impedance - Active Rectifier Unit

The third type of rectifier, considered here, is the ARU, with its schematics given in **Fig. 5.12**. A cascaded control scheme is used to control the ac-side currents and the dc-side voltage. The voltage control is based on DVC and its detailed description can be found in [105]. The schematics of DVC, current control and PLL are also shown in **Fig. 5.12**. The voltage and current loops are tuned using *symmetric optimum* and *magnitude optimum*, respectively and the PI gains are given in Table 5.2. Similar to DRU case, only a capacitive filter is required here. The ARU impedances for the parametric variations listed in Table 5.1 are illustrated in **Fig. 5.13**.

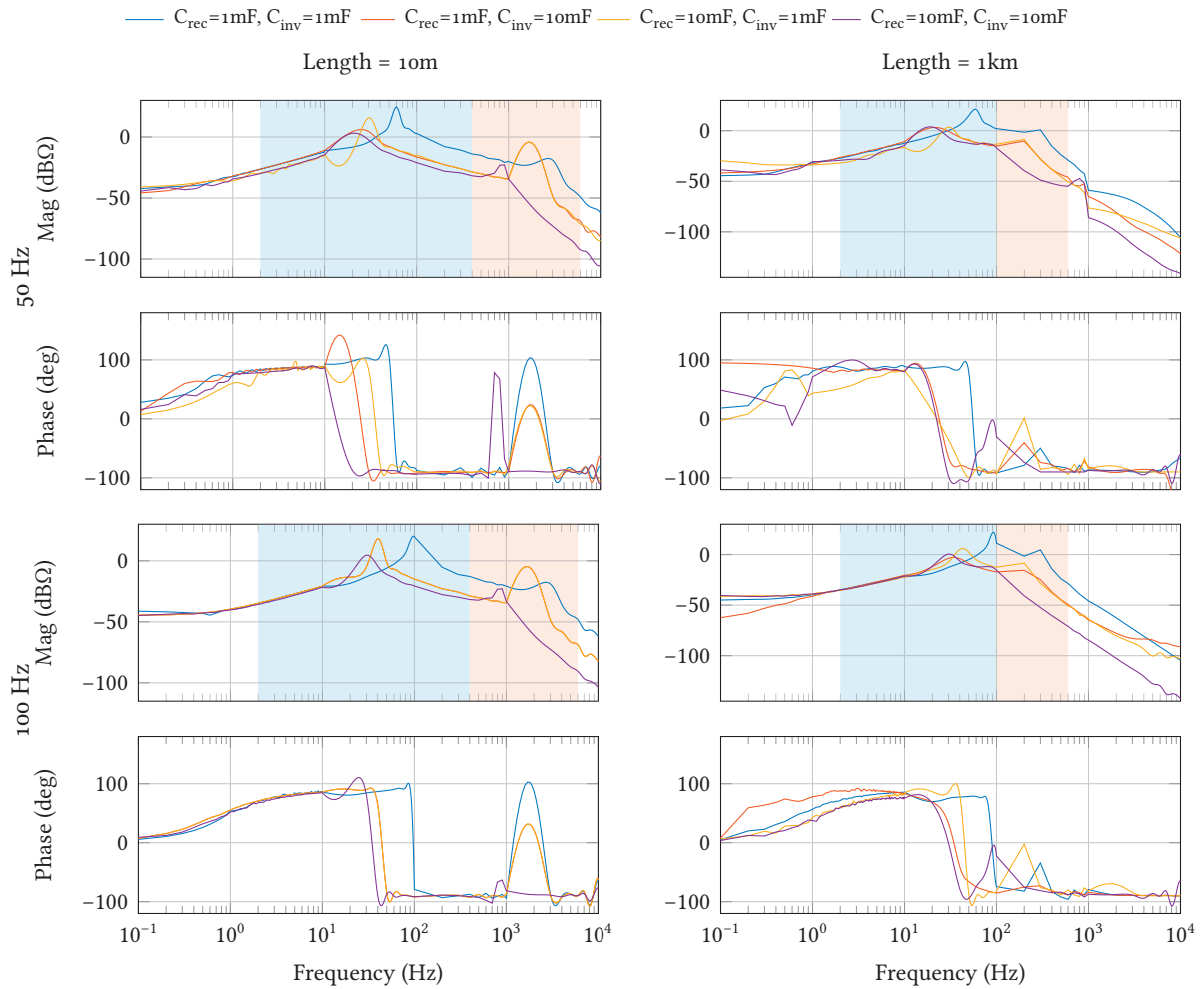


**Figure 5.11** TRU impedances in a frequency window of 0.1 - 10k Hz for different filtering efforts. The low frequency resonances, caused by the generator inductance and filter capacitors, are shaded blue. Whereas, the high frequency resonances, caused by cable inductance and filter capacitors, are shaded red.

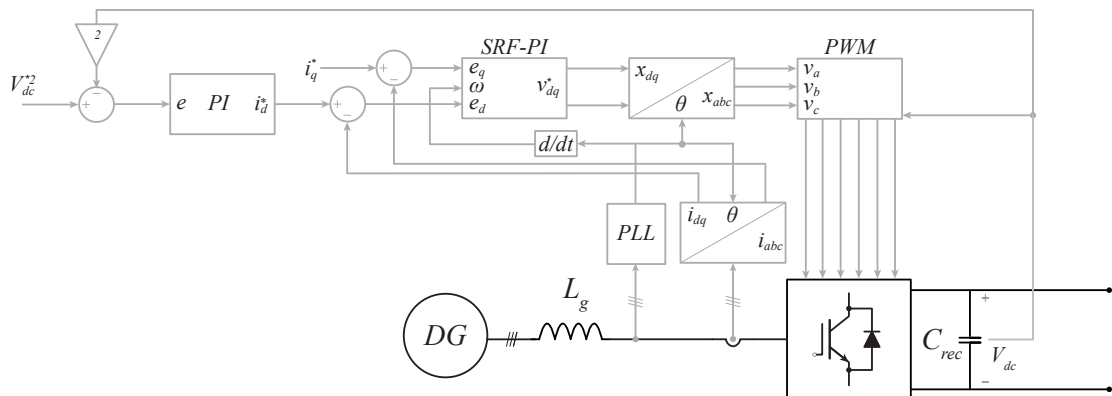


**Figure 5.12** Schematics of ARU and direct voltage control (DVC) for dc-side voltage control.

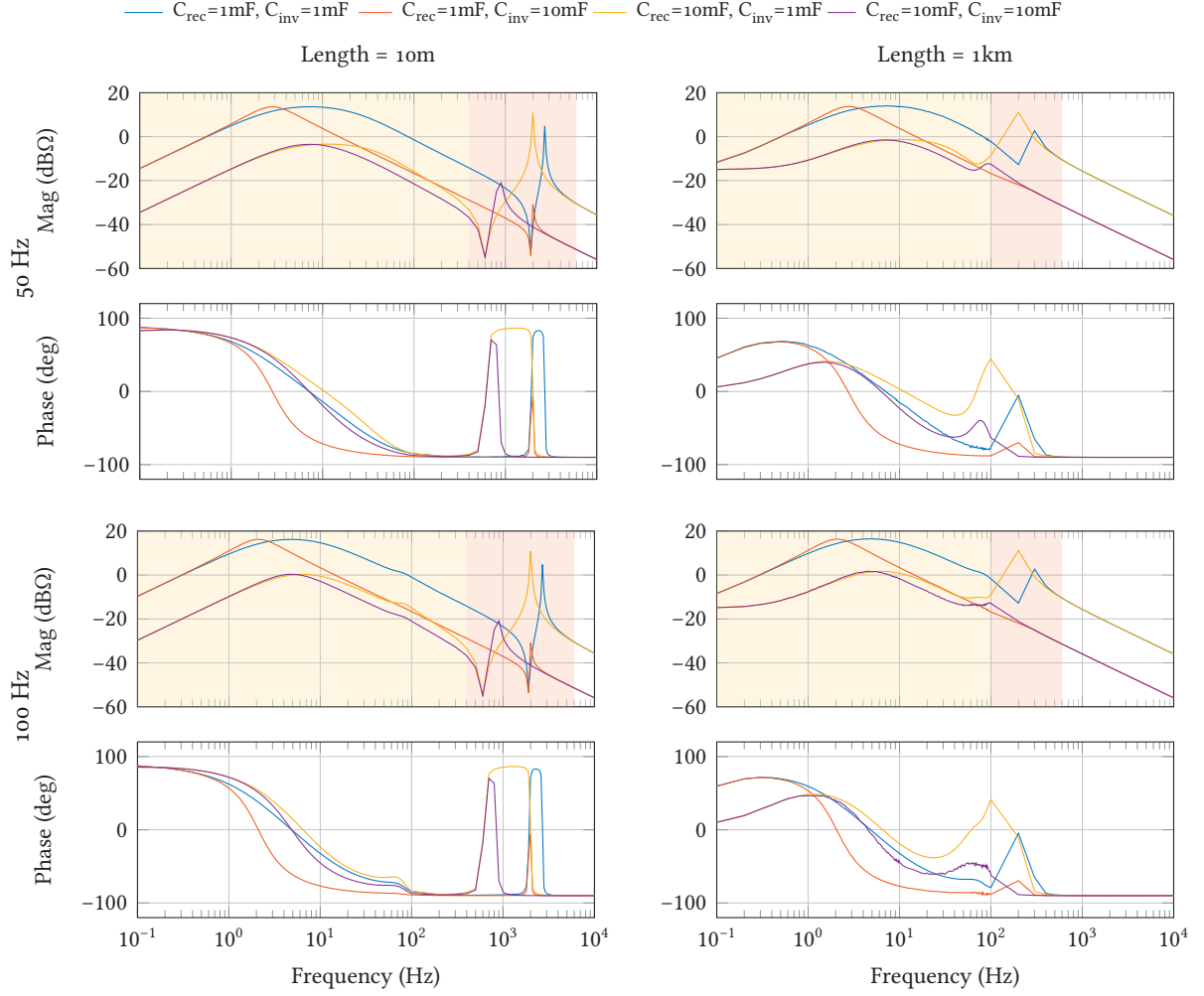


**Figure 5.13** ARU impedances in a frequency window of 0.1 - 10k Hz for different filtering efforts. The low frequency resonances, caused by the ARU control, are shaded yellow. Whereas, the high frequency resonances, caused by cable inductance and filter capacitors, are shaded red.

With sufficient simplification of the control and using the cable  $\pi$  - model, these impedances can be determined mathematically. Considering sufficient bandwidth of the current control, its impact on the voltage loop can be ignored. The converter impedance can be approximated as:

$$\frac{\tilde{v}_{dc}}{\tilde{i}_{dc}} = Z_{conv} = \frac{s}{s^2 C_{rec} + \frac{K_{pv,ARU}s}{\sqrt{3}} + \frac{K_{iv,ARU}}{\sqrt{3}}} \quad (5.12)$$

$\pi$ -section model of the cable is being considered for this study. From Table 5.1, it can be seen that the capacitances are very small and can be neglected in these theoretical considerations. Thus the cable can be represented just as a  $RL$  circuit:

$$Z_{cable} = sL_{cable} + R_{cable} \quad (5.13)$$

The impedance of capacitor bank on the inductor side can be represented as  $Z_{C_{inv}} = 1/sC_{inv}$ . Adding all these impedances gives us the expression for the total source output impedance, which can be

mathematically expressed as:

$$Z_o = (Z_{conv} + Z_{cable}) \parallel Z_{C_{inv}} \quad (5.14)$$

From **Fig. 5.13**, it can be seen that for the long cable, i.e., 1 km case, the higher resistance is also dominant at lower frequencies, i.e., less than 1 Hz. The low frequency resonance, shaded yellow in **Fig. 5.13**, is dependent on the controller parameters  $K_{pv,ARU}$  and  $K_{iv,ARU}$ . These parameters can be calculated by using *symmetric optimum* or as given in [105], while the high frequency resonance is given by (5.9).

## 5.5 Dynamic Assessment of the MVDC PDN

The dynamic interactions of the source and load subsystems in the equivalent two-port MVDC PDN, given in **Fig. 5.4(a)**, are analyzed for the different system configurations for the parametric

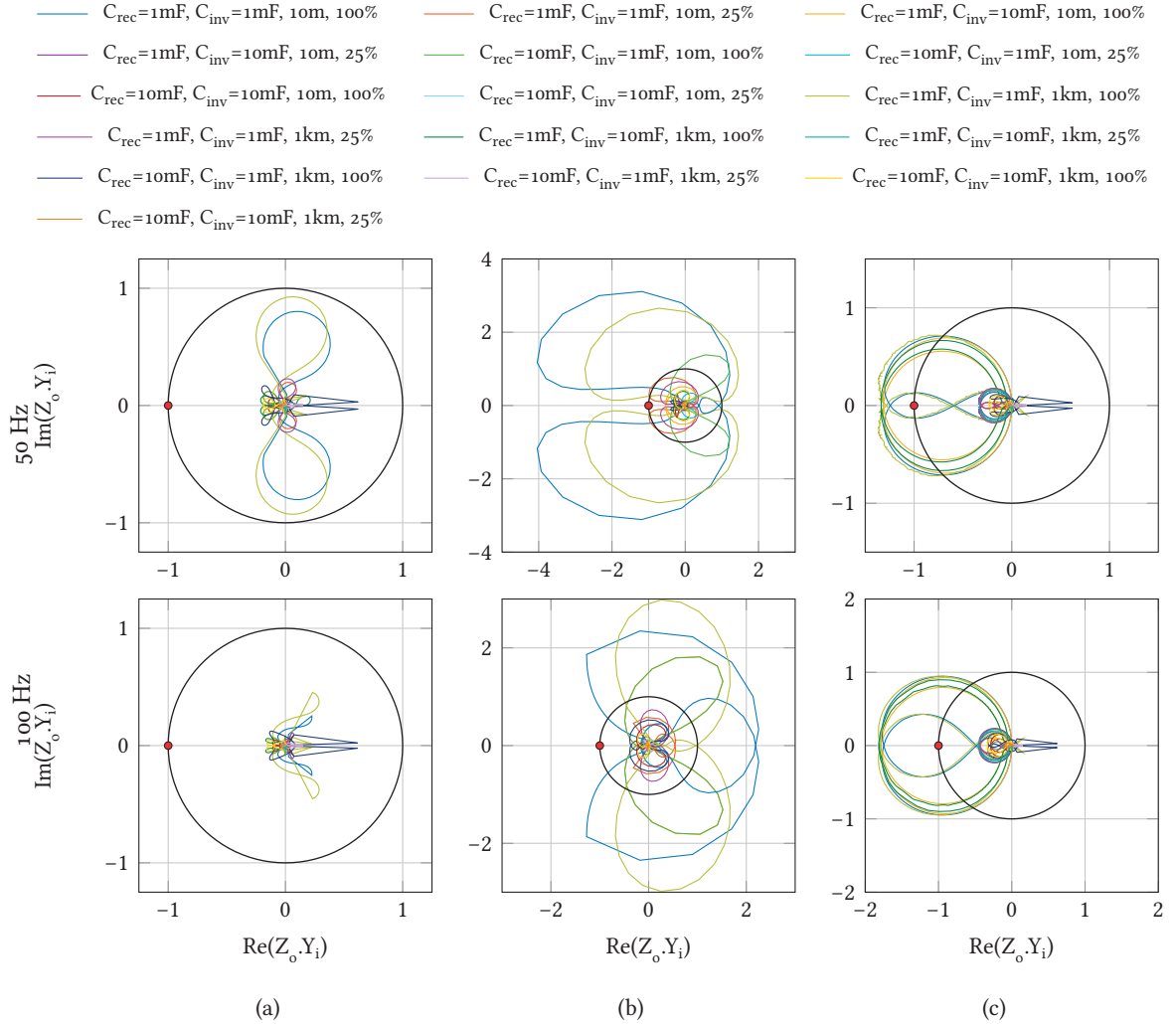


**Figure 5.14** Nyquist plots for the different system configurations and loadings. (a) DRU. (b) TRU. (c) ARU.

variations listed in Table 5.1. These parametric variations are expected to cover possible realistic MVDC PDN configurations. As discussed earlier, for a system to demonstrate absolute stability, the Nyquist Criterion must be satisfied, i.e., Nyquist trajectory must not encircle critical point of  $(-1,0)$ . Additionally, the IEEE Std. 1709-2010 ([20]) requires that a relative stability metric is employed. In this analysis, the *inverse of the sensitivity peak*  $\eta_I$  is used, as it is specially suited for system with resonances [106].  $\eta_I$  can be defined as the distance of the Nyquist contour from the critical point. Using this metric, the system can be characterized as demonstrating either a high stability margin for  $\eta_I \geq 0.5$ , low stability margin for  $0.5 > \eta_I > 0.1$ , or unstable behavior for  $0.1 \geq \eta_I$  [106], [107]. The characterization is possible by observing the Nyquist plots, which are given in Fig. 5.14. A discussion on the different observations from the Nyquist plots is provided below.

The Nyquist trajectories, shown in Fig. 5.14, cover the different source side converters, their respective configurations and the two different loading conditions at  $f_g = 50$  Hz and  $f_g = 100$  Hz. The Nyquist trajectories for DRU case are shown in Fig. 5.14(a), where the upper plot is for  $f_g = 50$  Hz and the bottom plot for  $f_g = 100$  Hz. It can be observed that none of the Nyquist trajectories for the parametric variations intersect the unit circle or encircle the critical point. For  $f_g = 50$  Hz, upper plot of Fig. 5.14(a), the Nyquist trajectories of two configurations, i.e.,  $C_{rec} = C_{inv} = 1$  mF and cable lengths of 10 m/1 km, come close to the unit circle but do not intersect it, thus the absolute stability criterion is satisfied for all system configurations. Furthermore, all configurations demonstrate high stability, i.e.,  $\eta_I \geq 0.5$ . The time domain simulation of a representative case is shown in Fig. 5.15(a).

Fig. 5.14(b) shows the Nyquist trajectories for the TRU case. The dc-side filter inductance, as

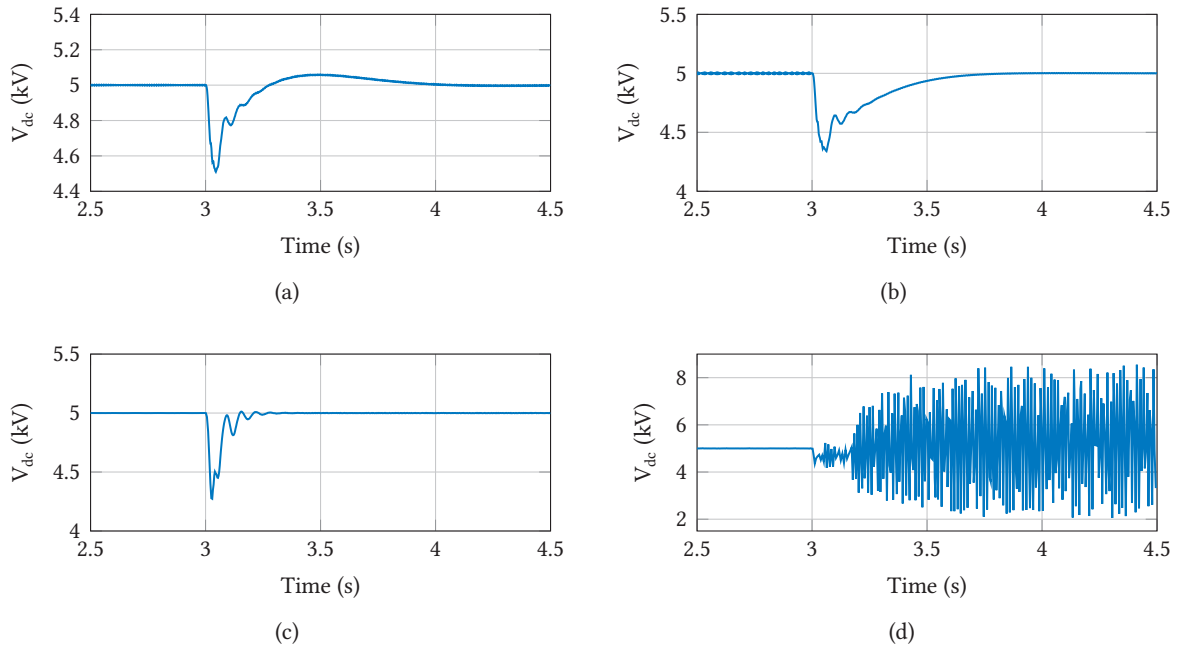


**Figure 5.15** Time domain simulations showing the dc-side voltage, for the different source converters, when a step change from 25% to 100% load is applied at 3 s. (a) DRU for 50 Hz,  $C_{rec} = C_{inv} = 1$  mF, 10 m. (b) TRU for 50 Hz,  $C_{rec} = C_{inv} = 1$  mF, 10 m. (c) ARU for stable case: 50 Hz,  $C_{rec} = 10$  mF,  $C_{inv} = 1$  mF, 10 m. (d) ARU for unstable case: 100 Hz,  $C_{rec} = C_{inv} = 1$  mF, 1 km. *Note: The bandwidths of AVR for DRU and voltage controller for TRU are the same.*

highlighted in the earlier section, impacts the low frequency resonance in the system, e.g., from Table 5.1, it can be observed that the value of  $L_f$  is quite high for lower generator frequency and lower filtering effort at the output of the TRU. Three systems configurations, as shown in Fig. 5.14(b) for  $f_g = 50$  Hz, intersect the unit circle. Although none of these configurations encircle the critical point, but two of these ( $C_{rec} = C_{inv} = 1$  mF and cable lengths of 10 m/1 km, for 100% and 25% loading) intersect the unit circle close to the critical point. In terms of the relative stability metric, introduced earlier, they demonstrate low stability as  $\eta_1$  lies in the range of 0.1 - 0.5. Such systems may exhibit under damped or self sustained oscillations. Another system configuration intersecting the unit circle is  $C_{rec} = 10$  mF,  $C_{inv} = 1$  mF and cable length of 10 m, but it has a higher relative stability as  $\eta_1 \geq 0.5$ . All of the above discussed system configurations, for  $f_g = 100$  Hz, also intersect the unit circle, however, they all have high relative stability margin, i.e.,  $\eta_1 \geq 0.5$ . Any possible instabilities, demonstrated by this case, might be a result of the higher inductance of the system due to the presence of  $LC$  filter at the output of the TRU. The time domain simulation of a representative case is given in Fig. 5.15(b), which shows the system is stable and the oscillations are well damped.

The measurements of the source impedance, for the ARU case, showed that the low frequency resonance is dependent on the voltage control of the ARU, while the high frequency resonance is dependent on the passive elements of the circuit similar to DRU and TRU case. As can be observed from Fig. 5.14(c), four system configurations for  $f_g = 50$  Hz, i.e.,  $C_{rec} = C_{inv} = 1$  mF/10 mF and cable lengths of 10 m/1 km, show unstable behavior. Similar behavior can be observed for  $f_g = 100$  Hz. The possible cause of these instabilities is the lower filtering effort at the output of the ARU, which in turn reduces the controllability of the dc-side voltage that leads to insufficient damping of the oscillations caused by  $L_g$ . Rest of the configurations demonstrate high relative stability of  $\eta_1 \geq 0.5$ , thus highlighting the oscillation damping capability of the voltage controller. The time domain simulations of the representative cases, i.e., stable and unstable are given in Fig. 5.15(c) and Fig. 5.15(d), respectively. Both these time-domain simulations verify the predictions of the Nyquist plots. From Fig. 5.15(c), it can be observed that the ARU, with proper filtering effort, exhibits well-damped response to the load change.

From the above discussions, which are also summarized in Table 5.4, it can be observed that among the different rectifiers considered the DRU demonstrates the best dynamic behavior for different system configurations and loadings. As discussed earlier, the DRUs are simple, robust and inexpensive, but are dependent on the AVR of the generator for maintaining the dc-side voltage. Due to the presence of the  $LC$  filter at the output of the TRUs, their dynamic behavior is slightly penalized and the filter inductance also impacts the low frequency resonance, which might lead to instability. The TRUs can control the dc-side voltage, but cannot step up the voltage levels and their control also has low impact on the dynamics of the system. However, their ability to control dc voltage provides them the ability to interrupt fault currents. The ARUs, with properly sized filter, can maintain the dc-side voltage under all operating conditions and also damp the low frequency resonance due to their higher bandwidths. However, the ability of the ARUs of 4-quadrant operation does not add any advantage and only increasing complexity and cost to the system.

**Table 5.4** Summary of the assessment of the different source side converters for  $f_g = 50$  Hz, 100 Hz at 100% loading.

|                                      | $\eta_i \geq 0.5$<br>(stable) | $0.5 > \eta_i > 0.1$<br>(weakly stable) | $0.1 \geq \eta_i$<br>(unstable) |
|--------------------------------------|-------------------------------|---|---------------------------------|
| Cable length 10 m, $C_{rec} = 1$ mF  |                               |   |                                 |
| $C_{inv} = 1$ mF                     | DRU                           | TRU                                     | ARU                             |
| $C_{inv} = 10$ mF                    | DRU, TRU                      | -                                       | ARU                             |
| Cable length 10 m, $C_{rec} = 10$ mF |                               |   |                                 |
| $C_{inv} = 1$ mF                     | DRU, TRU, ARU                 | -                                       | -                               |
| $C_{inv} = 10$ mF                    | DRU, TRU, ARU                 | -                                       | -                               |
| Cable length 1 km, $C_{rec} = 1$ mF  |                               |   |                                 |
| $C_{inv} = 1$ mF                     | DRU                           | TRU                                     | ARU                             |
| $C_{inv} = 10$ mF                    | DRU, TRU                      | -                                       | ARU                             |
| Cable length 1 km, $C_{rec} = 10$ mF |                               |   |                                 |
| $C_{inv} = 1$ mF                     | DRU, TRU, ARU                 | -                                       | -                               |
| $C_{inv} = 10$ mF                    | DRU, TRU, ARU                 | -                                       | -                               |

## 5.6 Summary

The assessment of the dynamic interactions of the source-load subsystems considering contributions from the generator inductances, dc-bus side capacitances, impact of cables, and the control strategies of source and load sides (CPL behavior), provides valuable insights about the dynamics of the marine MVDC PDN. Proper figures of merit are extracted from this assessment by utilization of the impedance stability criteria and the corresponding Nyquist trajectories. It has been proven that the increase in the source-side system inductance and the decrease in the capacitive filtering can lead to an unstable behavior, which is highlighted in the TRU and ARU cases. These insights from the stability studies can support designing the system with desired dynamic performances by aiding in proper tuning of control parameters, and sizing of filters and other passive components.

Additionally, the three different rectifier types, analyzed here, have their own advantages and disadvantages, e.g., DRU is simple and inexpensive, but requires the AVR of the generator to maintain dc-side voltage, the TRU provides limited controllability of the dc-side voltage and also can interrupt fault currents, but has reduced dynamics due to the  $LC$  filter at its output. Finally, the ARU offers a better dynamic response near rated conditions, but is sensitive to changes in the filtering effort, cables, and interaction between load and source leading to unstable behavior and also is more complex and expensive.

Both DRU and ARU are part of the state-of-the-art high performance VSDs, therefore, they may be preferred over TRU. The decision to utilize either of them will depend highly on additional factors, such as the presence of on-board energy storage (bidirectional power flow), requirement of high bandwidth dynamics of the source, cost, and reliability.





# 6

## Interactions of the MMC and CPLs in the MVDC Power Distribution Network

*In this chapter, the analysis of source-load interactions of a two-port MVDC PDN is extended to a modular multilevel converter (MMC) based rectifier feeding constant power loads (CPLs) in both onshore and offshore (marine) applications. Here, the impacts of varying distribution cable lengths between the source and the load, the filtering effort at the load end and the different loading conditions are analyzed for their impact on system stability.*

### 6.1 Introduction

The analysis presented in *Chapter 5* is extended here, considering an MVDC PDN with an MMC based rectifier supplying bandwidth limited CPLs. As discussed in *Chapter 2*, MMCs are the state-of-the-art technology in HVDC applications and are gaining interests as potential candidates for converters in the future MVDC PDNs due to their higher efficiency, modularity, scalability of the voltage and reduced filtering effort [56], [108]–[110]. The MMCs for MV application have much lower number of cells compared to HV applications. This leads to modified control and modulation methods for achieving low switching frequency for equal distribution of losses among cells [111]. This also opens up challenges which are being investigated and different solutions (topologies) have been proposed in [56], [108]–[110]. In addition to this, MMCs are being promoted for different applications at MV level. An MVDC PDN, based on point-to-point HVDC PDN, is being promoted in [59] with MMC as the principle converter interfacing different MVAC PDNs. MMC is also considered as an inverter in VSDs [112], [113] and, furthermore, [58] highlights its potential of reducing filtering effort in VSDs. A rectifier, based on MMC, for marine MVDC PDNs is reported in [61], which can also be used to interface energy storage in these systems [64].

With respect to ship on-board PDNs, MMCs have a larger footprint and a complex control structure compared to DRU, TRU and ARU and they may not be the first choice for such systems. Nevertheless, MMCs are prime candidates for onshore MVDC PDNs and an analysis of them in an MVDC PDN setting must be carried out. To analyze the stability of the PDNs with MMC as the source/load converter, its dc/ac-side impedance modeling is reported and analyzed for system stability in [61], [114]–[117]. In [114]–[116] dc/ac-side impedance models for MMCs operating as inverters are presented, whereas, [61], [117] present dc-side impedance of MMCs operating as rectifiers. The impedance models presented in [61], [114]–[117] model the impact of circulating currents, but consider approximations for voltage balancing among the MMC cells. Additionally, they have not analyzed the effects of the distribution cables and the inverter filters for system stability.

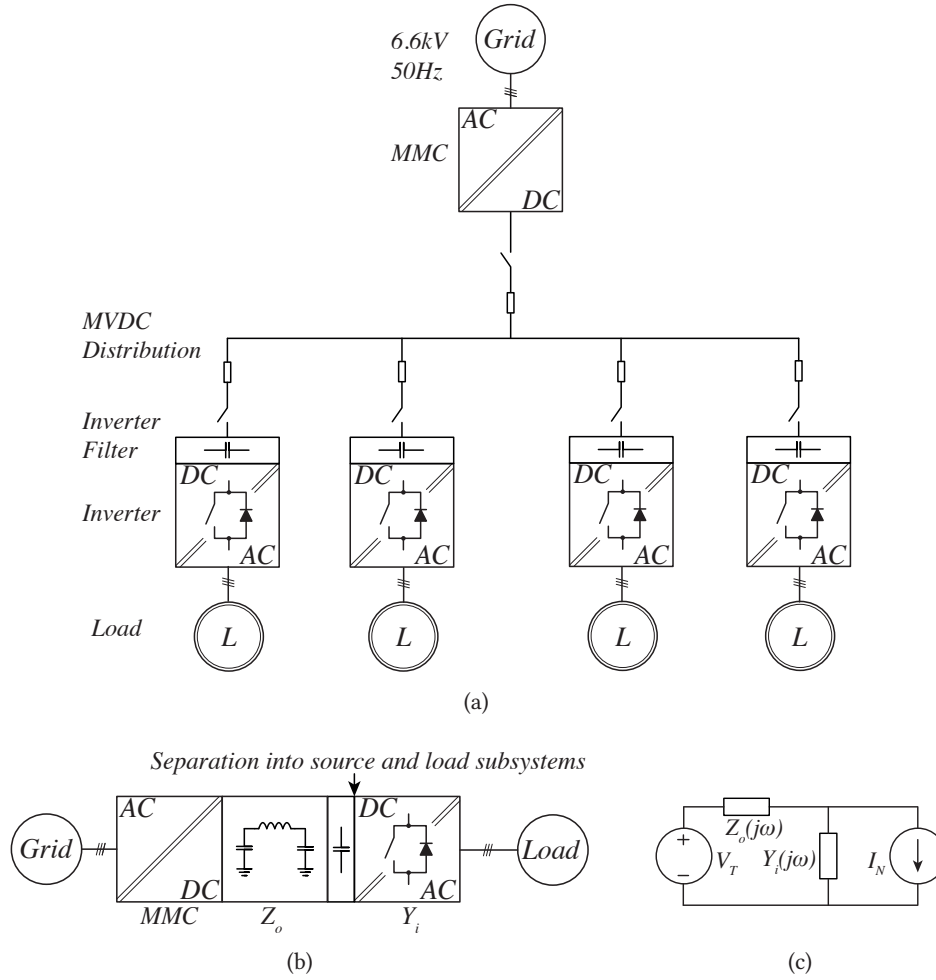


**Figure 6.1** (a) Simplified MVDC PDN. (b) Two-port MVDC PDN and its appropriate partitioning into source/load subsystems at the arrow [100]. (c) Linearized model for the stability analysis.

In this chapter, an MVDC PDN (several MWs) is considered with an MMC rectifier that is supplying bandwidth limited CPLs. Similar to *Chapter 5*, source impedances and load admittances are measured using simulations for different system parameters and loading conditions. The dynamic analysis is performed using Nyquist Criterion for the impact of the detailed control of MMC (based on [118]) and variations in cable lengths and filter on the inverter side. Figures of merit are extracted from the corresponding Nyquist plots, which provide useful insight into the design aspects of the future MVDC PDNs.

## 6.2 System Description

A generalized MVDC PDN similar to **Fig. 5.3** is shown in **Fig. 6.1(a)**, with MMC based rectifier as the sole rectifier feeding four different loads. The generalized MVDC PDN can be connected to a diesel generator set, a small wind farm or a solar farm, but for simplicity of the analysis a 3-phase balanced supply is considered. A 3-phase grid with voltage rating of 6.6 kV, a frequency of 50 Hz and power

**Table 6.1** System Parameters and their variations considered for this study.

| System Parameters                             |                | Equivalent Induction Motor Ratings |                    |
|---|----------------|------------------------------------|--------------------|
| <i>Rated Apparent Power</i>                   | 7 MVA          | <i>Rated Power</i>                 | 6.5 MW             |
| <i>Rated dc Voltage</i>                       | 10 kV          | <i>Rated Voltage</i>               | 6.1 kV             |
| <i>Rated ac Voltage</i>                       | 6.6 kV         | <i>Rated Current</i>               | 700 A              |
| <i>Rated Frequency</i>                        | 50 Hz          | <i>Power Factor</i>                | 0.92               |
| <i>Phase Reactor Inductance</i>               | 1 mH           | <i>Rated Frequency</i>             | 19 Hz              |
| <i>Switching frequency for load inverters</i> | 1 kHz          | <i>Rated Speed</i>                 | 376 rpm            |
| MMC Parameters                                |                | Cable Parameters                   |                    |
| <i>Rated Apparent Power</i>                   | 7 MVA          | <i>Cable Inductance</i>            | 0.347 mH/km        |
| <i>Rated Direct Voltage</i>                   | 10 kV          | <i>Cable Resistance</i>            | 0.089 $\Omega$ /km |
| <i>Number of cells per arm</i>                | 10             | <i>Cable Capacitance</i>           | 0.307 $\mu$ F/km   |
| <i>Switching frequency per cell</i>           | 315 Hz         | Parametric Variations              |                    |
| <i>Arm capacitance</i>                        | 0.65 mF        | <i>System Load</i>                 | 25% - 100%         |
| <i>Arm Inductance</i>                         | 1 mH           | <i>Cable Length</i>                | 100 m - 10 km      |
| <i>Arm Resistance</i>                         | 0.1 m $\Omega$ | <i>Inverter Filter</i>             | 1 mF - 10 mF       |

rating of 7 MVA is connected to the MMC rectifier. The MMC is maintaining a dc-side voltage of 10 kV and is connected through a disconnector to the PDN. The PDN is modeled as a single  $\pi$ -section for cables, for distance up to 10 km. For this study, a 12 kV XLPE MVAC cable from Brugg Cables is chosen [65]. The PDN is supplying four load inverters, which can be supplying power to another grid, a data center, driving a large electrical machine or a collection of smaller machines. In this case, each load inverter is considered to be supplying a motor with its own disconnector and filter. The load inverters are usually multi-level voltage source inverter (VSI) topologies [66], constructed with high power semiconductors that are usually switched less than 1 kHz to reduce switching losses [67]. In any case, due to constant power injection in the load for a given loading condition, a bandwidth limited CPL behavior is characteristic for the load side converters. The parameters for the system, MMC based supply side converter, cable and load parameters are given in Table 6.1.

### 6.3 Dynamic Assessment of MVDC Power Distribution Network

Using identical procedures as *Chapter 5*, the MVDC PDN shown in **Fig. 6.1(a)** can be simplified to **Fig. 6.1(b)** which shows equivalent source and loads. This can be carried out by considering similar small signal behavior for all the loads, connection of the loads with similar cable lengths to the source, and by neglecting the impact of the non-linear effects of each of the loads [93], [94]. The PDN of **Fig. 6.1(b)** helps in extracting the figures of merit for different load devices and their interactions with the source. Furthermore, **Fig. 6.1(b)** can be divided into source, i.e., grid, MMC rectifier, distribution cable (represented as an equivalent  $\pi$ -section model), and inverter filter, and load, i.e., inverter and motor. This partition of the PDN into source and load subsystems can be further simplified and represented as **Fig. 6.1(c)** [94], [100]. The minor loop gain, given in (6.1), is employed to plot the Nyquist contours to assess the stability of the system under consideration.

$$H_{mlg}(j\omega) = Z_o(j\omega)Y_i(j\omega) \quad (6.1)$$

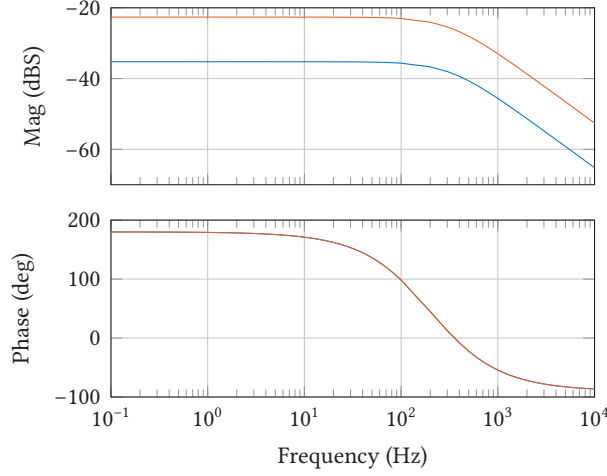


**Figure 6.2** Load admittance in a frequency window of 0.1 - 10k Hz for — 25% load and — 100% load.

The complete system is implemented in PLECS with detailed control implemented for the MMC rectifier and the inverter drive. The measurement of the source/load impedance/admittances is carried out by injection of a multi-tone perturbation as current/voltage at the terminals and by measuring the corresponding voltage/current. This arrangement is identical to one shown in **Fig. 5.5**. The ratio of the measured signal to the perturbation signal gives the impedance/admittance [119].

### 6.3.1 Load Admittance

The equivalent load subsystem considers an equivalent high performance inverter motor drive with FOC. The parameters of the equivalent induction motor are given in Table 6.1 and the control identical to the one shown in **Fig. 5.6**. The load considered here has a higher input voltage 10 kV compared to 5 kV for load in previous chapter, while the power rating is the same in both cases. Load admittances are shown in **Fig. 6.2** and are measured for full load, i.e., 100% of the rated speed and rated torque, and light load, i.e., 100% of the rated speed and 25% rated torque. As expected the admittances show a CPL behavior for the majority of the frequency window, but change to an inductive behavior reflecting the limitations on the current control bandwidth, i.e., 100 Hz. At higher frequencies, the motor inductance dominates the load admittances. This admittance  $Y_i(j\omega)$  is used for the small signal analysis.

### 6.3.2 Source Impedance

Large amount of work can be found on the design and operation of the MMC, but only a few works can be found on the MMC dc-side impedance modeling [61], [114]–[117]. In these works a rather simplified MMC control is considered and also the dc-side equipment is neglected. Here a detailed control of the MMC based on [118] is considered that is explained in the next section. As apparent from **Fig. 6.1(b)**, the source-side impedance consists of three parts: i) grid connected MMC rectifier, ii) cable, and iii) inverter filter. The cable and inverter filter are the passive components, which shape the source impedance beyond the bandwidth of the control of the MMC.

**Table 6.2** MMC control parameters.

|                |            |              |             |                |            |                |            |
|----------------|------------|--------------|-------------|----------------|------------|----------------|------------|
| $K_{p,dc}$     | 0.2184 A/V | $K_{i,dc}$   | 30.576 As/V | $K_{p,\Sigma}$ | 0.091 A/V  | $K_{i,\Sigma}$ | 12.74 As/V |
| $K_{p,\Delta}$ | 0.364 A/V  | $K_{p,circ}$ | 6.72 V/A    | $K_{i,circ}$   | 0.672 Vs/A | $K_{p,gc}$     | 0.84 V/A   |
| $K_{i,gc}$     | 0.084 Vs/A | $K_{p,pll}$  | 91.9 /V     | $K_{i,pll}$    | 46 s/V     |                |            |

## 6.4 MMC Control Structure

**Fig. 6.3** shows the schematics of the MMC rectifier with average representation of its branches. Furthermore, the  $\pi$ -section cable model and the inverter filter are also shown in **Fig. 6.3**. To model the impact of the control and discard any noise due to switching an average model is used for each MMC branch, which is shaded as purple while the average model is shaded as light brown in **Fig. 6.3**. In an MMC, different variables need to be controlled for proper operation, which can be classified into: (i) external variables and (ii) internal variables. The external variables are the ac-side grid current, tracking of the ac grid angle and dc-side voltage (only for MMCs operating as rectifiers). The internal variables are the energies stored in each cell and the circulating current in the branches of the MMC. In terms of the control implementation and its structural similarity with ARU, the outer loop acts on dc-side voltage and the energies stored in cell capacitance, whereas, the inner loops control the ac grid currents and circulating currents. The dc-side impedances of MMC (rectifier mode), presented in [61], [117], do not model the impact of the control of MMC cell energies, but in their place consider an arm energy estimator [120]. An explanation of the control structure used in this study is described as follows.

The outer loop of the MMC control effectively controls the cell capacitor voltages and is shown

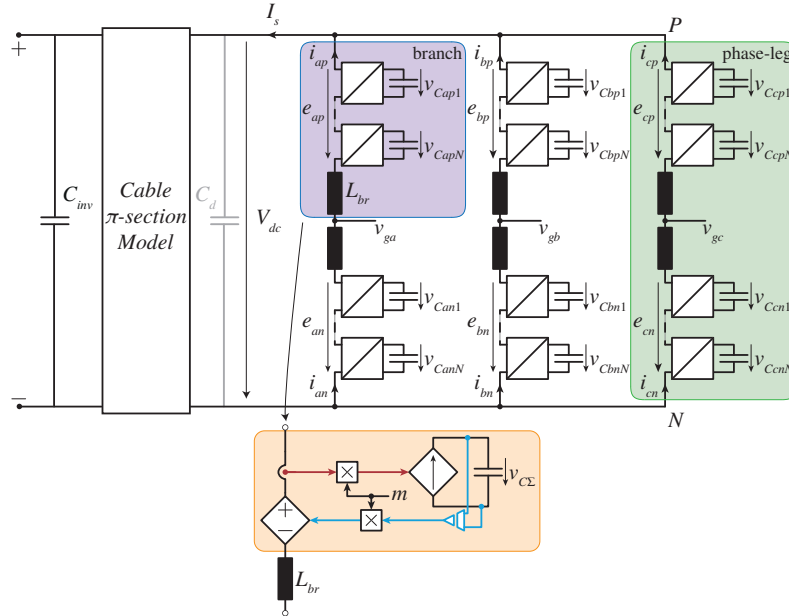


**Figure 6.3** Schematics of grid connected MMC based rectifier. The value of  $C_d$  is considered as 0.225 mF for this study, but for small cable lengths it can be neglected ( $C_d \ll C_{branch}$ ).

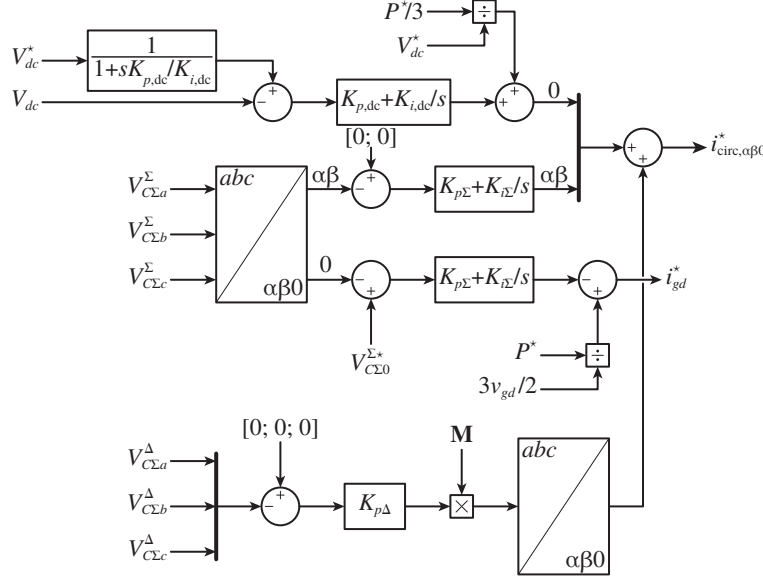


**Figure 6.4** MMC cell capacitor voltage controls: dc-side voltage control, and  $V_{C\Sigma}^\Sigma$  and  $V_{C\Delta}^\Delta$  controls for energy balancing.

in **Fig. 6.4**. The cell capacitor voltage control performs three functions, i.e., it controls: i) the sum ( $V_{C\Sigma}^\Sigma$ ) of and ii) the difference ( $V_{C\Delta}^\Delta$ ) of the summed capacitor voltages, and iii) dc-side control  $V_{dc}$ . The sum of the capacitor voltages maintains the total energy of the MMC and additionally provides horizontal balancing. The *horizontal balancing* ensures that each phase-leg of the MMC shares the same average energy. The *PI* controllers are used to control the  $V_{C\Sigma}^\Sigma$  voltages in the  $\alpha\beta o$ -frame to separate the horizontal energy balancing of  $\alpha\beta$ -axes and the total energy control  $o$ -axis [118]. The second function of the cell capacitor voltage control is to control the difference ( $V_{C\Delta}^\Delta$ ) of the summed capacitor voltages. This function maintains the *vertical balancing* by using the differential energy control, i.e., the energy balance among the positive and negative branches of the MMC phase-leg. The  $V_{C\Delta}^\Delta$  is controlled in the  $abc$ -axes, with a proportional  $P$  controller and matrix  $\mathbf{M}$  [118]. This matrix  $\mathbf{M}$  is established in accordance with the discussion provided in [121] and it can be expressed as:

$$\mathbf{M} = \begin{bmatrix} \cos(\theta_L) & \frac{-\sin(\theta_L)}{\sqrt{3}} & \frac{\sin(\theta_L)}{\sqrt{3}} \\ \frac{\sin(\theta_L - 2\pi/3)}{\sqrt{3}} & \cos(\theta_L - 2\pi/3) & \frac{-\sin(\theta_L - 2\pi/3)}{\sqrt{3}} \\ \frac{-\sin(\theta_L + 2\pi/3)}{\sqrt{3}} & \frac{\sin(\theta_L + 2\pi/3)}{\sqrt{3}} & \cos(\theta_L + 2\pi/3) \end{bmatrix} \quad (6.2)$$

Here  $\theta_L$  is the angle of  $V_L$  which is the line voltage. The adoption of  $\mathbf{M}$  ensures the cancellation of the fundamental frequency component of the circulating currents at the dc terminals by introducing reactive power flows that do not affect  $V_{C\Delta}^\Delta$ . These control schemes and the required filters are discussed in detail in [56], [118].

The *dc-side voltage* control is based on [122]. This control strategy is based on controlling the energy of the total capacitance, which in this case is a combination of the cell capacitances and the equivalent cable capacitance ( $C_d$  shown in **Fig. 6.3**). The plant for tuning dc-side voltage control is, therefore:

$$C_{eq} = C_d + C_{branch} = C_d + \frac{6C_{cell}}{N_{cell}} \quad (6.3)$$

Here,  $C_{cell}$  is the cell capacitance and  $N_{cell}$  is the number of cells. The dc-side voltage control is implemented as part of the total energy control.

The *circulating current* naturally exists in the MMC due to the voltage mismatch between the positive and negative branch. This causes steady state even harmonics (2<sup>nd</sup> and 4<sup>th</sup>) and odd harmonics in transient conditions. To control the circulating current, its references come from the total and differential energy control. The circulating current control is shown in **Fig. 6.5(a)**. It is implemented in  $\alpha\beta o$ -frame with  $\alpha\beta$ -axes having *PR* controllers, while a *PI* controller is used for the *o*-axis [118]. The *PR* regulators are tuned here to fundamental, second and fourth harmonics, which not only improves the vertical balancing dynamics, but also minimizes the even harmonics (2<sup>nd</sup> and 4<sup>th</sup>).

The *grid current control* is implemented in *dq*-frame with *PI* controllers, including axis decoupling and feed-forward as shown in **Fig. 6.5(b)**. The PLL, shown in **Fig. 6.5(c)**, synchronizes the system

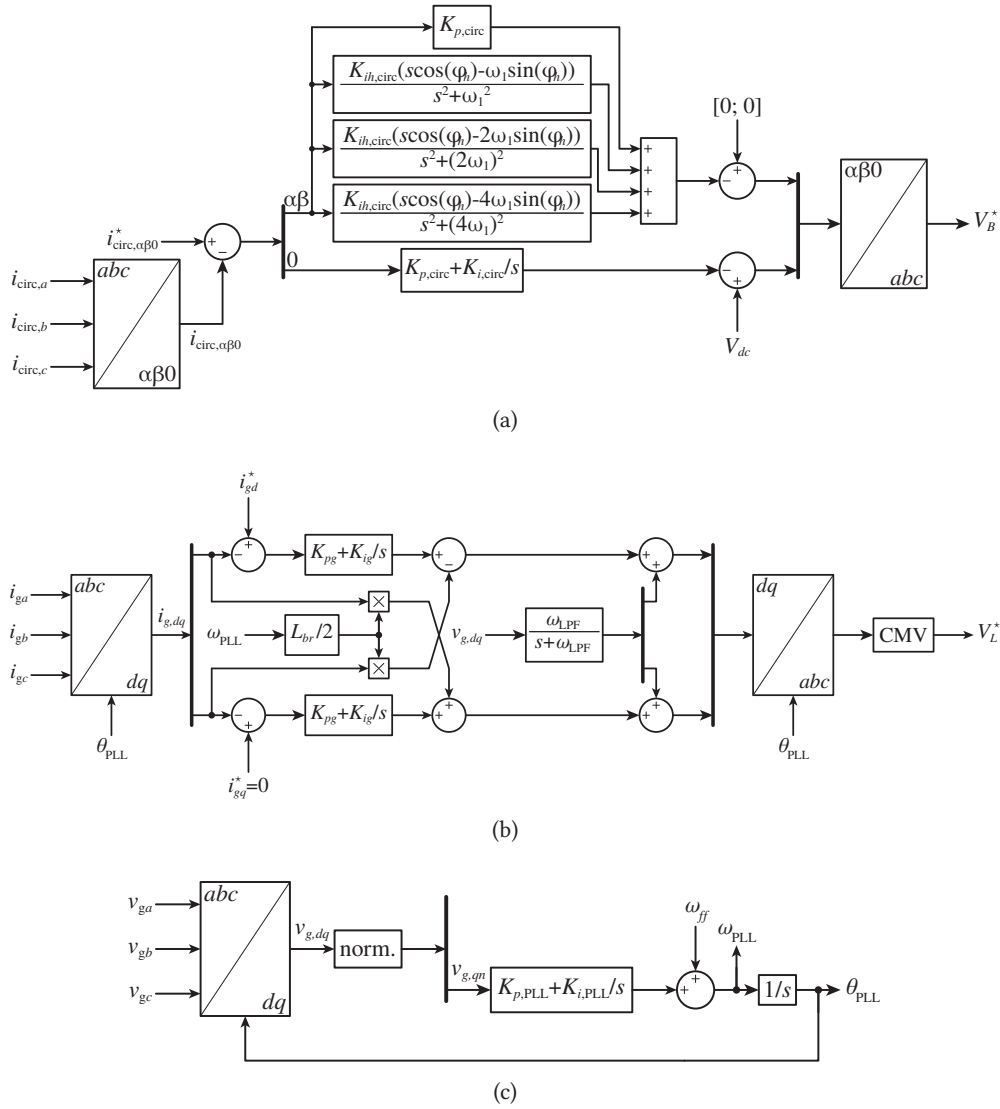


**Figure 6.5** (a) MMC circulating current control inspired by [118]. (b) MMC grid current controller. (c) PLL.

with the grid frequency. The controller gains for all of these controls are given in Table 6.2.

All of the different controls, considered here, play a role in shaping  $Z_{MMC}$ . The analytical expression for  $Z_{MMC}$  is not presented here due to the different non-linearities and the complexity of the controls implemented in this study. The source impedance also has contributions from cable and inverter filter, in addition to  $Z_{MMC}$  and a final approximation of the source impedance is:

$$Z_o = (Z_{MMC} + Z_{cable}) \parallel Z_{C_{inv}} \quad (6.4)$$

The impedance of the MMC, considering the impact of dc-side voltage control, with and without the consideration of cable (100 m) and inverter filter (1 mF) is illustrated in Fig. 6.6. The blue curve shown in Fig. 6.6, illustrates the impact of the dc-side voltage control at lower frequencies, i.e., 0.1 - 100 Hz, but for frequencies higher than 100 Hz the internal branch inductances dominate the impedance. However, adding the cable impedance and inverter input filter lead to yellow curve. In the high frequency range, the capacitive parts of the cable and the inverter filter become dominant in the  $Z_o$  shape. This is a good behavior in the sense that a low  $|Z_o|$  limits the possibility of load/source interactions at high frequencies.

Different source configurations are defined by varying the distribution lengths and the inverter filter, while the parameters of the grid connected MMC rectifier are kept constant. The parametric variations are given in Table 6.1. Fig. 6.7 shows the source impedances for the different system configurations. As pointed out earlier and as can be observed, from Fig. 6.7, at the lower frequencies the MMC cascaded control is dominant in the shaping of the impedance and the corresponding lower frequency resonance is due to the voltage control of the MMC. Furthermore, increase in the inverter filter shifts this resonance to slightly lower frequencies, as can be seen in Fig. 6.7. The second resonance is due to the interactions between the cable inductance and the inverter filter, but it is significantly damped. Higher cable length and filtering effort at the inverter side also shift the second resonance to lower frequencies. Additionally, the cable resistance for longer cable lengths has a pronounced effect as it damps the second resonance and also dominates at really low frequencies, as can be observed from Fig. 6.7(b) and Fig. 6.7(c).

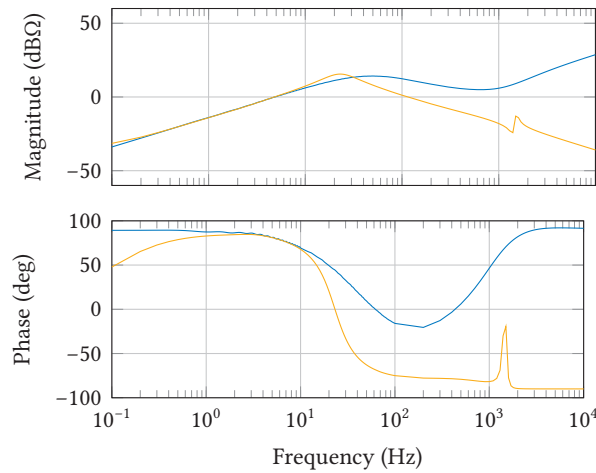


**Figure 6.6** MMC impedance (—  $Z_{MMC}$ ) with dc voltage control and source impedance (—  $Z_o$ ) considering a cable length of 100 m and  $C_{inv}$ .



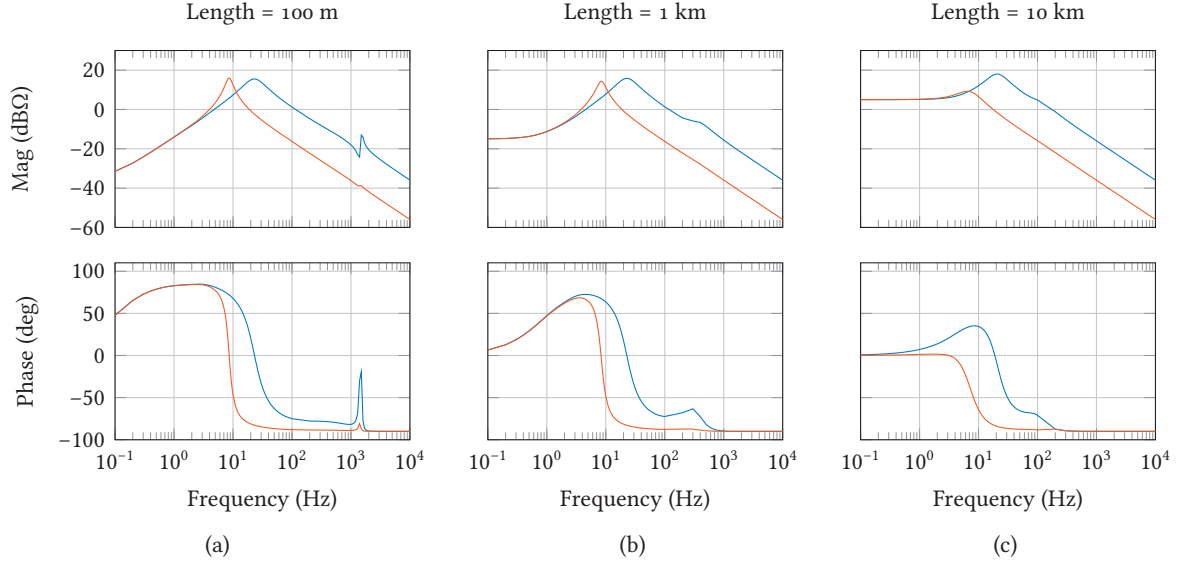


**Figure 6.7** Source impedance for different distribution lengths and load filters (— 1 mF and — 10 mF). It can be seen here that the resonance occurs between the MMC branch inductances and the inverter filter. For longer distance, case for onshore MVDC PDNs, the resistance of line has significant impact at lower frequencies.

## 6.5 Impedance Stability Assessment

The stability of the two-port MVDC PDN, shown in **Fig. 6.1(b)**, is evaluated for the parametric variations listed in **Table 6.1**. As discussed earlier in *Chapter 5*, for a system to be considered stable its Nyquist contour must not encircle the critical point of  $(-1,0)$  [100]. Additionally, a relative stability index based on the inverse of the sensitivity peak  $\eta$  is also employed [107]. This index helps in

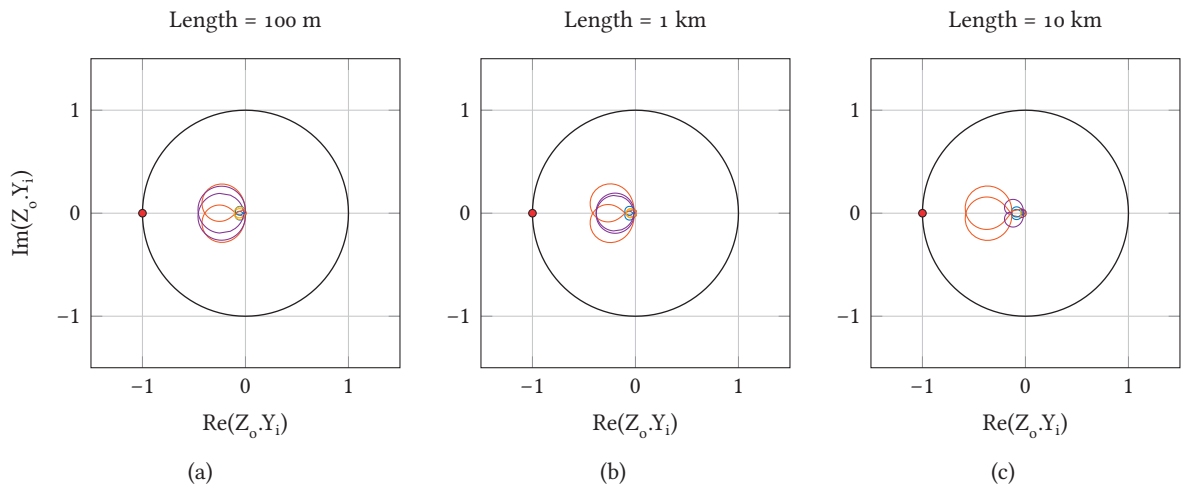


**Figure 6.8** Nyquist plots for different system configurations and loadings (— 1 mF-25% Load, — 1 mF-100% Load, — 10 mF-25% load, — 10 mF-100% load).

categorizing the system into three different stability zones, i.e., i)  $\eta \geq 0.5$  high stability, ii)  $0.5 > \eta > 0.1$  low stability, and iii)  $0.1 \geq \eta$  unstable. The Nyquist contours for three different distribution cable lengths are illustrated in **Fig. 6.8**. It can be observed that most of the system configurations, as a result of the parametric variations, exhibit relatively high stability, i.e.,  $\eta \geq 0.5$ . One system configuration with cable length of 10 km and  $C_{inv} = 1$  mF shows low stability i.e.,  $0.5 > \eta > 0.1$ . This relatively low stability is due to the increased inductance in the system and decreased filtering effort at the load side.

## 6.6 Time Domain Simulations

The time domain simulations for different system configurations are given in **Fig. 6.9**. **Fig. 6.9(a)** shows the dc-side voltage and current for the system configuration with 100 m cable length and inverter filter, while, **Fig. 6.9(b)** shows the same variables for the system configuration with 10 km cable length and the same inverter filter. The predictions made regarding system stability, in **Fig. 6.8(a)** and **Fig. 6.8(c)**, are fulfilled and the system is stable for variations in the different system parameters and the loading conditions.

## 6.7 Summary

MMCs are increasingly being considered for the different applications for MV level applications, e.g., VSDs, shaft generator applications, point-to-point MVDC PDN, etc. Additionally, some works are also considering them for the ship on-board applications. MMCs with the large footprint and complex control, compared to other rectifiers, may not be the first choice for the marine applications but have the potential to become prime converters for the onshore MVDC PDNs.

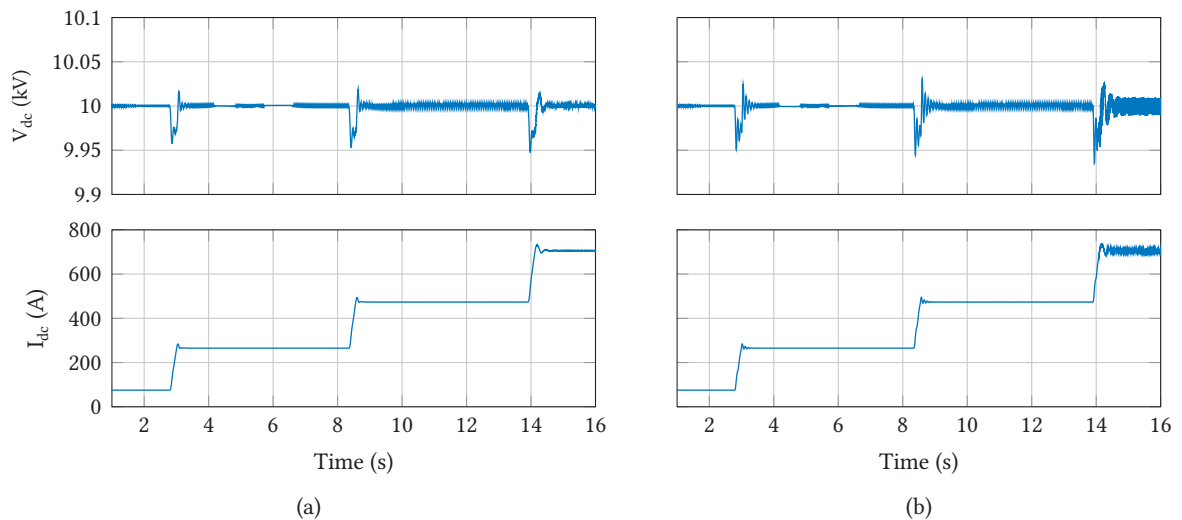


**Figure 6.9** Time domain simulation for different system configurations ((a) cable length 100 m and  $C_{inv} = 1$  mF, (b) cable length 10 km and  $C_{inv} = 1$  mF) and different loading conditions. The load has step changes at 3 s, 8.25 s and 13.9 s with increments of 25% till 100% load is reached.

The analysis of *Chapter 5* is extended here to discuss the dynamic interactions between an MMC based source side converter and bandwidth limited CPLs, when connected to each other through cables. A realistic and detailed control that includes dc-side voltage control, horizontal and vertical energy balancing, circulating current control and ac current control is employed for the MMC rectifier. The influence of this detailed MMC control, the inverter filter and distribution lengths have been observed on the shaping of the source-side impedance. From the analysis, it can be seen that high inductance due to long cable lengths and also lower filtering effort at the inverter side negatively impacts the system stability. Overall, it can be seen that due to the higher bandwidth of the control, MMC ensures good dynamic stability of the system.



# 7

## Dynamic Stability of the Multi-port MVDC Power Distribution Network

*In this chapter, multi-port MVDC PDNs are modeled and analyzed using state space techniques. The resultant system model is independent of the source operating conditions and the groupings of the different elements in the system. This model is utilized to map the impact of the variations of the passive elements by analyzing the closed-loop pole movements and the corresponding multi-variable Nyquist trajectories. Additionally, the unstable system configurations are identified and the findings are verified with time-domain simulations.*

### 7.1 Introduction

In the previous chapters, the complex system of **Fig. 5.3** is analyzed to identify the dynamic interactions of the source and the load subsystems. To carry out this analysis, super-position principle and small signal techniques are combined to simplify the multi-port MVDC PDN to a two-port MVDC PDN (SISO, **Fig. 5.4(a)**). The resulting source and load subsystems are represented as impedances and admittances that are measured, at the partition point, using simulations for different system parameters and loading conditions, and are utilized to determine the source-load dynamic interactions by means of *impedance stability criteria*. This analysis helps in highlighting the impact of the control strategies, filtering efforts and distribution lengths on the dynamic stability of a two-port MVDC PDN (SISO system).

The SISO analysis is a good benchmark for analyzing stability, however, it is dependent on the proper partitioning of the system into source and load subsystems [94] and also the steady state operation point [123]. Furthermore, real systems are expected to be multi-port MVDC PDNs and SISO approximations may not be always sufficient for the stability analysis, i.e., the interactions among the multiple sources and loads can not be ignored and must be analyzed. Therefore, to analyze these interactions, their implications on the system stability and to overcome deficiencies in the SISO analysis, a MIMO analysis, based on state space techniques, is required. Literature discussing the stability analysis of multi-port dc PDNs can be found [124]–[126]. Multi-terminal HVDC PDNs are modeled using state space modeling techniques and analyzed using eigenvalue analysis in [124], [125]. The analyses focus on control design to achieve stable operation of the HVDC PDNs. Additionally, in [126], state space modeling is used to represent a multi-port dc PDN with CPLs and a sufficient condition for stability is presented. This condition is dependent on elaborate steps to test whether the closed-loop system can be classified as negative imaginary or not. Supposing that the closed-loop system is classified as negative imaginary, then the system is stable for all operation points.

In this chapter, to analyze stability of a multi-terminal MVDC PDN, state space representation of MIMO systems is discussed and its application to determine system stability using eigenvalue analysis and multi-variable Nyquist Criteria is presented. Additionally, two topologies for multi-terminal MVDC PDNs are introduced and modeled using state space techniques, considering realistic control bandwidths and system parameters. The resulting model is analyzed for the impact of the control loops, filtering efforts and distribution cable lengths. The effects of variations in the different system parameters, on the system stability, are mapped using eigenvalue plots and the Nyquist trajectories. Furthermore, system configurations leading to unstable modes are highlighted and the time-domain simulations are carried out in PLECS to verify the findings.

## 7.2 Multiple Input Multiple Output Systems

In this section, a brief description of the state space representation of the MIMO systems is presented. The resulting models from this will be used in analyzing stability of the MIMO systems.

### 7.2.1 State Space Representation of MIMO System

To model a MIMO system with state space techniques, it is assumed to be a linear time invariant system. Following this assumption, a minimum continuous linear time invariant state space model of the MIMO system can be expressed as:

$$\begin{aligned}\frac{d\vec{x}(t)}{dt} &= \mathbf{A}\vec{x}(t) + \mathbf{B}\vec{u}(t) \\ \vec{y}(t) &= \mathbf{C}\vec{x}(t) + \mathbf{D}\vec{u}(t)\end{aligned}\tag{7.1}$$

Here  $\vec{x}(t)$  is the state vector,  $\vec{u}(t)$  is the input vector,  $\vec{y}(t)$  is the output vector,  $\mathbf{A}$  is the state matrix,  $\mathbf{B}$  is the input matrix,  $\mathbf{C}$  is the output matrix, and  $\mathbf{D}$  is the feed-forward matrix [127]. All the elements of these vectors and matrices are real. Applying Laplace transformation to (7.1) gives s-domain representation as:

$$\begin{aligned}s\vec{X}(s) - \vec{x}(0) &= \mathbf{A}\vec{X}(s) + \mathbf{B}\vec{U}(s) \\ \vec{Y}(s) &= \mathbf{C}\vec{X}(s) + \mathbf{D}\vec{U}(s)\end{aligned}\tag{7.2}$$

Considering  $\vec{x}(0) = 0$ , the output  $\vec{Y}(s)$  can be expressed in terms of  $\vec{U}(s)$  as:

$$\vec{Y}(s) = (\mathbf{C}(s\mathbf{I} - \mathbf{A})^{-1}\mathbf{B} + \mathbf{D})\vec{U}(s)\tag{7.3}$$

Equation (7.3) represents the relationship between input and output of a MIMO system. The *matrix transfer function* is usually represented as  $\mathbf{G}(s)$ , a square matrix, and given by:

$$\mathbf{G}(s) = \mathbf{C}(s\mathbf{I} - \mathbf{A})^{-1}\mathbf{B} + \mathbf{D}\tag{7.4}$$

As  $\mathbf{G}(s)$  maps the interactions between different inputs and outputs, therefore, each of its elements is a transfer function.  $\mathbf{G}(s)$  is called a *proper matrix* when all of its elements are proper transfer functions. Another property, arising from the transfer function nature of the elements of  $\mathbf{G}(s)$ , is the possibility

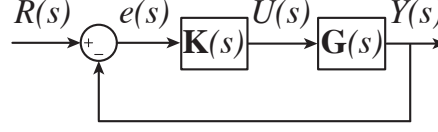


**Figure 7.1** Interconnected MIMO system with feedback.

to represent  $\mathbf{G}(s)$  in terms of two matrices having numerator and denominator polynomials. This representation is possible using *matrix fraction descriptions*. Following the steps highlighted in [127],  $\mathbf{G}(s)$  can also be represented as:

$$\mathbf{G}(s) = [\mathbf{G}_D(s)]^{-1}[\mathbf{G}_N(s)] \quad (7.5)$$

Here  $\mathbf{G}_D(s)$  and  $\mathbf{G}_N(s)$  are the matrices with denominator and numerator polynomials, respectively. Further discussions on *matrix fraction descriptions* can be found in [127].

### 7.2.2 Stability of the MIMO Systems

Considering the terms introduced earlier to describe the MIMO system, an interconnected MIMO system with feedback control is shown in **Fig. 7.1**. Here  $\mathbf{K}(s)$  represents the control of the MIMO system. From the observation of **Fig. 7.1**, the closed-loop gain of the system can be expressed as:

$$\mathbf{T}(s) = [\mathbf{G}(s)\mathbf{K}(s)][\mathbf{I} + \mathbf{G}(s)\mathbf{K}(s)]^{-1} \quad (7.6)$$

Here  $\mathbf{I}$  is the identity matrix. For the MIMO system to be stable, all the poles of the system must be in the LHP. In order to determine the stability of the closed system of **Fig. 7.1**, the denominator of (7.6) is of the most importance. For MIMO system this can be expressed as:

$$\mathbf{S}^{-1}(s) = \mathbf{I} + \mathbf{G}(s)\mathbf{K}(s) \quad (7.7)$$

Here  $\mathbf{S}(s)$  is the sensitivity matrix [128], [129]. To check for the stability of the MIMO system, the determinant of (7.7) is taken that results in a transfer function. The numerator polynomial of this transfer function gives the characteristic equation of the system, and from here the poles of the system can be determined. There is a possibility that during this operation unstable pole zero cancellation occurs, therefore, in order to prevent that the *matrix fraction descriptions* can be applied on (7.7) [127], [129], which results in:

$$\mathbf{S}^{-1}(s) = \mathbf{G}_D(s)\mathbf{K}_D(s) + \mathbf{G}_N(s)\mathbf{K}_N(s) \quad (7.8)$$

The zeros of the following expression give the poles of the closed-loop MIMO system:

$$\det[\mathbf{S}^{-1}(s)] = \det[\mathbf{G}_D(s)\mathbf{K}_D(s) + \mathbf{G}_N(s)\mathbf{K}_N(s)] = 0 \quad (7.9)$$

Equation (7.9) is used later to plot the pole movement of the closed-loop MIMO system for the variations in the different system parameters. This method to determine stability is known as *eigenvalue analysis*.

Another frequency domain method to determine stability is to plot the *minor loop gain* of the MIMO system and use *multi-variable Nyquist Criteria* to determine stability of the MIMO system [130]. This, similar to the discussion provided earlier in *section 5.2*, is the MIMO equivalent to the *minor loop gain* of the SISO system. From observation of (7.6), the *minor loop gain* of the MIMO system is given by:

$$\mathbf{H}_{mlg}(s) = \mathbf{G}(s)\mathbf{K}(s) \quad (7.10)$$

Equation (7.10) is only valid under the assumption that *no unstable pole-zero cancellation* occurs [127]. Calculation of the eigenfunctions of (7.10) and plotting them on complex plane, as function of  $s$ , results in characteristic loci or Nyquist trajectories of the MIMO system [127]. These eigenfunctions can be calculated as:

$$\det[\mathbf{H}_{mlg}(s)] = \det[\mathbf{G}(s)\mathbf{K}(s)] = \prod_{i=1}^n \Lambda_i(s) \quad (7.11)$$

Here  $\Lambda_i(s)$ ,  $i = 1, 2, \dots, n$  are the eigenfunctions of the  $\mathbf{G}(s)\mathbf{K}(s)$  and  $n$  is the order of the square matrix.

Both these methods are used to determine the stability of the multi-terminal MVDC PDNs described later in the chapter.

### 7.3 Modeling of Multi-Terminal MVDC PDN

In order to carry out MIMO modeling and analysis, a simple three-port MVDC PDN is considered in this thesis. This PDN is based on the two-port MVDC PDN (**Fig. 5.4(a)**), which is expanded to consider another load connected through a distribution cable to the main source converter. This provides enough complexity to demonstrate the procedure and the effectiveness of the MIMO analysis explained earlier. Two different topologies are considered here for representing a multi-terminal MVDC PDN:

- *Case 1*: One drive connected to the source converter through the main dc-link and the second one connected through a distribution cable. This is a special case in which one drive is located very close to the source and can be connected to it using short bus-bars.
- *Case 2*: Both drives connected to the source converter through distribution cables to the main dc-link. This is a generalized version of Case 1.

These two MVDC PDNs are shown in **Fig. 7.2**. The MVDC supply, in these cases, is considered to be sufficiently sized to support both loads. The control strategies for both source and load side converters are the same as described in *Chapter 5*. The MVDC PDN, shown in **Fig. 7.2(a)**, is supplied by a 3.3 kV, 50 Hz source connected to a rectifier through a phase reactor. The two drives, in this case, are rated at 7.3 MVA each. The first drive is connected to the main capacitor bank  $CBU_1$ , while, the second drive is connected through a cable and has another capacitor bank  $CBU_2$ . The system is generalized by considering that the first drive is also connected through a cable and it is illustrated in **Fig. 7.2(b)**. This leads to the consideration of an additional capacitance bank in the system and the three capacitor banks are named  $CFU$ ,  $CBU_1$  and  $CBU_2$ .  $CFU$  is the filter capacitance of the rectifier unit, while  $CBU_1$  and  $CBU_2$  are input filters for the inverter drives. The system parameters used, in this case, are given in *Table 7.1*.



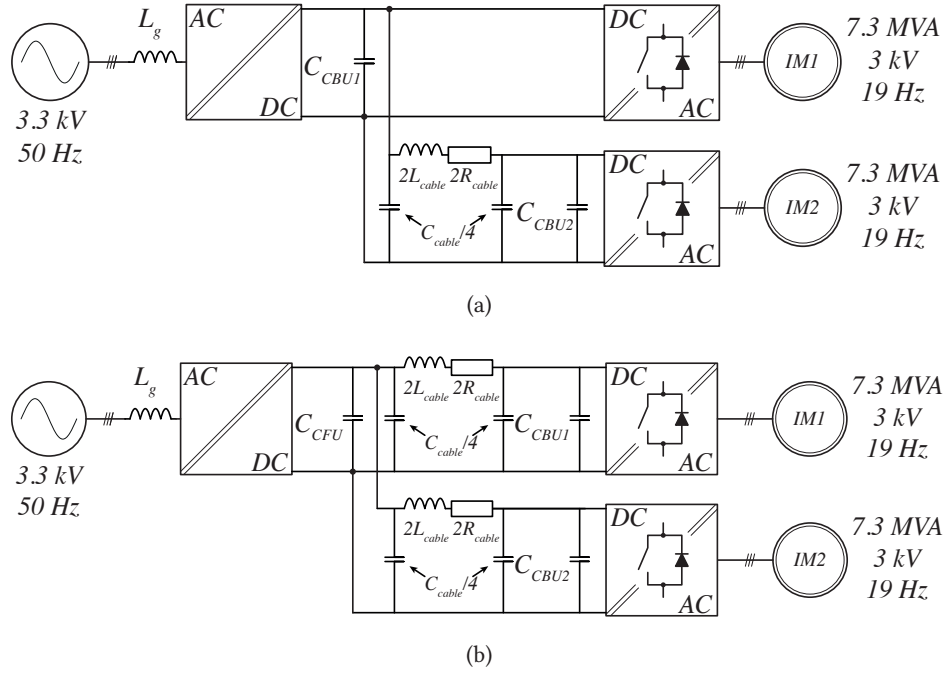


**Figure 7.2** Multi-terminal MVDC PDNs. (a) Case 1. (b) Case 2.

**Table 7.1** System Parameters used for this study.

| System Parameters        |             | Induction Motor Ratings |         | Cable Parameters  |                    |
|--------------------------|-------------|-------------------------|---------|-------------------|--------------------|
| Rated Apparent Power     | 14.6 MVA    | Rated Power             | 6.9 MW  | Cable Inductance  | 0.347 mH/km        |
| Rated Direct Voltage     | 5 kV        | Rated Voltage           | 3.05 kV | Cable Resistance  | 0.089 $\Omega$ /km |
| Rated Frequency          | 50 Hz       | Rated Current           | 1.4 kA  | Cable Capacitance | 0.307 $\mu$ F/km   |
| Phase Reactor Inductance | 0.0025 p.u. | Rated Frequency         | 19 Hz   |                   |                    |
| Phase Reactor Resistance | 0.0025 p.u. | Rated Speed             | 376 rpm |                   |                    |
| Switching Frequency      | 250 Hz      | Power Factor            | 0.92    |                   |                    |

In order to determine the stability limits of the systems, shown in **Fig. 7.2**, their linearized representation is required. In the following sub-sections the derivation of the linearized state space models is explained by considering **Fig. 7.2(a)** and **Fig. 7.2(b)**.

### 7.3.1 Case 1 - One Drive Connected Remotely

The linearized state space MIMO models are derived by modeling passive components separately from the active components (power electronic converters). Following this objective, the schematics of the passive components for case 1 is shown in **Fig. 7.3(a)**. The variables defining the dynamics of this system are: (i)  $i_1$  the current through the cable inductance, (ii)  $v_1$  the voltage of  $C_1$ , where  $C_1 = C_{BU1} + C_{cable}/4$ , and (iii)  $v_2$  the voltage of  $C_2$ , where  $C_2 = C_{BU2} + C_{cable}/4$ . The differential equations

defining this system are expressed as:

$$\begin{aligned}\frac{di_1}{dt} &= -\frac{R}{L}i_1 + \frac{1}{L}v_1 - \frac{1}{L}v_2 \\ \frac{dv_1}{dt} &= -\frac{1}{C_1}(i_s + i_{l1}) - \frac{1}{C_1}i_1 \\ \frac{dv_2}{dt} &= \frac{1}{C_2}i_1 - \frac{1}{C_2}i_{l2}\end{aligned}\quad (7.12)$$

Here  $L = 2 \cdot l_{cable} \cdot L_{cable}$  and  $R = 2 \cdot l_{cable} \cdot R_{cable}$  are the inductance and resistance of the cable,  $l_{cable}$  is length of the cable, and  $i_s$ ,  $i_{l1}$  and  $i_{l2}$  are currents flowing in the ARU and the two load converters, respectively. The state-space representation of (7.12) is expressed as:

$$x = \begin{bmatrix} i_1 \\ v_1 \\ v_2 \end{bmatrix}, \mathbf{A} = \begin{bmatrix} -\frac{R}{L} & \frac{1}{L} & -\frac{1}{L} \\ -\frac{1}{C_1} & 0 & 0 \\ \frac{1}{C_2} & 0 & 0 \end{bmatrix}, \mathbf{B} = \begin{bmatrix} 0 & 0 \\ -\frac{1}{C_1} & 0 \\ 0 & -\frac{1}{C_2} \end{bmatrix}, \mathbf{C} = \begin{bmatrix} 0 & 1 & 0 \\ 0 & 0 & 1 \end{bmatrix}, \mathbf{D} = \begin{bmatrix} 0 & 0 \\ 0 & 0 \end{bmatrix} \quad (7.13)$$

Here  $i_1$ ,  $v_1$  and  $v_2$  are the state variable,  $v_1$  and  $v_2$  are also the output variables and  $i_s$ ,  $i_{l1}$  and  $i_{l2}$  are the inputs of the system. Using (7.3) the input-output relation can be derived for this system that is also the equivalent impedance of the passive components. This can expressed as:

$$\vec{v}_{dc}(s) = \mathbf{Z}_{sys}(s) \vec{i}_{dc}(s) \quad (7.14)$$

Here  $\vec{v}_{dc}$  is the voltage vector of the capacitor voltages and  $\vec{i}_{dc}$  is the vector of all dc-side currents flowing out of the capacitors. In order to calculate the impedance ( $\mathbf{Z}_{sys}(s)$ ) of the system from its state space representation, given in (7.13), (7.4) is used and can now be expressed as:

$$\mathbf{Z}_{sys}(s) = -(\mathbf{C}s\mathbf{I} - \mathbf{A})^{-1}\mathbf{B} + \mathbf{D} \quad (7.15)$$

Here -ve sign compensates for the convention of the current. Equation (7.15) results in:

$$\mathbf{Z}_{sys}(s) = \frac{1}{s(s^2LC_1C_2 + sRC_1C_2 + C_1 + C_2)} \begin{bmatrix} s^2LC_2 + sRC_2 + 1 & 1 \\ 1 & s^2LC_1 + sRC_1 + 1 \end{bmatrix} \quad (7.16)$$

From (7.16), it can be seen that  $\mathbf{Z}_{sys}(s)$  contains the passive elements of the system, it can be deduced that none of its poles lies in the right half plane (RHP) and that it is passive. The passive nature of  $\mathbf{Z}_{sys}(s)$  ensures that no unstable poles-zeros are canceled in (7.10).

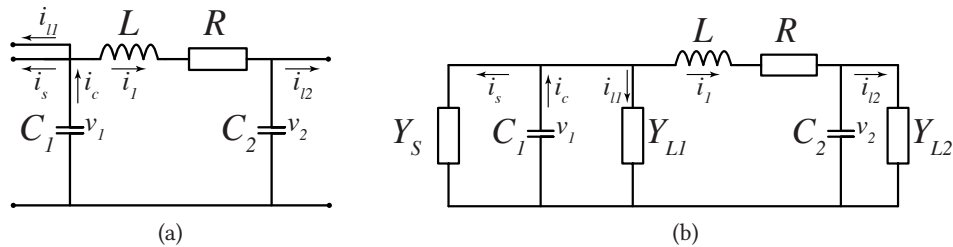


**Figure 7.3** Linearized model of the system given in Fig. 7.2(a). (a) Passive circuit. (b) The multi-drive system as a combination of impedances and admittances.

In the second part of the MIMO modeling, linearized behaviors of the rectifier and the inverter drives that are dominated by the control loops are modeled. In general, the control is usually modeled as inverse of the plant model where it can cancel the dominant poles of the system [117], [131]. Therefore, the impact of control of the converters, of the MIMO system, can be modeled as:

$$\vec{i}_{dc}(s) = -\mathbf{K}(s)\vec{v}_{dc}(s) \quad (7.17)$$

Here  $\mathbf{K}(s)$  represents the active components of the system and is also the admittance of the system. The following necessary assumptions and steps are followed to model the power electronic converters as admittances:

- The slower outer voltage control loop, of the cascaded control of the ARU, determines its behavior in the frequency domain.
- The inverter drives are tightly regulating the speed and the torque of the machine and are maintaining a constant input power for a given loading condition. Therefore, they are behaving as CPLs within a bandwidth of their current control loops.

Considering the above assumptions and a *PI* voltage controller, the rectifier can be represented as:

$$Y_s(s) = \frac{sK_{pv} + K_{iv}}{s} \times K_{comp} \quad (7.18)$$

Here  $K_{pv}$  and  $K_{iv}$  are the proportional and integral gains of the voltage control and  $K_{comp} = 3V_d/2V_{dc}$  is the compensation factor for the current control loop, considering zero reactive power. The CPL behavior of the inverter drives, within their current control bandwidths, can be expressed as:

$$Y_{l1}(s) = -\frac{P_1}{V_1^2} \frac{1}{s\tau + 1} \quad (7.19)$$

$$Y_{l2}(s) = -\frac{P_2}{V_2^2} \frac{1}{s\tau + 1} \quad (7.20)$$

Here  $P_1$ ,  $P_2$ ,  $V_1$  and  $V_2$  are the input powers and voltages of the inverter drives and based on the operation point of the drive, while  $\tau = 10/(\pi f_s)$  is the inverse of the bandwidth of the current control<sup>1</sup> [131]. Following the conventions given in Fig. 7.3(a), the converters are supplied by the currents from their respective nodes that they are connected to, therefore, the resulting  $\mathbf{K}(s)$  matrix is a diagonal matrix and is given below:

$$\mathbf{K}(s) = \begin{bmatrix} Y_s + Y_{l1} & 0 \\ 0 & Y_{l2} \end{bmatrix} \quad (7.21)$$

The complete representation of the system as a combination of impedances and admittances is given in Fig. 7.3(b). Fig. 7.4 shows the linearized representation of a generalized MIMO applicable to Fig. 7.2(a) and Fig. 7.2(b) as a block model with feedback. This model defines the dynamics of the system and is inspired from [126].

<sup>1</sup> $f_s$  is the sampling frequency and is four times the switching frequency, considering 3L-NPC.

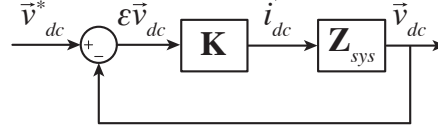


**Figure 7.4** Linearized representation of the MIMO systems with feedback.

### 7.3.2 Case 2 - Two Drives Connected Remotely

The state space modeling techniques are extended to model the system given in **Fig. 7.2(b)**. The schematics of the passive components of this system are illustrated in **Fig. 7.5**. The variables defining the dynamics of this system are: (i)  $i_1$  the current through the cable inductance connecting the first drive to the CFU, (ii)  $i_2$  the current flows through the second cable connecting the second drive, (iii)  $v_1$  the voltage of  $C_1$ , where  $C_1 = CFU + C_{cable}/2$ , (iv)  $v_2$  the voltage of  $C_2$ , where  $C_2 = CBU1 + C_{cable}/4$ , and (v)  $v_3$  the voltage of  $C_3$ , where  $C_2 = CBU1 + C_{cable}/4$ . The differential equations defining this system are expressed as:

$$\begin{aligned} \frac{di_1}{dt} &= -\frac{R_1}{L_1}i_1 + \frac{1}{L_1}v_1 - \frac{1}{L_1}v_2 \\ \frac{di_2}{dt} &= -\frac{R_2}{L_2}i_2 + \frac{1}{L_2}v_1 - \frac{1}{L_2}v_3 \\ \frac{dv_1}{dt} &= -\frac{1}{C_1}i_s - \frac{1}{C_1}i_1 - \frac{1}{C_1}i_2 \\ \frac{dv_2}{dt} &= \frac{1}{C_2}i_1 - \frac{1}{C_2}i_{l1} \\ \frac{dv_3}{dt} &= \frac{1}{C_3}i_2 - \frac{1}{C_3}i_{l2} \end{aligned} \quad (7.22)$$

Here  $L_1 = 2 \cdot l_{cable1} \cdot L_{cable}$ ,  $L_2 = 2 \cdot l_{cable2} \cdot L_{cable}$ ,  $R_1 = 2 \cdot l_{cable1} \cdot R_{cable}$  and  $R_2 = 2 \cdot l_{cable2} \cdot R_{cable}$  are the inductances and resistances of the cables,  $l_{cable1}$  and  $l_{cable2}$  are the lengths of the two cables, and  $i_s$ ,  $i_{l1}$  and  $i_{l2}$  are currents flowing in the ARU and the two load converters, respectively. The state-space representation of (7.22) is given in (7.23), where  $i_1$ ,  $i_2$ ,  $v_1$ ,  $v_2$  and  $v_3$  are the state variables and  $v_1$ ,  $v_2$  and  $v_3$  are also the output variables, and  $i_s$ ,  $i_{l1}$  and  $i_{l2}$  are the inputs of the system:

$$\begin{aligned} x = \begin{bmatrix} i_1 \\ i_2 \\ v_1 \\ v_2 \\ v_3 \end{bmatrix}, \mathbf{A} = \begin{bmatrix} -\frac{R_1}{L_1} & 0 & \frac{1}{L_1} & -\frac{1}{L_1} & 0 \\ 0 & -\frac{R_2}{L_2} & \frac{1}{L_2} & 0 & -\frac{1}{L_2} \\ -\frac{1}{C_1} & -\frac{1}{C_1} & 0 & 0 & 0 \\ \frac{1}{C_2} & 0 & 0 & 0 & 0 \\ 0 & \frac{1}{C_3} & 0 & 0 & 0 \end{bmatrix}, \mathbf{B} = \begin{bmatrix} 0 & 0 & 0 \\ 0 & 0 & 0 \\ -\frac{1}{C_1} & 0 & 0 \\ 0 & -\frac{1}{C_2} & 0 \\ 0 & 0 & -\frac{1}{C_3} \end{bmatrix}, \\ \mathbf{C} = \begin{bmatrix} 0 & 0 & 1 & 0 & 0 \\ 0 & 0 & 0 & 1 & 0 \\ 0 & 0 & 0 & 0 & 1 \end{bmatrix}, \mathbf{D} = \begin{bmatrix} 0 & 0 & 0 \\ 0 & 0 & 0 \\ 0 & 0 & 0 \end{bmatrix} \end{aligned} \quad (7.23)$$

In order to calculate the impedance of the system from its state space representation, given in (7.23), the following equation is used:

$$\mathbf{Z}_{sys}(s) = -(\mathbf{C}(s\mathbf{I} - \mathbf{A})^{-1}\mathbf{B} + \mathbf{D}) \quad (7.24)$$

This results in:

$$\mathbf{Z}_{sys}(s) = \begin{bmatrix} \frac{Z_4 Z_3}{Z_1} & \frac{Z_3}{Z_1} & \frac{Z_4}{Z_1} \\ \frac{Z_3}{Z_1} & \frac{Z_5}{Z_1} & Z_2 \\ \frac{Z_4}{Z_1} & Z_2 & \frac{Z_6}{Z_1} \end{bmatrix} \quad (7.25)$$

$Z_1, Z_2, Z_3, Z_4, Z_5$  and  $Z_6$  are defined in (7.26):

$$\begin{aligned} Z_1 &= s^4(L_1 L_2 C_1 C_2 C_3 + s^3(L_1 R_2 C_1 C_2 C_3 + L_2 R_1 C_1 C_2 C_3) + s^2 R_1 R_2 C_1 C_2 C_3 + s(L_1 C_1 C_2 + \\ &\quad L_2 C_1 C_3 + L_1 C_2 C_3 + L_2 C_2 C_3 + R_1 C_1 C_2 + R_2 C_1 C_3 + R_1 C_2 C_3 + R_2 C_2 C_3) + \\ &\quad C_1 + C_2 + C_3) \\ Z_2 &= 1/(s^5(L_1 L_2 C_1 C_2 C_3) + s^4(L_1 R_2 C_1 C_2 C_3 + L_2 R_1 C_1 C_2 C_3) + s^3(L_1 C_1 C_2 + L_2 C_1 C_3 + \\ &\quad L_1 C_2 C_3 + L_2 C_2 C_3 + R_1 R_2 C_1 C_2 C_3) + s^2(R_1 C_1 C_2 + R_2 C_1 C_3 + R_1 C_2 C_3 + R_2 C_2 C_3) + \\ &\quad s(C_1 + C_2 + C_3)) \\ Z_3 &= s^2 L_2 C_3 + s R_2 C_3 + 1 \\ Z_4 &= s^2 L_1 C_2 + s R_1 C_2 + 1 \\ Z_5 &= s^4 L_1 L_2 C_1 C_3 + s^3(L_1 R_2 C_1 C_3 + L_2 R_1 C_1 C_3) + s^2(L_1 C_1 + L_1 C_3 + L_2 C_3 + R_1 R_2 C_1 C_3) + \\ &\quad s(R_1 C_1 + R_1 C_3 + R_2 C_3) + 1 \\ Z_6 &= s^4 L_1 L_2 C_1 C_2 + s^3(L_1 R_2 C_1 C_2 + L_2 R_1 C_1 C_2) + s^2(L_2 C_1 + L_1 C_2 + L_2 C_2 + R_1 R_2 C_1 C_2) + \\ &\quad s(R_2 C_1 + R_1 C_2 + R_2 C_2) + 1 \end{aligned} \quad (7.26)$$

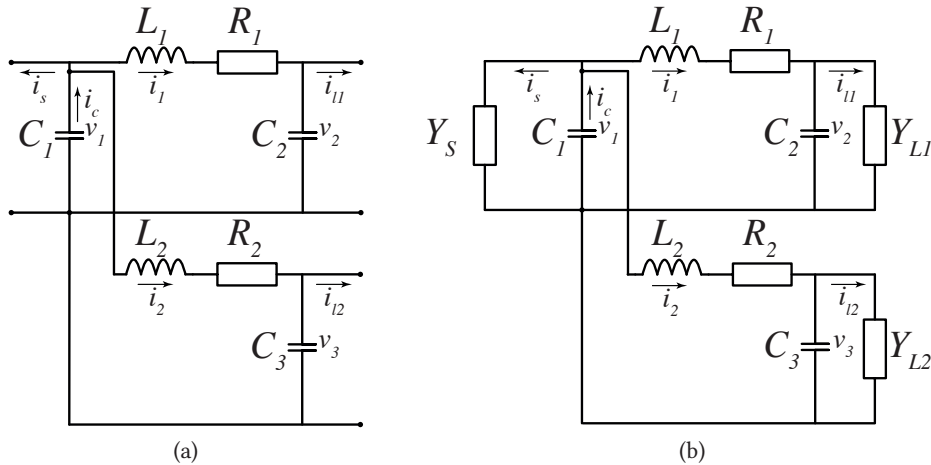


**Figure 7.5** Linearized model of the system given in Fig. 7.2(b). (a) Passive circuit of the multi-drive system. (b) The multi-drive system as a combination of impedances and admittances.

The rectifier and inverter drive admittances are the same as the ones discussed earlier, therefore, (7.18), (7.19) and (7.20) are valid for this case as well. Following the steps, explained above, the resulting  $\mathbf{K}(s)$  matrix is:

$$\mathbf{K}(s) = \begin{bmatrix} Y_s & 0 & 0 \\ 0 & Y_{l1} & 0 \\ 0 & 0 & Y_{l2} \end{bmatrix} \quad (7.27)$$

The modeling, presented here, is limited to ARUs because of the linear behavior of DVC control loops. The models can be further extended by considering the non-linear control schemes and behaviors of the DRUs, TRUs, MMCs and also droop control for multi-source MVDC PDNs.

## 7.4 Dynamic Analysis of Multi-Terminal MVDC PDN

The dynamic analysis of the MIMO system, described and modeled earlier, is carried out by the two methods described earlier. The first method calculates the eigenvalues of the MIMO system shown in Fig. 7.4. In order to calculate the eigenvalues, the sensitivity matrix is used:

$$\mathbf{S}(s) = [\mathbf{I} + \mathbf{Z}_{sys}(s)\mathbf{K}(s)]^{-1} \quad (7.28)$$

The poles of (7.28) define the closed-loop dynamics of the system. Stability is ensured if all the poles are in the LHP. These poles can be calculated by:

$$\det[\mathbf{S}^{-1}(s)] = \det[\mathbf{I} + \mathbf{Z}_{sys}(s)\mathbf{K}(s)] = 0 \quad (7.29)$$

To avoid unstable pole-zero cancellations, the determinant in (7.29) is calculated using *matrix fraction descriptions*. Therefore, (7.30) can be rewritten as:

$$\det[\mathbf{S}^{-1}(s)] = \det[\mathbf{Z}_{sys,D}(s)\mathbf{K}_D(s) + \mathbf{Z}_{sys,N}(s)\mathbf{K}_N(s)] = 0 \quad (7.30)$$

Here  $\mathbf{Z}_{sys,D}(s)$ ,  $\mathbf{Z}_{sys,N}(s)$ ,  $\mathbf{K}_D(s)$  and  $\mathbf{K}_N(s)$  are the denominator and numerator matrices of  $\mathbf{Z}_{sys}(s)$  and  $\mathbf{K}(s)$  matrices respectively. Furthermore, let the complex roots of (7.30) be given by  $r_1, r_2, \dots, r_n$ , this leads to a simple representation of the stability criterion as:

$$\Re(r_1, r_2, \dots, r_n) < 0 \quad (7.31)$$

This implies that the real part of the roots of the characteristic equation should be located in the LHP to ensure the system stability.

The second method is based on using the *minor loop gain* of the MIMO system to calculate the eigenfunctions and plot them on the complex plane to get the Nyquist trajectories of the MIMO system. In accordance to earlier explanation, the *minor loop gain* is given by:

$$\mathbf{H}_{mlg}(s) = \mathbf{Z}_{sys}(s)\mathbf{K}(s) \quad (7.32)$$

These eigenfunctions can be calculated as:

$$\det[\mathbf{H}_{mlg}(s)] = \det[\mathbf{Z}_{sys}(s)\mathbf{K}(s)] = \prod_{i=1}^n \Lambda_i(s) \quad (7.33)$$

The possible parametric variations, for the multi-terminal MVDC PDNs under consideration, are given in Table 7.2.

**Table 7.2** Parametric variations for stability tests. Longer cable lengths are considered here to cover both land based and marine MVDC PDNs.

|            |           |             |           |             |           |                      |            |
|------------|-----------|-------------|-----------|-------------|-----------|----------------------|------------|
| <i>CFU</i> | 1 - 20 mF | <i>CBU1</i> | 1 - 20 mF | <i>CBU2</i> | 1 - 20 mF | <i>Cable Lengths</i> | 1 - 5000 m |
|------------|-----------|-------------|-----------|-------------|-----------|----------------------|------------|

**7.4.1 Analysis and Discussion - Case 1**

In the case of one drive remotely connected to the dc-link, the  $Z_N(s)$  and  $Z_D(s)$  can be extracted from (7.16). They are defined as:

$$\mathbf{Z}_{sys,N}(s) = \begin{bmatrix} s^2 LC_2 + sRC_2 + 1 & 1 \\ 1 & s^2 LC_1 + sRC_1 + 1 \end{bmatrix} \quad (7.34)$$

$$\mathbf{Z}_{sys,D}(s) = s(s^2 LC_1 C_2 + sRC_1 C_2 + C_1 + C_2)\mathbf{I}$$

Here  $\mathbf{I}$  is the identity matrix of order  $2 \times 2$ . The matrices  $K_N(s)$  and  $K_D(s)$  are extracted from (7.21) and defined as:

$$\mathbf{K}_N(s) = \begin{bmatrix} (s\tau + 1)(sK'_{pv} + K'_{iv}) - s\frac{P_1}{V_1^2} & 0 \\ 0 & -s\frac{P_2}{V_2^2} \end{bmatrix} \quad (7.35)$$

$$\mathbf{K}_D(s) = s(s\tau + 1)\mathbf{I}$$

Here  $K'_{pv} = K_{pv} \times K_{comp}$  and  $K'_{iv} = K_{iv} \times K_{comp}$ . In order to map the pole movements for the parametric variations listed in Table 7.2, (7.34) and (7.35) are substituted in (7.30) and MATLAB is utilized to calculate the determinant and then correspondingly the roots of the resultant characteristic polynomial. As these roots are the poles of the closed-loop system, they are used to determine the stability of the system. **Fig. 7.6** shows the eigenvalue movements for variations in  $CBU1$ ,  $CBU2$ , and the distribution cable length as listed in Table 7.2. From **Fig. 7.6(a)**, it can be observed that increasing  $CBU1$  from

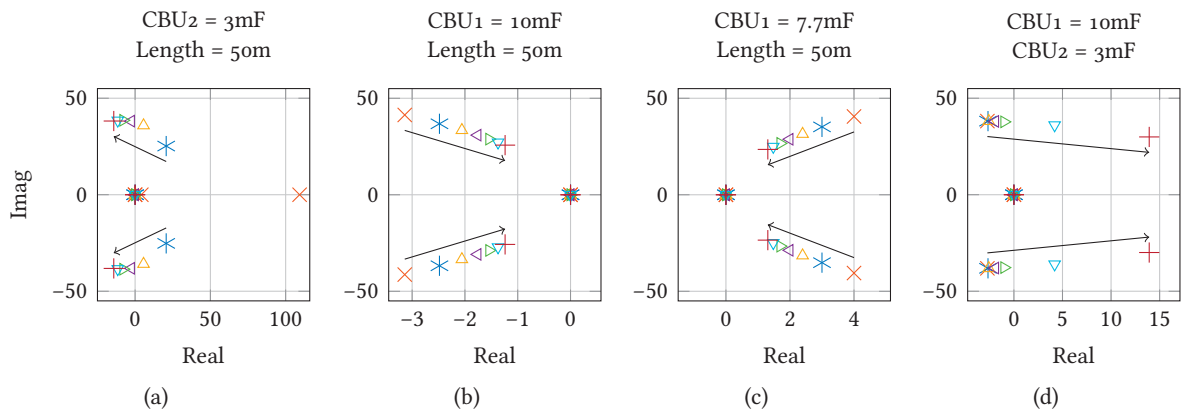


**Figure 7.6** Eigenvalue movements with changes in cable length,  $CBU1$  and  $CBU2$ .  $\times$  represents the lower value of the parameter, while  $+$  represents the highest value. (a)  $CBU1$  variations with fixed  $CBU2$  and cable length. (b)  $CBU2$  variations with fixed  $CBU1$  and cable length for a stable configuration. (c)  $CBU2$  variations with fixed  $CBU1$  and cable length for an unstable configuration. (d) Distribution cable length variations with fixed  $CBU1$  and  $CBU2$ .

1 mF to 20 mF has a positive affect on the system stability and the eigenvalues move towards LHP. As explained in *Chapter 5*,  $CBU_1$  directly impacts the tuning of the voltage controller of the ARU and thus impacts stability the most. Additionally, it can be seen from **Fig. 7.6(b)** and **Fig. 7.6(c)** that the  $CBU_2$  variations have minimal impact on the stability of the system for both stable and unstable system configurations. In **Fig. 7.6(d)** the impact of distribution cable is shown, and it can be observed that increasing cable lengths increases the distribution inductances in the system, therefore, causing instability in the system.

**Fig. 7.7** alternatively shows the impact on the stability of the system in terms of Nyquist trajectories on complex plane. This helps representation of dominant poles more effectively, while avoiding poles at origin. As can be seen from **Fig. 7.7**, there are two eigenfunctions defining the dynamic behavior of case 1<sup>2</sup>. The blue trajectory represents the first eigenfunction  $\Lambda_1$  and it can be seen that it exits the unit circle, therefore, it can be considered the dominant eigenfunction. In order to declare a system absolutely unstable, the trajectories are expected to encircle the critical point of (-1,0). However, from **Fig. 7.7**, it can be observed that there are no visible encirclements. In this scenario to test for the system stability *conformal mapping* property of Nyquist trajectories can be applied [132]. This property is briefly explained here.

The Laplace variable  $s$  can be defined as:

$$s = \sigma + j\omega \quad (7.36)$$

Applying (7.36) to (7.34), the *minor loop gain* of MIMO system can be expressed as:

$$\mathbf{H}_{mlg}(\sigma, \omega) = \mathbf{H}_{\Re,mlg}(\sigma, \omega) + j\mathbf{H}_{\Im,mlg}(\sigma, \omega) \quad (7.37)$$

This implies that the eigenfunction  $\Lambda_1$  becomes:

$$\Lambda_1(\sigma, \omega) = \Lambda_{\Re,1}(\sigma, \omega) + j\Lambda_{\Im,1}(\sigma, \omega) \quad (7.38)$$

For absolute stability of the system, the Nyquist trajectories plotted using (7.37) and crossing unit circle must have stable eigenfunction for every frequency. In order to calculate poles visually from **Fig. 7.7**, the following expression can be used:

$$\sigma_1 = \Delta\omega \frac{\Lambda_{\Im,1}(\omega_1)}{\Lambda_{\Re,1}(\omega_1) - \Lambda_{\Re,1}(\omega_1 - \Delta\omega)} \quad (7.39)$$

Here  $\sigma_1$  represents real part of the eigenfunction, while  $\omega_1$  is the corresponding imaginary part and  $\Delta\omega$  is frequency step between two consecutive data points. Now, from **Fig. 7.7(a)**, it can be observed that low value of  $CBU_1$ , i.e., 7 mF,  $\Lambda_1$  lies in the II-quadrant and by applying (7.39), it can be seen that the real part of eigenfunction is positive. This implies that the system is unstable for this system configuration. For the other two system configurations of  $CBU_1$ , i.e., 10 mF and 15 mF, the real part of the eigenfunction is negative, implying that the system absolutely stable. From extension of this concept to **Fig. 7.7(b)** and **Fig. 7.7(c)**, it can be observed that  $CBU_2$  has minimum impact on the system stability, whereas, long distribution cable lengths, i.e., 5 km<sup>3</sup>, cause instabilities in the system.

<sup>2</sup>The mathematical expressions of these eigenfunctions are not given, in the thesis, as they are highly complex and do not provide any useful information visually.

<sup>3</sup>Emulation of distribution lengths for industrial grids.



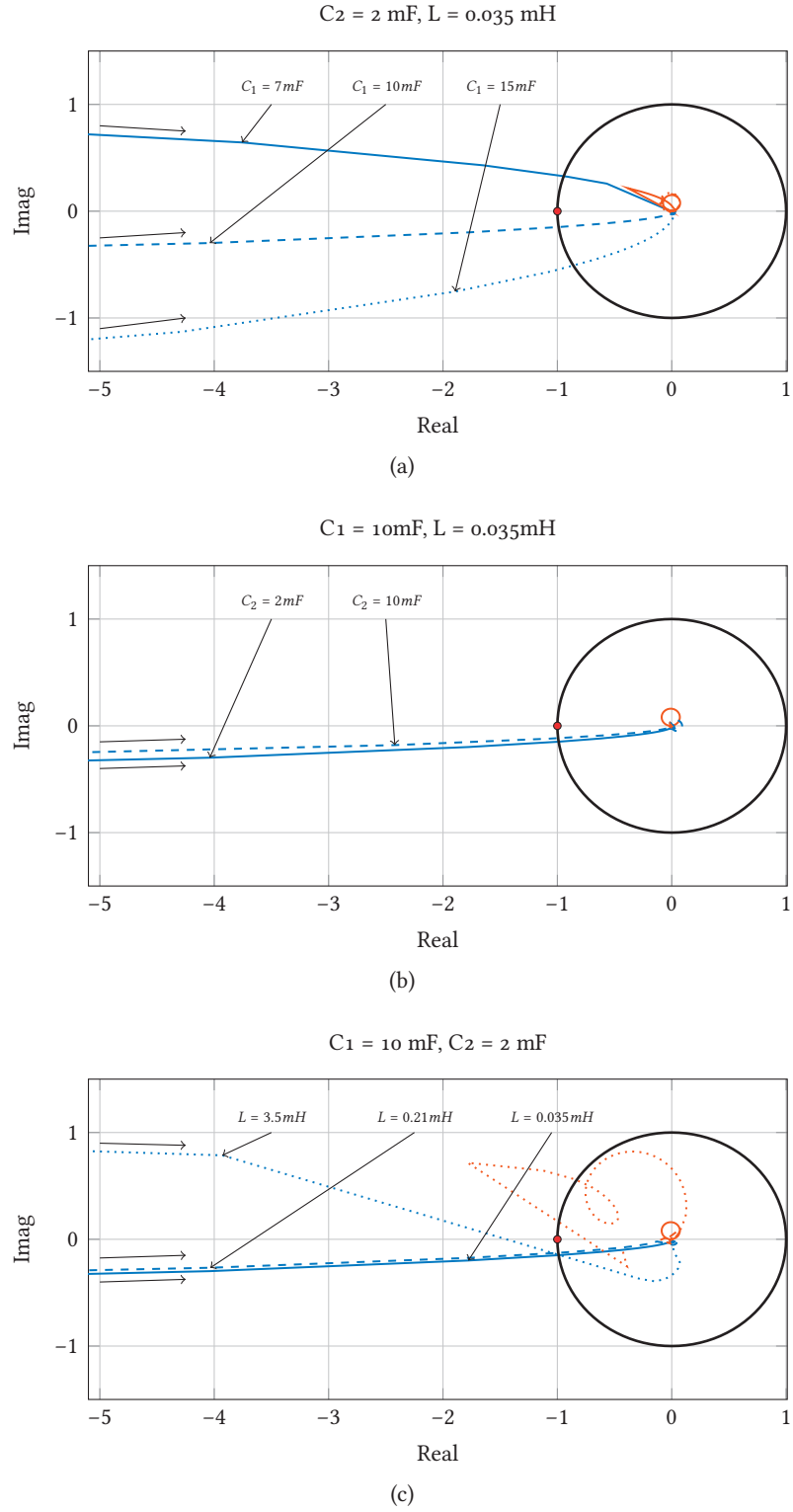


**Figure 7.7** Multi-variable Nyquist trajectories for case 1. The arrows on the figures show the direction of the trajectory for increase in frequency. (a) Variations in  $CBU_1$  (7 mF, 10 mF, 15 mF). (b) Variations in  $CBU_2$  (2 mF, 10 mF). (c) Variations in distribution cable length (10 m, 300 m, 5 km).

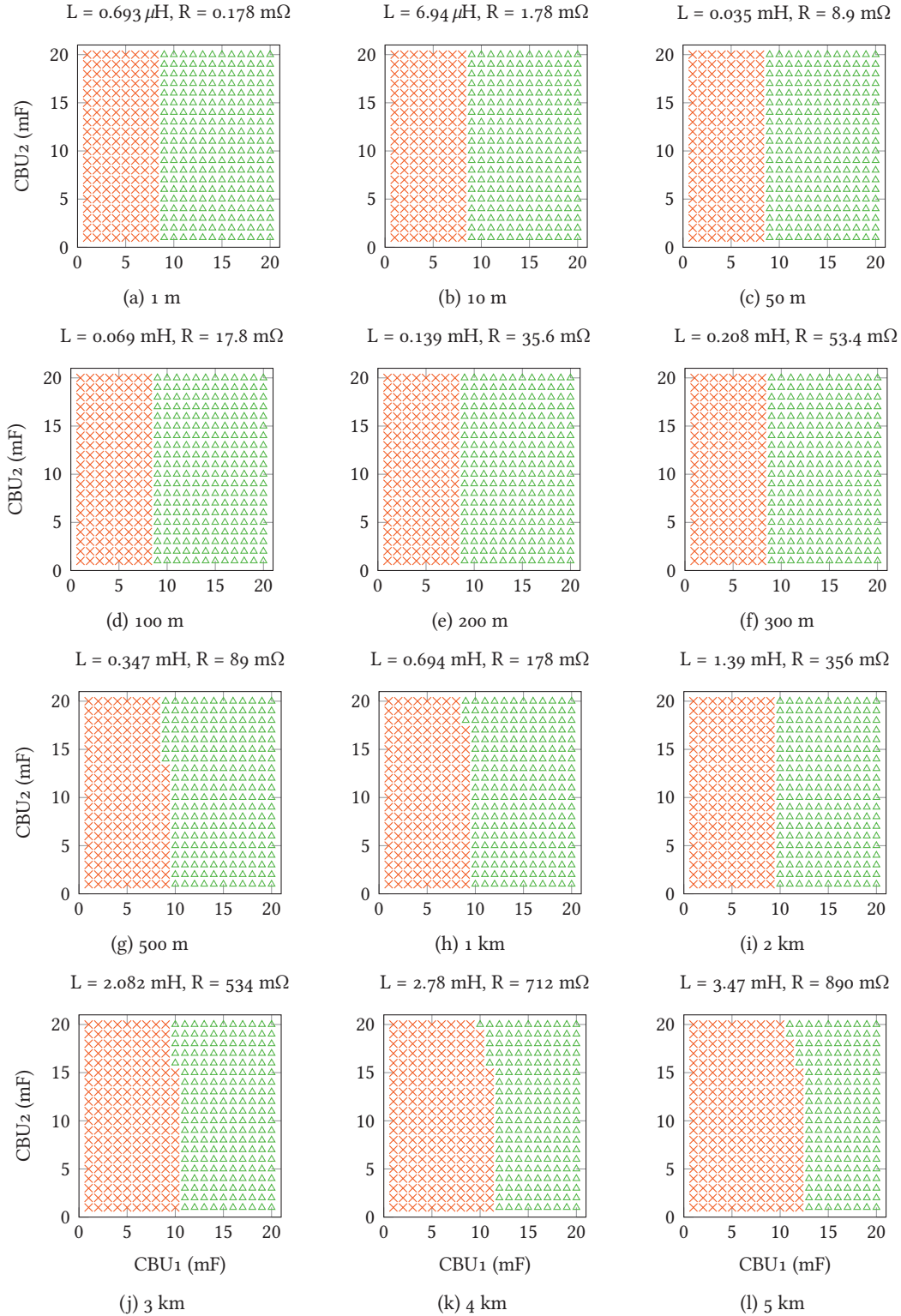


**Figure 7.8** Impact of filter capacitors and cable length on system stability:  $\times$  for unstable and  $\Delta$  for stable configurations respectively.

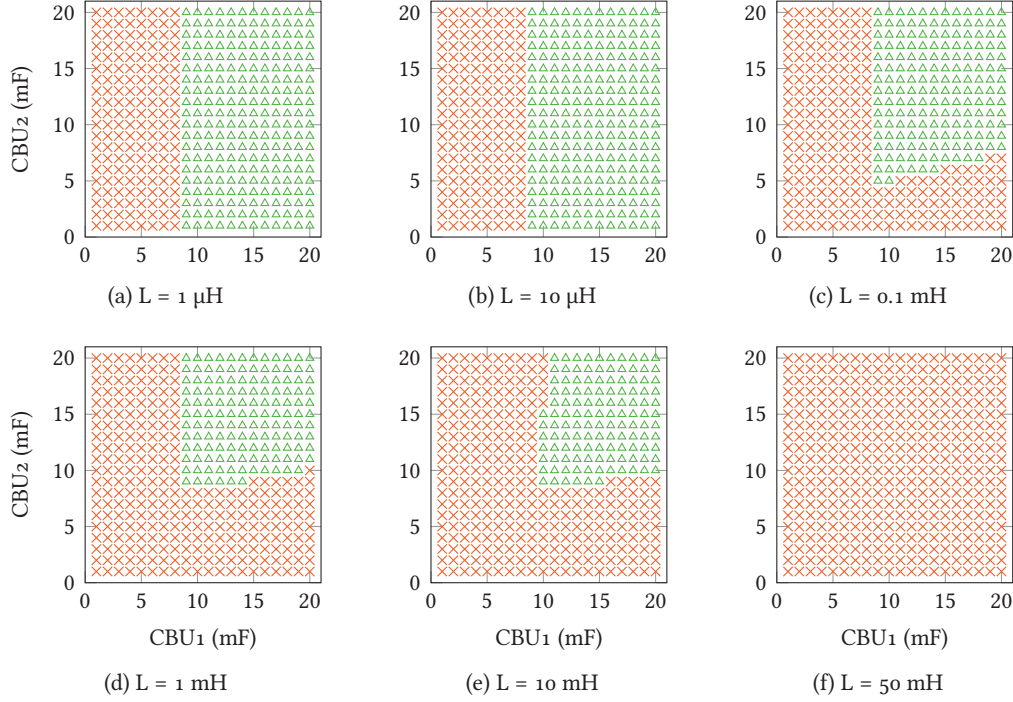


**Figure 7.9** Impact of inductance on the system stability with small  $R_{cable} = 0.1 \text{ m}\Omega$ :  $\times$  for unstable and  $\Delta$  for stable configurations respectively.

The variations in  $CBU_1$ ,  $CBU_2$  and cable length are used to determine which system configurations lead to an overall unstable system. **Fig. 7.8** shows the possible stable and unstable states for the parametric variations of Table 7.2. The stability of the system configurations is directly dependent on  $CBU_1$  and this can be observed from **Fig. 7.8(a)**-**Fig. 7.8(f)**. Here the cable length is varied from 1 - 300 m and  $CBU_2$  from 1 - 20 mF, but these two have very little impact on the system stability. As given in [105],  $K_{pv} = a_d CBU_1$  (here  $a_d$  is the bandwidth of the voltage controller and is approximately 1/50 times switching frequency), another observation is made from these results that whenever  $K_{pv}$  is greater than the sum of  $-P_1/V_1$  and  $-P_2/V_2$ , condition (7.31) is true and the system is stable. This new condition for system stability follows the system stability dependence directly on  $CBU_1$ , when  $a_d$  is constant, and can be expressed as:

$$\text{trace}[\mathbf{K}(0)] > 0 \quad (7.40)$$

This condition is true for cable lengths upto 300 m, where damping from the  $R$  is high. Once the cable length is increased beyond 300 m, the impact of  $L$  and  $CBU_2$  becomes more and more apparent, as can be seen from **Fig. 7.8(g)**-**Fig. 7.8(l)**. This fact is further illustrated in **Fig. 7.9**. Here, it can be clearly observed that very high  $L$  causes higher instability in the system and higher  $CBU_2$  is required to mitigate this instability. These impacts are further verified in time domain simulations.

#### 7.4.2 Analysis and Discussion - Case 2

The dynamic analysis of the system, given in **Fig. 7.2(b)**, is similar to the earlier described case. Here, again the numerator and denominator matrices of  $\mathbf{Z}_{sys}(s)$ , (7.25), and  $\mathbf{K}(s)$ , (7.27), are calculated to

perform the *matrix fraction descriptions*. This is done using MATLAB and then (7.31) is applied and the roots are calculated for the resultant characteristic equation, which gives the actual poles of case 2.

In order to understand the impact of different passive elements on the system stability, the parametric variations given in Table 7.2 are utilized. The pole movements directly resulting from these parametric variations are illustrated in **Fig. 7.10**. It can be seen from **Fig. 7.10(a)** that once again filter capacitance  $CFU$ , used for tuning the voltage control of the rectifier  $K_{pv} = a_d CFU$ , plays the biggest role in determining the system stability. The other parameters,  $CBU_1$ ,  $CBU_2$  and cable lengths, have the least impact on the system stability. These observations lead to the condition specified in (7.40), that a properly tuned  $K_{pv}$  and sized  $CFU$  ensure stability. Similar conclusions can be drawn from **Fig. 7.11**. Here it can be observed that  $CFU$  is the most critical among all the system parameters and directly impacts the ability of voltage control to damp the resonances and maintain the dc-side voltage. The inverter filter capacitors  $CBU_1$  and  $CBU_2$  have minimal impact on stability. The distribution cables cause instability for long lengths, i.e., above 2 km, as they introduce high inductance.

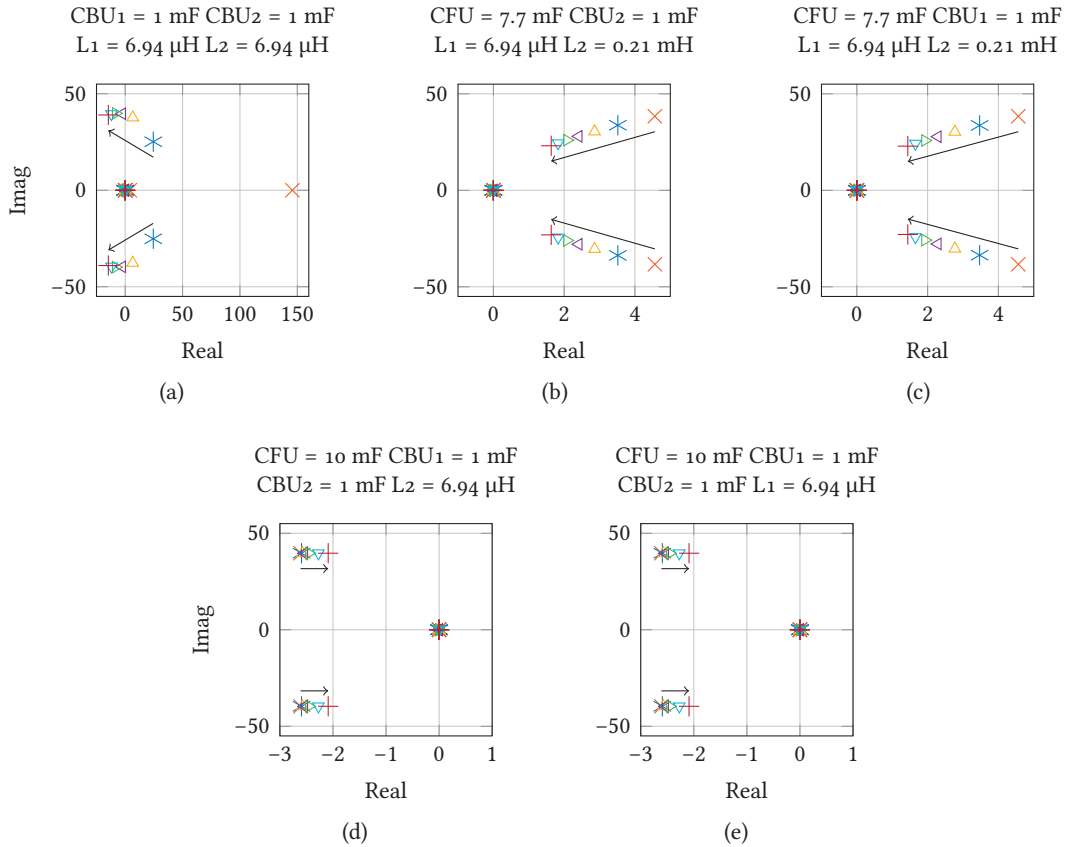


**Figure 7.10** Eigenvalue movements with changes in cable lengths,  $CFU$ ,  $CBU_1$  and  $CBU_2$ . 'x' represents the lower value of the parameter, while '+' represents the highest value. (a)  $CFU$  variations with fixed  $CBU_1$ ,  $CBU_2$  and cable lengths at 10 m. (b)  $CBU_1$  variations with fixed  $CFU$ ,  $CBU_2$  and cable lengths at 10 m and 300 m. (c)  $CBU_2$  variations with fixed  $CFU$ ,  $CBU_1$  and cable lengths at 10 m and 300 m. (d) and (e) variations in cable lengths from 10 m to 300 m with fixed  $CFU$ ,  $CBU_1$  and  $CBU_2$ .

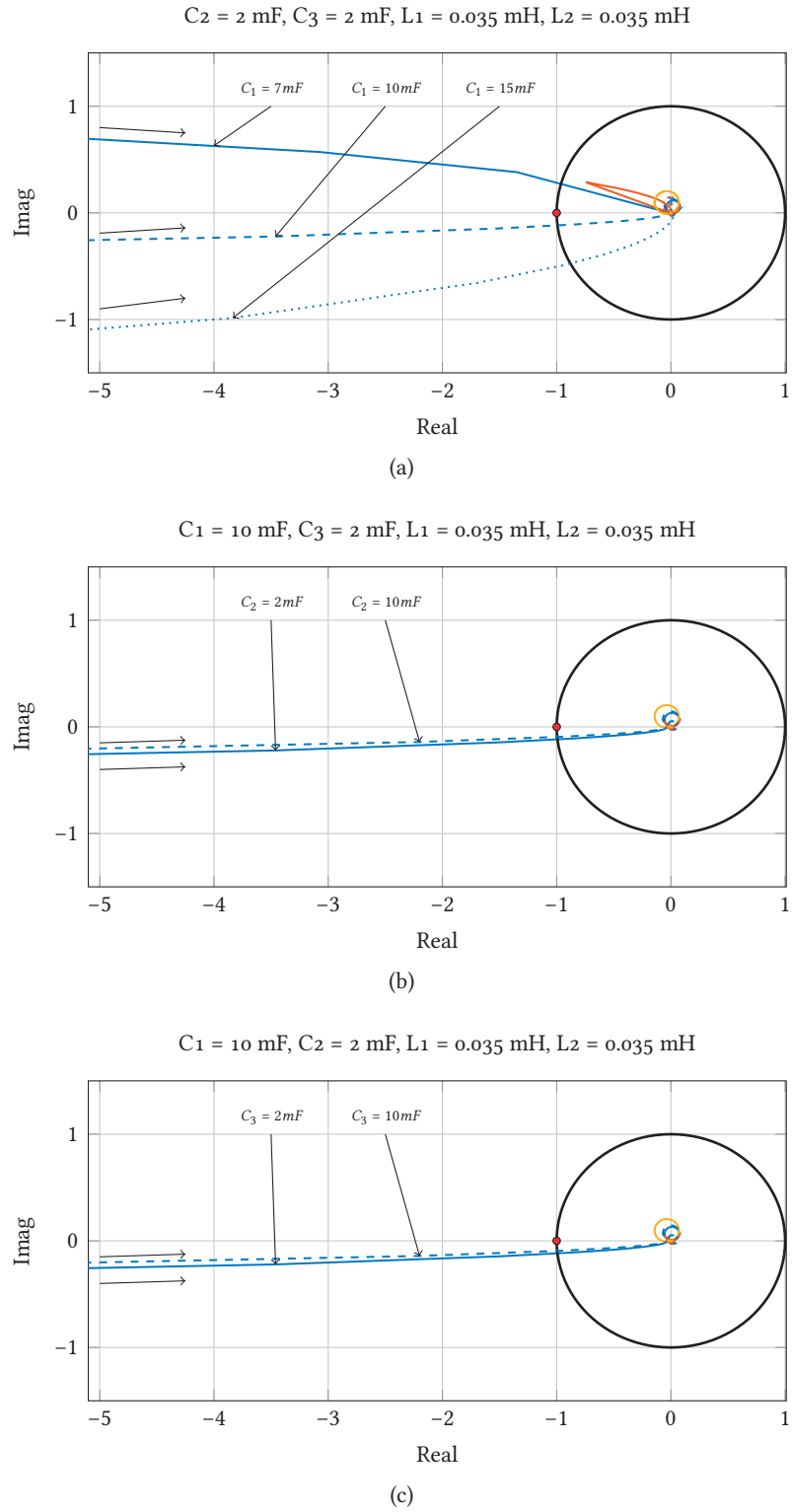


**Figure 7.11** Multi-variable Nyquist trajectories for case 2 - part 1. The arrows on the figures show the direction of the trajectory for increase in frequency. (a) Variations in *CFU* (7 mF, 10 mF, 15 mF). (b) Variations in *CBU1* (2 mF, 10 mF). (c) Variations in *CBU2* (2 mF, 10 mF). (d) & (e) Variations in distribution cable lengths (10 m, 300 m, 5 km).

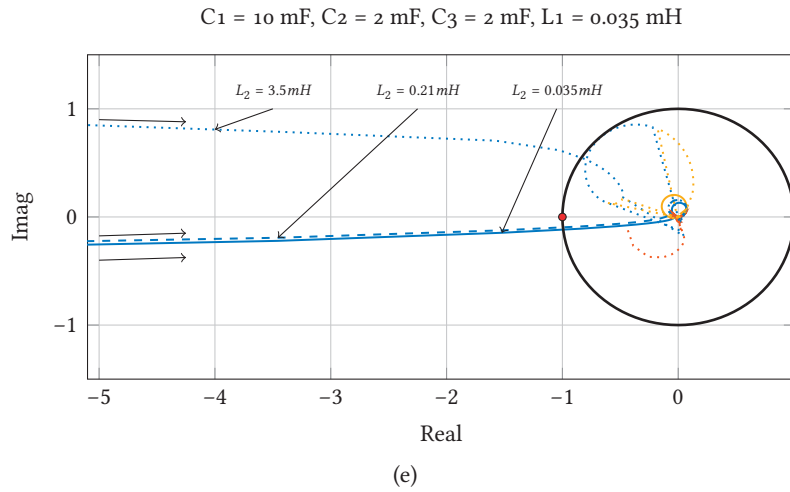
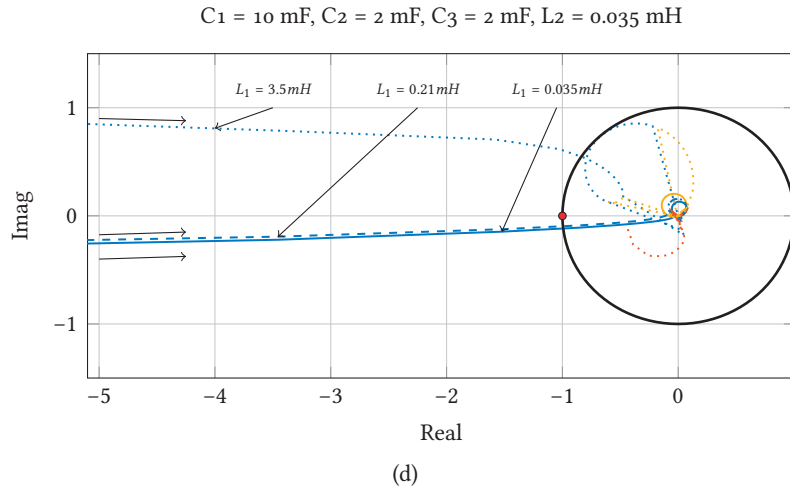


**Figure 7.11** Multi-variable Nyquist trajectories for case 2 - part 2. The arrows on the figures show the direction of the trajectory for increase in frequency. (d) & (e) Variations in distribution cable lengths (10 m, 300 m, 5 km).

**Fig. 7.12** shows stable and unstable system configurations for a few representative cases. As the dimensionality of the system is higher, compared to the previous case, thus **Fig. 7.12** shows only variations of  $CBU_1$  and  $CBU_2$ , while fixed values are considered for  $CFU$  and cable lengths. It can be seen that the properly sized  $CFU$  is required to maintain system stability. In this case, as both drives are fed remotely through cables, the voltage drop along these cables increases the load admittances and, therefore, a slightly higher  $CFU$  is required to maintain system stability, for the same  $a_d$ . Impact of high inductance of the cable is expected to be similar to the first case and is, therefore, not explored here. A summary of stable system configurations is given in Table 7.3 for cable lengths upto 300 m (300 m is chosen to emulate only the expected industrial MVDC distribution).

*Note:* Equation (7.40) is valid for both cases, given that there is only one dominant eigenfunction (modeling impact of  $CBU_1/CFU$  for case 1/case 2.)

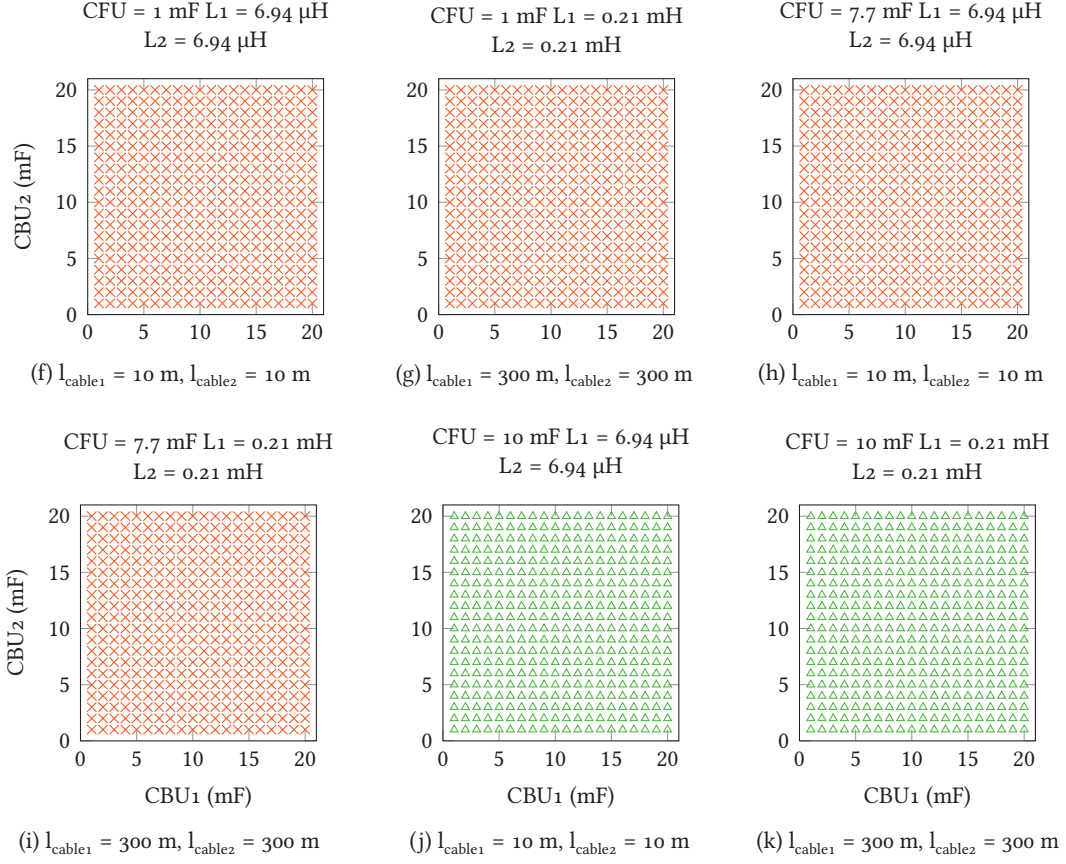


**Figure 7.12** Impact of filter capacitors and cable length on system stability:  $\times$  for unstable and  $\triangle$  for stable configurations respectively.

**Table 7.3** Stable configurations for the system with two drives connected remotely.

| <i>Parameter</i>       | <i>Variations</i> |
|------------------------|-------------------|
| <i>CFU</i>             | 10 - 20 mF        |
| <i>CBU<sub>1</sub></i> | 1 - 20 mF         |
| <i>CBU<sub>2</sub></i> | 1 - 20 mF         |
| <i>Cable Lengths</i>   | 1 - 300 m         |

## 7.5 Time Domain Simulation

The time domain simulations, using average converter models, for the systems shown in **Fig. 7.2(a)** and **Fig. 7.2(b)** are given in **Fig. 7.13** and **Fig. 7.14**, respectively. These simulations are carried for different configurations. For the case 1, it can be seen from **Fig. 7.13** that higher *CBU<sub>1</sub>* results in stable response for different loading conditions, as can be observed from **Fig. 7.13(a)** where the system configuration is *CBU<sub>1</sub>* = 10 mF, *CBU<sub>2</sub>* = 3 mF and cable length is 50 m. The system configuration of *CBU<sub>1</sub>* = 7.7 mF, *CBU<sub>2</sub>* = 3 mF and 50 m cable length, with time domain results shown in **Fig. 7.13(b)**, is expected to be unstable, from the analysis presented above, but it shows slightly longer settling times

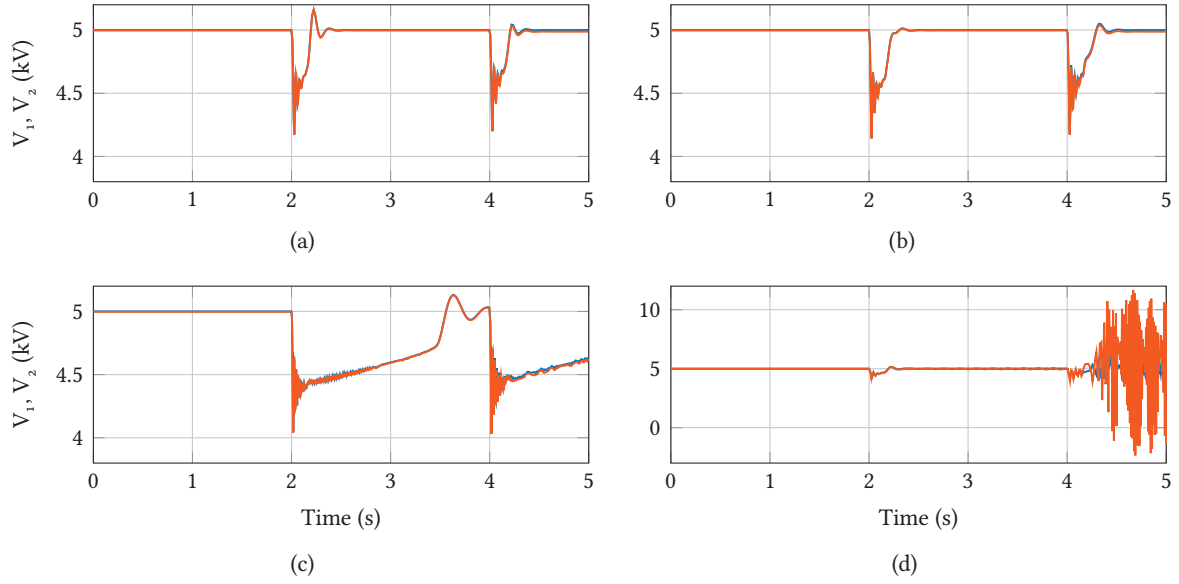


**Figure 7.13** Case 1: **Fig. 7.2(a)**. Time domains simulations for load changes from 25% load to 62.5% at 2 s and 100% at 4 s. Here  $V_1$  and  $V_2$  are the two variables presented. (a)  $CBU1 = 10$  mF,  $CBU2 = 3$  mF and  $l_{cable} = 50$  m. (b)  $CBU1 = 7.7$  mF,  $CBU2 = 3$  mF and  $l_{cable} = 50$  m. (c)  $CBU1 = 1$  mF,  $CBU2 = 3$  mF and  $l_{cable} = 50$  m. (d) Impact of high cable inductance  $CBU1 = 10$  mF,  $CBU2 = 3$  mF and  $L_{cable} = 2.5$  mH.

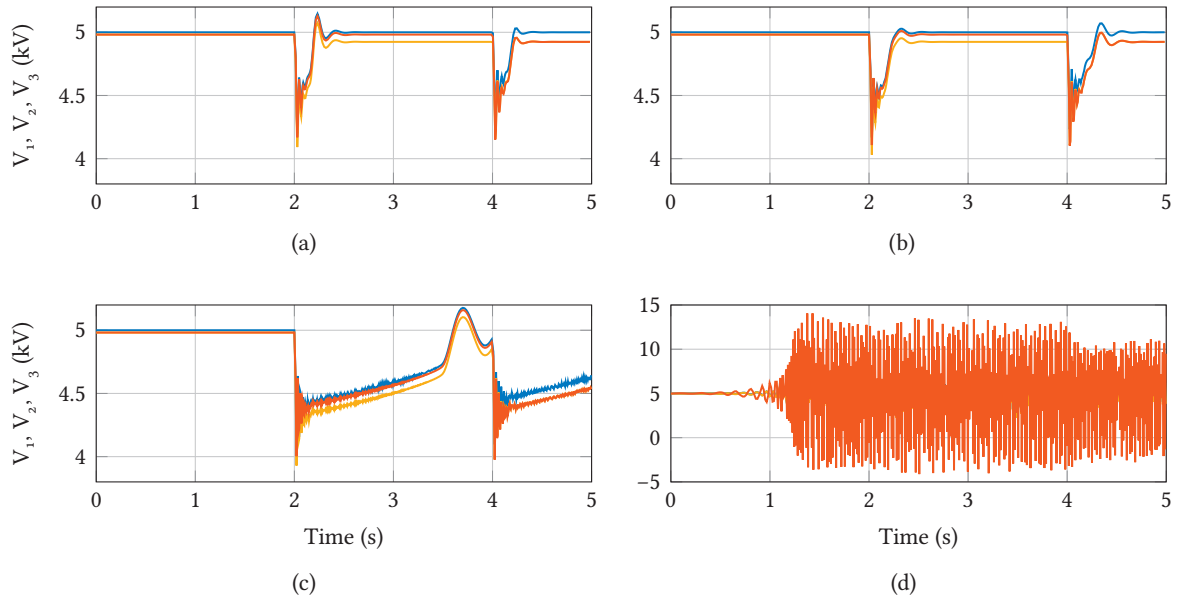


**Figure 7.14** Case 2: **Fig. 7.2(b)**. Time domains simulations for load changes from 25% load to 62.5% at 2 s and 100% at 4 s. Here  $V_1$ ,  $V_2$  and  $V_3$  are the three variables presented. (a)  $CFU = 10$  mF,  $CBU1 = 3$  mF,  $CBU2 = 3$  mF,  $l_{cable1} = 300$  m and  $l_{cable2} = 300$  m. (b)  $CFU = 7.7$  mF,  $CBU1 = 3$  mF,  $CBU2 = 3$  mF,  $l_{cable1} = 300$  m and  $l_{cable2} = 300$  m. (c)  $CFU = 1$  mF,  $CBU1 = 3$  mF,  $CBU2 = 3$  mF,  $l_{cable1} = 300$  m and  $l_{cable2} = 300$  m. (d)  $CFU = 10$  mF,  $CBU1 = 3$  mF,  $CBU2 = 3$  mF,  $L_{cable} = 0.21$  mH and  $L_{cable2} = 3.5$  mH.



but stable behavior. One of the possible reasons is that the representation of the source admittance in (7.18) is not equal to the actual source admittance, due to the simplification of cascaded control and the stability is overestimated.

The system configuration of  $CBU_1 = 1$  mF,  $CBU_2 = 3$  mF and 50 m cable length, simulation shown in **Fig. 7.13(c)**, is also expected to be unstable but it only shows quite long response time compared to **Fig. 7.13(a)** and **Fig. 7.13(b)**. This is possible due to the introduction of stable poles by the PLECS's stiff solver [133]. **Fig. 7.13(d)** shows the time domain response for the system with high  $L$ , i.e.,  $CBU_1 = 10$  mF,  $CBU_2 = 3$  mF,  $L = 2.5$  mH and  $R = 0.1$  m $\Omega$ . Here, it can be observed that the system is highly unstable for very large  $L$ .

As the first drive is connected far from the rectifier, therefore, three voltages are observed in **Fig. 7.14**. Similar results to the first case, **Fig. 7.2(a)**, are expected for **Fig. 7.2(b)** and can be seen in **Fig. 7.14**. Higher  $CFU$  implies faster response of voltage control, while higher inductance, in either cable, leads to instability.

## 7.6 Summary

In this chapter, modeling and analysis of a multi-terminal MVDC PDN is presented. State space modeling techniques have been used to model the small signal dynamics of the system and the resulting MIMO model is analyzed using *eigenvalue analysis* and *multi-variable Nyquist Criteria*. ARU is considered as the source converter to simplify and highlight the different advantages of the MIMO analysis.

Two different multi-terminal MVDC PDNs are analyzed here. The first system considers two inverter drives supplied by a common ARU with one of them directly connected to the source, while the other is connected through a cable. In the second case, a generalized representation with both drives connected through cables. The system models, using state space techniques, are then used to calculate the eigenvalues of the systems and also plot multi-variable Nyquist trajectories, which are in turn used to analyze the stability of the system. For stability, the eigenvalues must be placed in the LHP. A parametric sweep of different passive elements is used to determine the stable and unstable system configurations. It is found that the proper selection of rectifier filter and tuning of voltage control of rectifier play significant role in determining the stability of the system. Furthermore, very high inductance in cable ( $\approx 0.25$  mH) introduces low frequency resonances which lead to system instability. Time domain simulations are carried out in PLECS. The models verify the approach, with some minor divergences, clearly identified as the damping introduced by the simulation solver.

### 7.6.1 Future Work

The model generated for the multi-terminal MVDC PDN, based on the assumptions given earlier, can be further complicated by considering DRU, TRU and MMCs as source converters. These converters have a nonlinear behavior and would require appropriate linearization to be modeled as linearized source admittances. Furthermore, the state space model allows the introduction of 'voltage droop control' for a multiple source system. In this case, proportional gain of the ARU voltage control with droop gain are sufficient to model this effect. In addition to consideration of different source

converters, higher order system, e.g., MVDC PDN of **Fig. 5.3** can be utilized. Reduction methods can be applied on this higher order state space model to represent it as a reduced system by underlining the dominant poles or dominant eigenfunctions.

# 8

## Conclusions and Future Work

### 8.1 Summary and Contributions

With improvements in the power electronic technologies, MVDC PDNs are gaining interest for high power industrial installations. One particular area of interest is the ship on-board PDNs, where MVDC PDNs are expected to support higher fuel savings, energy density and flexibility in the system design. The implementation of the MVDC PDNs, albeit with various commercial benefits, face different technological challenges, e.g., lack of commercial standalone MVDC equipment, lack of dc breakers, lack of dc-dc converters, lack of real world multi-terminal MVDC PDNs and the subsequent absence of MVDC PDN stability studies, to name a few. Various literature can be found that target different challenges and also propose new technologies for the implementation of MVDC PDNs. However, the first adopters of the MVDC PDNs are expected to utilize the available commercial technologies. With this consideration, this thesis aims to identify and propose solutions for some of the challenges arising from the implementation of the MVDC PDN with focus on the main power chain.

Different commercial technologies are part of the main power chain and it is important to analyze their possible role in the future MVDC PDN. In this regard, *Chapter 2* provides a critical review of the commercially available technologies, for the main power chain, used at the moment in the MVAC PDNs and few of the technologies proposed in the literature for the future MVDC PDNs. It is seen that for these technologies to be utilized in the MVDC PDNs, the equipment layouts will have to be shuffled and additional functionality will be required from them. One such example is the VSD, as it will now be effectively spread across the complete system. Each of the subsystems, such as rectifiers, filters and inverters of the VSDs, will have an impact across the whole PDN, in contrast to the MVAC PDN, where they are galvanically isolated from the PDN by the LF VCTs.

Building on the critical review and considering the expected benefits from MVDC PDNs, *Chapter 3* analyzes the evolution of the state-of-the-art MVAC PDNs, of two real world cases (*LNG tanker* and *drill ship*), into the future MVDC PDNs. From this analysis, it is clear that despite the advantages of MVDC PDN, the transformation from MVAC to MVDC is not straightforward. It is highly influenced by the power requirements and the functionality of the ship. Two different PDNs are proposed here for implementation of the MVDC PDN. The first one is a hybrid between MVAC and MVDC PDNs, it is less invasive and ensures removal of LF VCTs, but does not provide any fuel savings. The second one is a full blown MVDC PDN that ensures all benefits from the dc distribution, but it requires development of new technologies, e.g., dc-dc converters, protection-coordination for MVDC PDNs, and so on. All in all, the absence of technologies in different parts of the system is a hurdle in the full realization of the MVDC PDN.

One of the challenges, identified by the discussions and analyses of *Chapter 2* and *3*, is the expected

removal of LF VCTs that opens up both challenges and opportunities for the realization of high quality MVDC supplies. In *Chapter 4*, possible MVDC supply configurations are discussed and multi-phase multi-pulse configurations are chosen to ensure high quality MVDC supplies. The concept of multi-phase multi-pulse supplies is explored further by presentation of two possible MVDC supplies, namely the parallel and series connection of rectifiers. Between these, the multi-pulse parallel rectifiers increase the redundancy and fault tolerance of the system, while the multi-pulse series rectifiers bring flexibility in the selection of voltage classes of the generators and the motors in the system. These supplies are also expected to ensure fuel efficiency, which can be achieved by utilizing medium speed ICEs (operated in DAC mode) as the prime movers that are driving multi-phase SMs. To achieve high quality MVDC supplies, a DRU sub-module is designed, with commercially available diodes, for these multi-pulse rectifiers that can withstand the thermal load of the normal operation and also the initial fault currents for dc-side faults but requires fast fuses for clearing faults. This sub-module can be arranged in parallel and series configurations to achieve multi-pulse parallel and multi-pulse series rectifiers, respectively. The selection of either multi-pulse parallel or series rectifiers depends on the system designers, the requirements and the function of the vessels and the availability of appropriate equipment.

Another broad challenge analyzed in this thesis, for implementation of the MVDC PDNs, arises from the presence of CPLs in the MVDC PDNs and their implication on the stability of the PDNs. In this regard, *Chapter 5* provides an assessment of the dynamic interactions of the source-load subsystems considering contributions from the generator inductances, dc-side capacitances, impact of cables, and the control strategies of source and load sides (CPL behavior). This analysis provides valuable insights about the dynamics of the marine MVDC PDNs. Using linearization techniques and small signal modeling, the PDN is reduced to a two-port MVDC PDN and the sources and loads are modeled as impedances and admittances. Impedance stability criterion is then utilized and corresponding Nyquist trajectories are plotted to extract proper figures of merit. This SISO assessment showed that increase in the source-side inductance and the decrease in the capacitive filtering can lead to an unstable behavior. Additionally, the insights from this assessment can support in designing the system with desired dynamic performances by aiding in proper tuning of the control parameters, and sizing of filters and selection of the other passive components.

The three different analyzed rectifiers, i.e., DRU, TRU and ARU, have their own advantages and disadvantages. DRU is simple and inexpensive, but requires the AVR of the generator to maintain dc-side voltage. The TRU provides limited controllability of the dc-side voltage and also can interrupt fault currents, but has reduced dynamics due to the *LC* filter at its output. Finally, the ARU offers a better dynamic response near rated conditions, but is sensitive to changes in the filtering effort, cables, and interaction between load and source leading to unstable behavior and also is more complex and expensive. The choice among the three would be dependent on the system designer and the requirements of high bandwidth dynamics of the source, cost, and reliability.

The analysis of *Chapter 5* is extended in *Chapter 6* to discuss the dynamic interactions between an MMC and bandwidth limited CPLs, in a two-port MVDC PDN setting. MMCs have bigger footprint and complex control structure and may not be the first choice for ship on-board MVDC PDNs, but they are one of the prime candidates for land based MVDC PDNs. To carry out the assessment of this system, a realistic and detailed control that includes dc-side voltage control, horizontal and vertical energy balancing, circulating current control and line current control is used for the MMC rectifier. This detailed control coupled with inverter filter and distribution cables shape the source-side

impedance. From the assessment, it was seen that longer cables and lower filtering efforts have a negative impact on the stability of the PDN, but the superior dynamics of the MMC ensure good dynamic performance.

The stability analysis presented in *Chapter 5* and *6* is based on small signal modeling and SISO analysis. It provides a good benchmark for analyzing stability, however, it is dependent on the proper partitioning of the system into source and load subsystems and also the steady state operation point. The real MVDC PDNs are expected to be multi-terminal and it would be necessary to analyze the interactions of various sources and loads. SISO analysis does not cover this aspect and, therefore, a MIMO analysis is required. MIMO analysis is presented in *Chapter 7* that is independent from the groupings and partition point, and also the operation point of the system. Multi-terminal MVDC PDNs are modeled using state space techniques and analyzed using eigenvalue analysis and multi-variable Nyquist Criteria. ARU is considered as the source converter to simplify and highlight the different advantages of the MIMO analysis. The state space models are used to calculate the eigenvalues of the systems and also plot multi-variable Nyquist trajectories. These methods analyze the impact of the variations in the different components on the system stability. It was concluded that the reduction in source-side filtering and increase in the distribution cable lengths adversely impact the system stability. Furthermore, unstable system configurations are highlighted, which can play an important role when designing the system for desired dynamic performance.

## 8.2 Overall Conclusion

From the work presented in the thesis and experience gained by the author, it can be concluded that to make MVDC PDNs a reality a few technological developments are required for full exploitation of the expected benefits. However, many commercial technologies can either be used directly or with few modifications in the future MVDC PDN. The prime example of this is the high power VSD that will be distributed over the whole PDN. Another opportunity from MVDC PDNs is to consider multi-phase machines as generators. Additionally, from the system stability point of view, with proper sizing of filters and selection of distribution cables, good dynamic performance and reliable operation of PDN can be assured.

## 8.3 Future Work

The thesis work opens up new avenues on both MVDC PDN development and implementation, and stability analysis. With respect to MVDC PDN development and implementation, different technological developments are required, however, some of these are key to full exploitation of these PDNs:

- High power dc-dc converters, for interface between LVDC and MVDC.
- Integration of energy storage.
- MVDC breaker.
- Protection-coordination of the MVDC PDN.

All these require further research and development efforts.

On the stability analysis presented in this thesis, it would be of interest to carry out experimental verification of the findings on MV setup. This would pave way for practical implementation of the MVDC PDNs. Additionally, the MIMO stability analysis presented here can be further enhanced by considering DRU, TRU and MMC admittances to map the impact of these converters. In case of multiple source converters, droop control can be also be added to the state space model of the system. The consideration of more than three nodes, will increase the mathematical load of this analysis. As the system produces sparse matrices, it would be of interest to utilize model reduction methods to identify the dominant eigenfunctions/eigenvalues. This identification can lead to simpler representation of the system and reduce the mathematical load. Another level of complexity that can be considered is the generalized state space representation of the system. This representation can introduce the switching harmonics (also its multiples) of the converters in the analysis. This can lead to identification of impact of these harmonics.

# A

## Time Domain Models

Here, time domain models of the different converters used in this thesis are given.

### A.1 DRU time domain model

The DRU model given in PLECS is used as such and arranged in different configurations for three-phase, six-phase and nine-phase generators used in the thesis. The schematics of the different time domain simulation models are given in **Fig. A.1**.

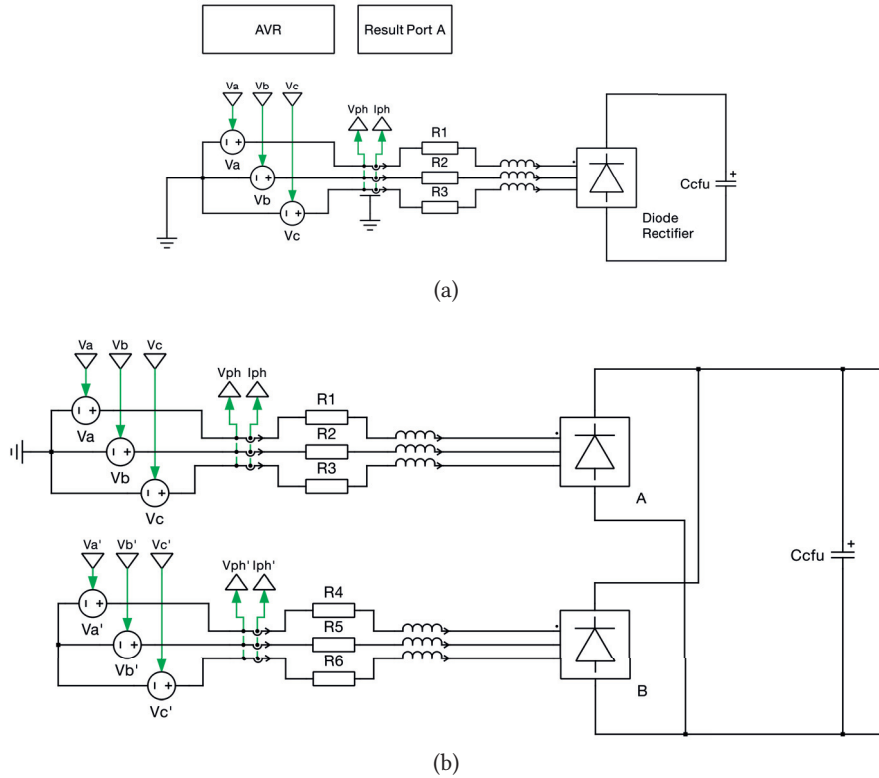


**Figure A.1** (a) Three-phase, six-pulse arrangement. (b) Six-phase, twelve-pulse parallel arrangement.

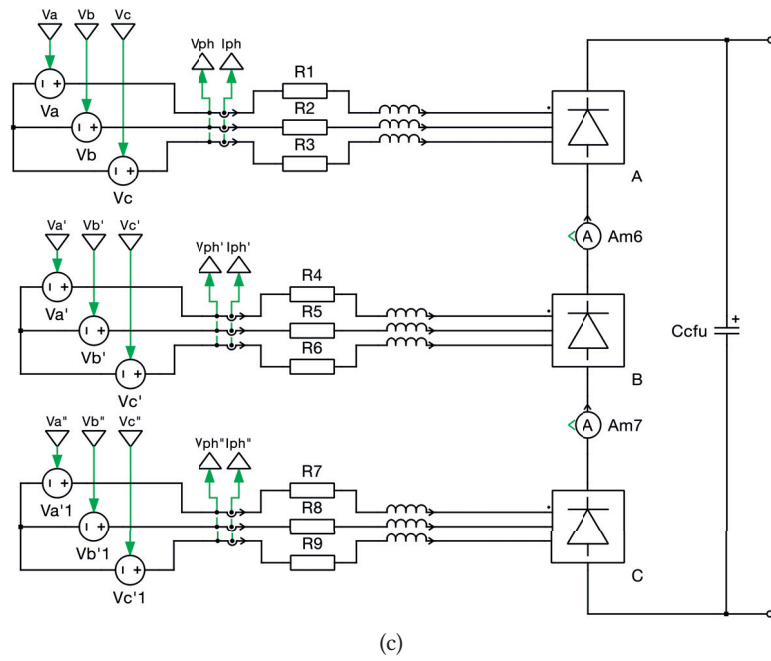


**Figure A.1** (c) Nine-phase, eighteen-pulse series arrangement.



## A.2 TRU time domain model

The TRU model is made from discrete components given in PLECS. The schematics of the six-pulse TRU and its control are given in **Fig. A.2**.

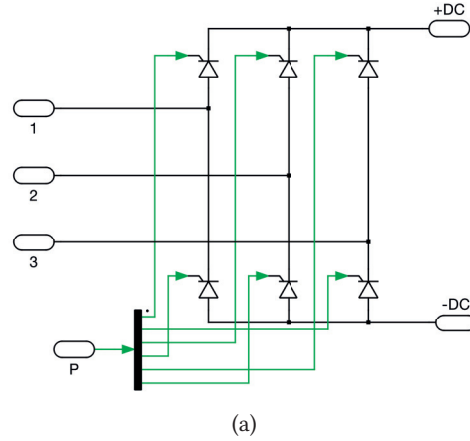


**Figure A.2** (a) Three-phase, six-pulse arrangement.

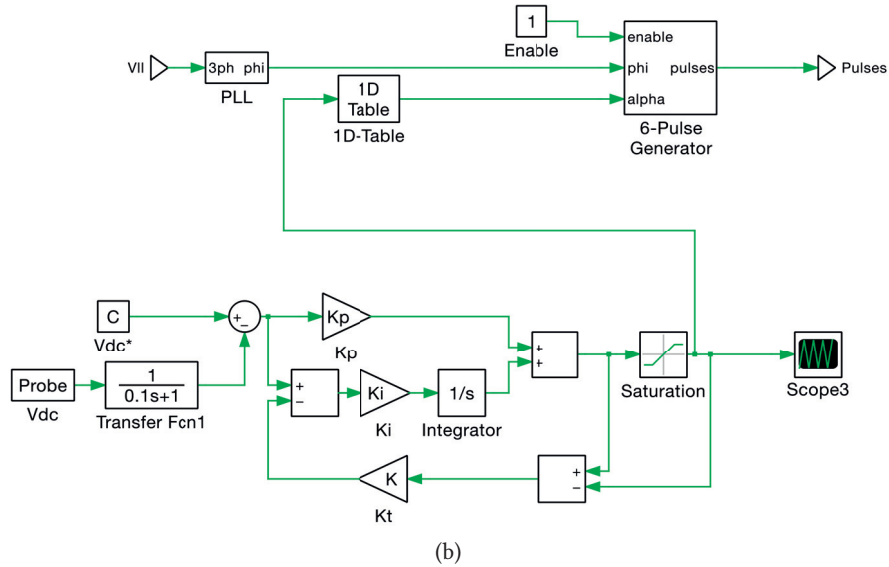


**Figure A.2** (b) Modified inverse cosine control for TRU.

### A.3 ARU time domain model

An average model is used for both ARU and inverter. This model is same for classic 2-L or multi-level VSC topologies and given in **Fig. A.3**.

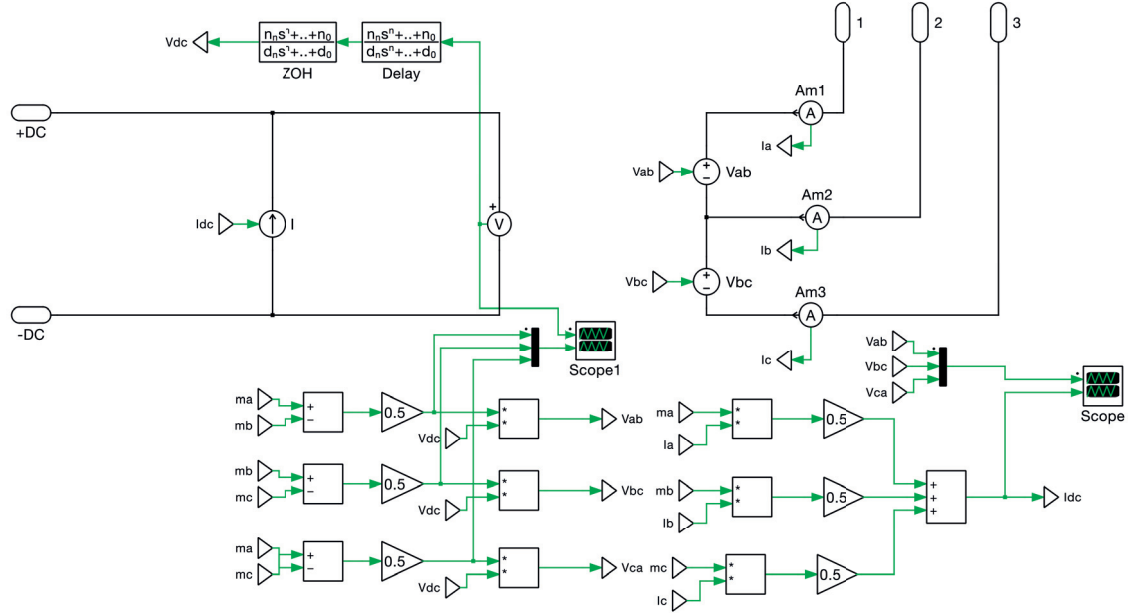


**Figure A.3** Average model used for simulating ARU and inverter.

## A.4 MMC time domain model

An average model is used for the MMC branch and is similar to the schematics given in Fig. 6.3. The models for the MMC branch and whole converter are given in Fig. A.4.

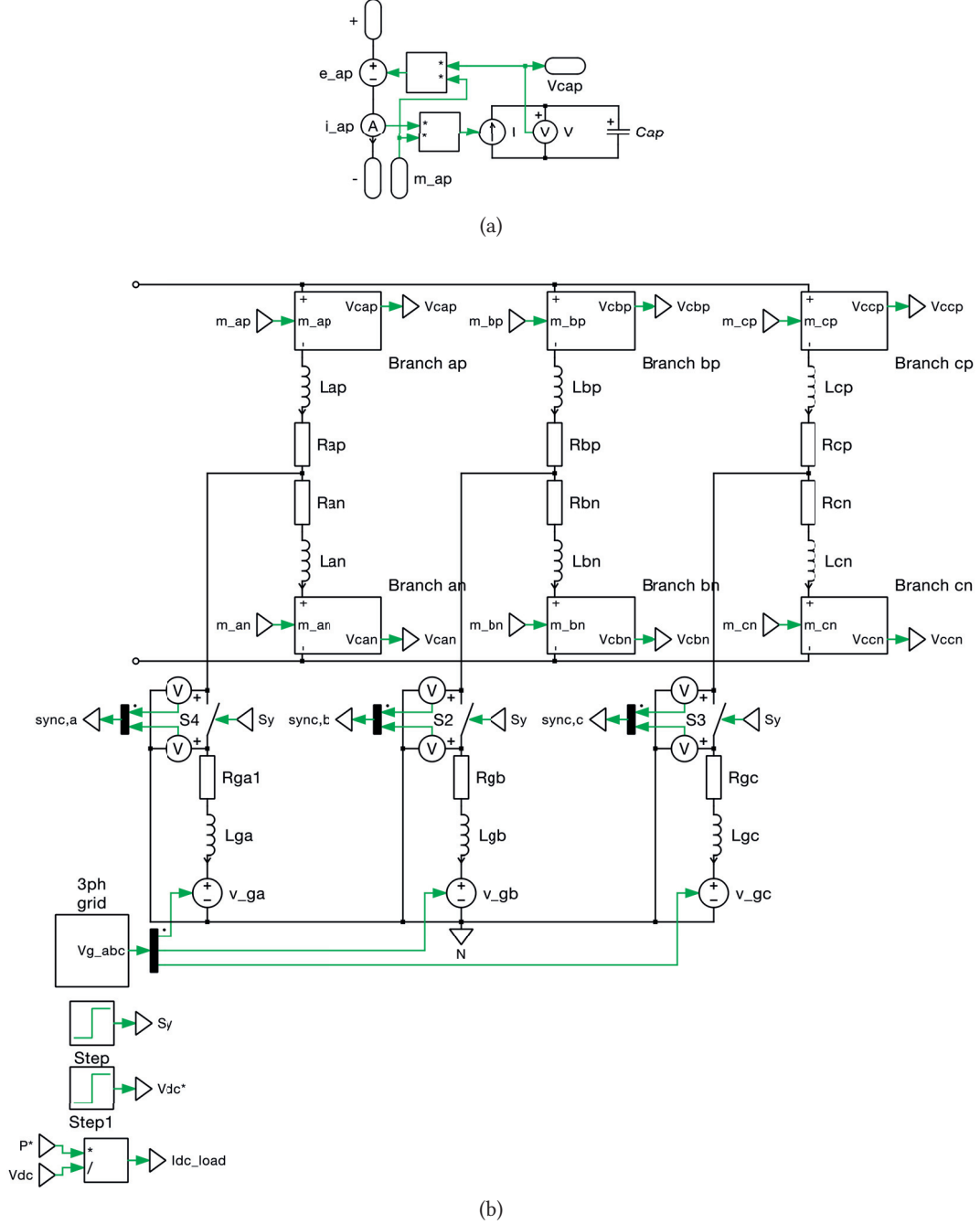


**Figure A.4** (a) Average branch model for MMC. (b) MMC model used for time domain simulations.



# References

- [1] S. Kenzelmann, “Modular dc/dc converter for dc distribution and collection networks,” PhD thesis, École Polytechnique Fédérale de Lausanne, 2012.
- [2] ABB. (Nov. 2011). Tesla vs Edison: the war of currents, [Online]. Available: <http://www.abb.com/cawp/seitp202/c646c16ae1512f8ec1257934004fa545.aspx>.
- [3] A. Lantero. (Nov. 2014). The war of the currents: Ac vs. dc power, [Online]. Available: <https://energy.gov/articles/war-currents-ac-vs-dc-power>.
- [4] H. Rissik, *Mercury-arc current converters*, 2nd. Pitman, London, 1941, Reprint 1960.
- [5] ABB Drives. (2010). Medium voltage AC drive - ACS 6000, 3 – 36 MW, up to 3.3 kV, [Online]. Available: [https://library.e.abb.com/public/5e7f2eb1c4d429c948257e12004d4282/ACS%206000%20EN%20Rev%20F\\_lowres.pdf](https://library.e.abb.com/public/5e7f2eb1c4d429c948257e12004d4282/ACS%206000%20EN%20Rev%20F_lowres.pdf).
- [6] S. D. Sudhoff, “Currents of change,” *IEEE Power Energy Magazine*, vol. 9, no. 4, pp. 30–37, Jul. 2011.
- [7] T. J. McCoy, “Trends in ship electric propulsion,” in *IEEE Power Engineering Society Summer Meeting*, vol. 1, Jul. 2002, pp. 343–346.
- [8] Rolls Royce. (2016). Marine marine products and systems, [Online]. Available: <https://www.rolls-royce.com/~media/Files/R/Rolls-Royce/documents/marine-product-finder/MPS%202017%20LR.pdf>.
- [9] Siemens AG. (2013). SINAMICS S120 cabinet modules application shaft generator drive, [Online]. Available: [https://www.industry.usa.siemens.com/drives/us/en/electric-drives/ac-drives/high-performance-and-servo-drives/sinamics-s120-drive-cabinet-modules/Documents/SINAMICS\\_S120\\_CM-Marine-Brochure.pdf](https://www.industry.usa.siemens.com/drives/us/en/electric-drives/ac-drives/high-performance-and-servo-drives/sinamics-s120-drive-cabinet-modules/Documents/SINAMICS_S120_CM-Marine-Brochure.pdf) (visited on ).
- [10] Brunvoll Holding AS. (2017). Integrated propulsion systems, [Online]. Available: <http://scanapropulsion.com/products/>.
- [11] STADT. (2017). System, [Online]. Available: <http://www.stadt.no/system.html>.
- [12] ABB, *Azipod® gearless propulsors*, 2017.
- [13] A. K. Aadnanes, “Maritime electrical installations and diesel electric propulsion,” Tech. Rep., 2003.
- [14] A. Tessarolo, S. Castellan, R. Menis, and G. Sulligoi, “Electric generation technologies for all-electric ships with medium-voltage dc power distribution systems,” in *IEEE Electric Ship Technologies Symposium (ESTS)*, Apr. 2013, pp. 275–281.
- [15] I. Fazlagic, J.-F. Hansen, and A. K. Aadnanes, *Onboard dc grid - one year in operation*, 2013.
- [16] R. M. Calfo, J. A. Fulmer, and J. E. Tessaro, “Generators for use in electric marine ship propulsion systems,” in *IEEE Power Engineering Society Summer Meeting*, vol. 1, Jul. 2002, pp. 254–259.
- [17] ABB AS. (2012). Onboard dc grid - the newest design for marine power and propulsion systems, [Online]. Available: [https://library.e.abb.com/public/b4f3f099e9d21360c1257a8a003beac2/ABB%20Generations\\_20%20Onboard%20DC%20grid.pdf](https://library.e.abb.com/public/b4f3f099e9d21360c1257a8a003beac2/ABB%20Generations_20%20Onboard%20DC%20grid.pdf).
- [18] Siemens Marine and Shipbuilding. (2014). BlueDrive PlusC - Makes vessels safer, more profitable and environmentally friendly, [Online]. Available: [https://w3.siemens.no/home/no/no/sector/industry/marine/Documents/Orig.BDPC\\_16pages.pdf](https://w3.siemens.no/home/no/no/sector/industry/marine/Documents/Orig.BDPC_16pages.pdf).
- [19] Y. Khersonsky and G. Sulligoi, “New IEEE & IEC standards for ships and oil platforms,” in *2014 IEEE Petroleum and Chemical Industry Technical Conference (PCIC)*, Sep. 2014, pp. 191–199.
- [20] *IEEE Recommended Practice for 1 kV to 35 kV Medium-Voltage DC Power Systems on Ships*. IEEE Standard 1709, 2010.
- [21] Rolls Royce. (2016). Tomorrow’s ferry technology delivered today, [Online]. Available: <https://www.rolls-royce.com/~media/Files/R/Rolls-Royce/documents/customers/marine/rr-b-ferry-0317-sp.pdf>.
- [22] S. Salomon, G. Avigad, R. C. Purshouse, and P. J. Fleming, “Gearbox design for uncertain load requirements using active robust optimization,” *Engineering Optimization*, vol. 48, no. 4, pp. 652–671, 2016.
- [23] B. Zahedi, L. E. Norum, and K. B. Ludvigsen, “Optimized efficiency of all-electric ships by dc hybrid power systems,” *Journal of Power Sources*, vol. 255, pp. 341–354, 2014.
- [24] S. Kanerva, P. Pohjanheimo, and M. Kajava, “Dynamic ac concept for variable speed power generation,” ABB Marine and Ports, Helsinki, Finland, Tech. Rep., 2016.
- [25] S. Z. Vijlee, A. Ouroua, L. N. Domaschk, and J. H. Beno, “Directly-coupled gas turbine permanent magnet generator sets for prime power generation on board electric ships,” in *IEEE Electric Ship Technologies Symposium (ESTS)*, May 2007, pp. 340–347.
- [26] Wartsila, *Wartsila generating sets*, 2017.
- [27] —, *Improving efficiency*, 2014.
- [28] MAN Diesel and Turbo, *Marine engine IMO Tier II and Tier III program 2nd ed.* 2016.

## References

- [29] —, *Thermo efficiency system for reduction of fuel consumption and CO<sub>2</sub> emission*.
- [30] GE Power Conversion, *GE showcases innovative and efficient solutions for the maritime industry at SMM*, 2014.
- [31] Bergen Engines AS, *Bergen engines products and applications*.
- [32] GE Aviation, *Commercial gas turbines*.
- [33] Rolls Royce, *Gas turbines*.
- [34] L. Mahon, *Diesel generator handbook*. Newnes, 1992.
- [35] J. F. Hansen, J. O. Lindtjørn, K. Vanska, and O. ABB, "Onboard dc grid for enhanced dp operation in ships," in *Dynamic Positioning Conference*, 2011.
- [36] MAN Diesel and Turbo, "EPROX Energy-saving electric propulsion system," Tech. Rep.
- [37] GE Power and Water, "Fast, Flexible Power Aeroderivative Product and Service Solutions," Tech. Rep., 2013.
- [38] ABB, *Marine generators - proven generators for reliable power on board*.
- [39] —, *Product note - wind power generators - high speed permanent magnet synchronous generator (HS PMG)*.
- [40] D. M. Saban, C. Bailey, D. Gonzalez-Lopez, and L. Luca, "Experimental evaluation of a high-speed permanent-magnet machine," in *55th IEEE Petroleum and Chemical Industry Technical Conference*, Sep. 2008, pp. 1–9.
- [41] Z. W. Vilar and R. A. Dougal, "Load following ability of a ship generating plant comprising a mixed set of high-speed and synchronous turbo-generators," in *IEEE Electric Ship Technologies Symposium (ESTS)*, May 2007, pp. 335–339.
- [42] G. Sulligoi, A. Tassarolo, V. Benucci, A. M. Trapani, M. Baret, and F. Luise, "Design, implementation and testing of a shipboard medium-voltage dc generation system based on a ultra-high speed 12-phase alternator," in *IEEE Electric Ship Technologies Symposium (ESTS)*, Apr. 2011, pp. 388–395.
- [43] N. Bianchi, S. Bolognani, and F. Luise, "Potentials and limits of high-speed pm motors," *IEEE Transactions on Industry Applications*, vol. 40, no. 6, pp. 1570–1578, Nov. 2004.
- [44] E. Levi, "Multiphase electric machines for variable-speed applications," *IEEE Transactions on Industrial Electronics*, vol. 55, no. 5, pp. 1893–1909, May 2008.
- [45] Siemens, *Siemens electric machines s.r.o., factory drasov*, 2010.
- [46] GE Power Conversion, *Generators - 2500 to 80000 kVA - up to 22000 kVA*, 2014.
- [47] Siemens AG, *Wind is our element*, 2012.
- [48] *NORSOK standards*, 2017.
- [49] *Power transformers - Part 11: Dry-type transformers*. IEC 60076-11:2004.
- [50] ABB. (2017). RESIBLOC transformers, [Online]. Available: <http://new.abb.com/products/transformers/dry-type/transmission-distribution/resibloc-transformers>.
- [51] D. Dujic, J. Wahlstroem, J. A. M. Sosa, and D. Fritz, "Modular medium voltage drive for demanding applications," in *International Power Electronics Conference (IPEC-Hiroshima - ECCE ASIA)*, May 2014, pp. 3476–3481.
- [52] N. Mohan and T. M. Undeland, *Power electronics: converters, applications, and design*. John Wiley & Sons, 2007.
- [53] D. Dong, Y. Pan, R. Lai, X. Wu, and K. Weeber, "Active fault-current foldback control in thyristor rectifier for dc shipboard electrical system," *IEEE Journal of Emerging and Selected Topics in Power Electronics*, vol. 5, no. 1, pp. 203–212, Mar. 2017.
- [54] J. Rodriguez, S. Bernet, B. Wu, J. O. Pontt, and S. Kouro, "Multilevel voltage-source-converter topologies for industrial medium-voltage drives," *IEEE Transactions on Industrial Electronics*, vol. 54, no. 6, pp. 2930–2945, Dec. 2007.
- [55] N. Chaudhuri, B. Chaudhuri, R. Majumder, and A. Yazdani, *Multi-terminal direct-current grids: Modeling, analysis, and control*. John Wiley & Sons, 2014.
- [56] A. Christe and D. Dujic, "Galvanically isolated modular converter," *IET Power Electronics*, vol. 9, no. 12, pp. 2318–2328, 2016.
- [57] P. Blaszczyk, M. Steurer, D. Soto, F. Bogdan, J. Hauer, M. Sloderbeck, and K. Schoder, "Modular multilevel converter based test bed for mvdc applications - a case study with a 12 kV, 5 MW setup," in *IEEE International Power Electronics and Motion Control Conference (PEMC)*, Sep. 2016, pp. 139–145.
- [58] D. Krug, S. Busse, and M. Beuermann, "Complete performance test of mv drive with modular multilevel topology for high power oil gas applications," in *IEEE Petroleum and Chemical Industry Technical Conference (PCIC)*, Sep. 2016, pp. 1–6.
- [59] Siemens AG. (2017). MVDC PLUS, [Online]. Available: <https://www.siemens.com/global/en/home/products/energy/medium-voltage/solutions/mvdc.html#Ordertechnicaldetails> (visited on ).
- [60] —, (2018). SINAMICS SM120 CM, [Online]. Available: <https://www.industry.siemens.com/drives/global/en/converter/mv-drives/Pages/sinamics-sm120-cm.aspx> (visited on ).
- [61] R. Mo, Q. Ye, and H. Li, "Dc impedance modeling and stability analysis of modular multilevel converter for mvdc application," in *IEEE Energy Conversion Congress and Exposition (ECCE)*, Sep. 2016, pp. 1–5.
- [62] H. Mirzaee, B. Parkhideh, and S. Bhattacharya, "Design and control of series dc active filter (sdaf) for shipboard medium-voltage dc power system," in *IEEE Electric Ship Technologies Symposium (ESTS)*, Apr. 2011, pp. 452–458.

- [63] Y.-C. Jeung, D. C. Lee, and H.-H. Lee, "Feedback linearization control of series active dc filters for mvdc shipboard power systems," in *16th European Conference on Power Electronics and Applications*, Aug. 2014, pp. 1–9.
- [64] R. Mo, R. Li, and H. Li, "Isolated modular multilevel (imm) dc/dc converter with energy storage and active filter function for shipboard mvdc system applications," in *IEEE Electric Ship Technologies Symposium (ESTS)*, Jun. 2015, pp. 113–117.
- [65] *Brugg cables - mittelspannungskabel - mittelspannungskabel (cu) - xkdt 1-leiter ms-polymerkabel 20/12kv*, Nov. 2011.
- [66] J. Wahlstroem, D. Dujic, M. A. Luescher, and S. Reist, "High power igct based multilevel inverter," in *Proceedings of International Exhibition and Conference for Power Electronics, Intelligent Motion, Renewable Energy and Energy Management (PCIM)*, May 2014, pp. 1–6.
- [67] J. K. Steinke, "Control strategy for a three phase ac traction drive with three-level gto pwm inverter," in *19th Annual IEEE Power Electronics Specialists Conference (PESC)*, Apr. 1988, 431–438 vol.1.
- [68] Siemens AG, *High voltage motors*, 2017.
- [69] ABB, *Energy storage systems*, 2017.
- [70] Y. K. Tran and D. Dujic, "A multiport isolated dc-dc converter," in *IEEE Applied Power Electronics Conference and Exposition (APEC)*, Mar. 2016, pp. 156–162.
- [71] N. H. Doerry and H. Fireman, "Designing all electric ships," in *Proceedings of the 9th International Marine Design Conference*, 2006, pp. 475–498.
- [72] G. Sulligoi, A. Vicenzutti, and R. Menis, "All-electric ship design: From electrical propulsion to integrated electrical and electronic power systems," *IEEE Transactions on Transportation Electrification*, vol. 2, no. 4, pp. 507–521, Dec. 2016.
- [73] A. Hasanzadeh, C. S. Edrington, D. M. Soto, and G. M. Rivera, "Comparative study of intensive pulse load impact on active and passive rectification system in mvdc ship power generation unit," in *IEEE International Electric Machines Drives Conference (IEMDC)*, May 2013, pp. 1326–1332.
- [74] R. T. Wang, L. J. Fu, F. Xiao, and X. X. Fan, "System protection for vessel dc zonal electrical system supplied by medium voltage dc," in *IEEE International Conference on Applied Superconductivity and Electromagnetic Devices (ASEMD)*, Oct. 2013, pp. 89–93.
- [75] A. Ouroua, L. Domaschk, and J. H. Beno, "Electric ship power system integration analyses through modeling and simulation," in *IEEE Electric Ship Technologies Symposium (ESTS)*, Jul. 2005, pp. 70–74.
- [76] B. Zahedi and L. E. Norum, "Modeling and simulation of all-electric ships with low-voltage dc hybrid power systems," *IEEE Transactions on Power Electronics*, vol. 28, no. 10, pp. 4525–4537, Oct. 2013.
- [77] G. Sulligoi, D. Bosich, G. Giadrossi, L. Zhu, M. Cupelli, and A. Monti, "Multiconverter medium voltage dc power systems on ships: Constant-power loads instability solution using linearization via state feedback control," *IEEE Transactions on Smart Grid*, vol. 5, no. 5, pp. 2543–2552, Sep. 2014.
- [78] B. Zahedi and L. E. Norum, "Efficiency analysis of shipboard dc power systems," in *39th Annu. Conf. of the IEEE Industrial Electronics Soc. (IECON)*, Nov. 2013, pp. 689–694.
- [79] *Maritime connector*.
- [80] A. K. Aadnanes, A. J. Sorensen, and T. Hackman, "Essential characteristics of electrical propulsion and thruster drives in dp vessels," in *Dynamic Positioning Conference*, Houston, Oct. 1997.
- [81] C. Zhao, D. Dujic, A. Mester, J. K. Steinke, M. Weiss, S. Lewdeni-Schmid, T. Chaudhuri, and P. Stefanutti, "Power electronic traction transformer - medium voltage prototype," *IEEE Trans. Ind. Electron.*, vol. 61, no. 7, pp. 3257–3268, Jul. 2014.
- [82] M. H. Rashid, *Power electronics handbook: devices, circuits and applications*. Academic press, 2010.
- [83] J. M. Meyer and A. Rufer, "A DC hybrid circuit breaker with ultra-fast contact opening and integrated gate-commutated thyristors (IGCTs)," *IEEE Transactions on Power Delivery*, vol. 21, no. 2, pp. 646–651, Apr. 2006.
- [84] K. A. Corzine and R. W. Ashton, "Structure and analysis of the z-source mvdc breaker," in *IEEE Electric Ship Technologies Symposium (ESTS)*, Apr. 2011, pp. 334–338.
- [85] H. Mirzaee, S. Bhattachary, and S. Bala, "Design issues in a medium-voltage dc amplifier with a multi-pulse thyristor bridge front-end," in *IEEE Energy Conversion Congress and Exposition (ECCE)*, Sep. 2012, pp. 603–609.
- [86] ABB drives, "Technical guide no. 6 guide to harmonics with AC drives," ABB, Tech. Rep., 2015.
- [87] ABB, *Application Note 5SYA 2029-03: High power rectifier diodes*, 2013.
- [88] —, *Application Note 5SYA 2051: Voltage ratings of high power semiconductors*, 2013.
- [89] Ferraz Shawmut, Mersen, *Special Purpose Fuses*, 2013.
- [90] Eaton, *Application Guide 10507: Protecting semiconductors with high speed fuses*, 2016.
- [91] A. Emadi, A. Khaligh, C. H. Rivetta, and G. A. Williamson, "Constant power loads and negative impedance instability in automotive systems: Definition, modeling, stability, and control of power electronic converters and motor drives," *IEEE Transactions on Vehicular Technology*, vol. 55, no. 4, pp. 1112–1125, Jul. 2006.



## References

- [92] P. Liutanakul, A. B. Awan, S. Pierfederici, B. Nahid-Mobarakeh, and F. Meibody-Tabar, "Linear stabilization of a dc bus supplying a constant power load: A general design approach," *IEEE Transactions on Power Electronics*, vol. 25, no. 2, pp. 475–488, Feb. 2010.
- [93] A. Riccobono and E. Santi, "Comprehensive review of stability criteria for dc power distribution systems," *IEEE Transactions on Industry Applications*, vol. 50, no. 5, pp. 3525–3535, Sep. 2014.
- [94] S. D. Sudhoff, S. F. Glover, P. T. Lamm, D. H. Schmucker, and D. E. Delisle, "Admittance space stability analysis of power electronic systems," *IEEE Transactions on Aerospace and Electronic Systems*, vol. 36, no. 3, pp. 965–973, Jul. 2000.
- [95] J. Sun, "Autonomous local control and stability analysis of multiterminal dc systems," *IEEE Journal of Emerging and Selected Topics in Power Electronics*, vol. 3, no. 4, pp. 1078–1089, Dec. 2015.
- [96] G. Sulligoi, D. Bosich, L. Zhu, M. Cupelli, and A. Monti, "Linearizing control of shipboard multi-machine mvdc power systems feeding constant power loads," in *IEEE Energy Conversion Congress and Exposition (ECCE)*, Sep. 2012, pp. 691–697.
- [97] M. Cupelli, M. Mirz, and A. Monti, "Application of backstepping to mvdc ship power systems with constant power loads," in *International Conference on Electrical Systems for Aircraft, Railway, Ship Propulsion and Road Vehicles (ESARS)*, Mar. 2015, pp. 1–6.
- [98] —, "A comparison of backstepping and lqg control for stabilizing mvdc microgrids with constant power loads," in *IEEE Eindhoven PowerTech*, Jun. 2015, pp. 1–6.
- [99] M. Cupelli, A. Monti, E. D. Din, and G. Sulligoi, "Case study of voltage control for mvdc microgrids with constant power loads - comparison between centralized and decentralized control strategies," in *18th Mediterranean Electrotechnical Conference (MELECON)*, Apr. 2016, pp. 1–6.
- [100] R. D. Middlebrook, "Input filter considerations in design and application of switching regulators," *IAS Record*, 1976.
- [101] C. M. Wildrick, F. C. Lee, B. H. Cho, and B. Choi, "A method of defining the load impedance specification for a stable distributed power system," *IEEE Transactions on Power Electronics*, vol. 10, no. 3, pp. 280–285, May 1995.
- [102] C. M. Wildrick, "Stability of distributed power supply systems," Master's thesis, Virginia Polytechnic Institute and State University, Blacksburg, VA, USA, Feb. 1993.
- [103] X. Feng, J. Liu, and F. C. Lee, "Impedance specifications for stable dc distributed power systems," *IEEE Transactions on Power Electronics*, vol. 17, no. 2, pp. 157–162, Mar. 2002.
- [104] *Dc stability toolbox source code and manual*.
- [105] L. Harnefors, M. Bongiorno, and S. Lundberg, "Input-admittance calculation and shaping for controlled voltage-source converters," *IEEE Transactions on Industrial Electronics*, vol. 54, no. 6, pp. 3323–3334, Dec. 2007.
- [106] F. de Bosio, L. A. de Souza Ribeiro, F. D. Freijedo, M. Pastorelli, and J. M. Guerrero, "Effect of state feedback coupling and system delays on the transient performance of stand-alone vsi with lc output filter," *IEEE Transactions on Industrial Electronics*, vol. 63, no. 8, pp. 4909–4918, Aug. 2016.
- [107] K. J. Astrom and T. Hagglund, *PID controllers: Theory, design, and tuning*. International Society of Automation, 1995.
- [108] R. Feldman, M. Tomasini, E. Amankwah, J. C. Clare, P. W. Wheeler, D. R. Trainer, and R. S. Whitehouse, "A hybrid modular multilevel voltage source converter for hvdc power transmission," *IEEE Transactions on Industry Applications*, vol. 49, no. 4, pp. 1577–1588, Jul. 2013.
- [109] M. M. C. Merlin, T. C. Green, P. D. Mitcheson, D. R. Trainer, R. Critchley, W. Crookes, and F. Hassan, "The alternate arm converter: A new hybrid multilevel converter with dc-fault blocking capability," *IEEE Transactions on Power Delivery*, vol. 29, no. 1, pp. 310–317, Feb. 2014.
- [110] H. Nademi, A. Das, R. Burgos, and L. E. Norum, "A new circuit performance of modular multilevel inverter suitable for photovoltaic conversion plants," *IEEE Journal of Emerging and Selected Topics in Power Electronics*, vol. 4, no. 2, pp. 393–404, Jun. 2016.
- [111] M. Hagiwara and H. Akagi, "Control and experiment of pulsewidth-modulated modular multilevel converters," *IEEE Transactions on Power Electronics*, vol. 24, no. 7, pp. 1737–1746, Jul. 2009.
- [112] A. J. Korn, M. Winkelnkemper, P. Steimer, and J. W. Kolar, "Direct modular multi-level converter for gearless low-speed drives," in *Proceedings of the 14th European Conference on Power Electronics and Applications*, Aug. 2011, pp. 1–7.
- [113] P. K. Steimer, O. Senturk, S. Aubert, and S. Linder, "Converter-fed synchronous machine for pumped hydro storage plants," in *IEEE Energy Conversion Congress and Exposition (ECCE)*, Sep. 2014, pp. 4561–4567.
- [114] X. Shi, Z. Wang, B. Liu, Y. Li, L. M. Tolbert, and F. Wang, "Dc impedance modelling of a mmc-hvdc system for dc voltage ripple prediction under a single-line-to-ground fault," in *IEEE Energy Conversion Congress and Exposition (ECCE)*, Sep. 2014, pp. 5339–5346.
- [115] J. Lyu, X. Cai, and M. Molinas, "Impedance modeling of modular multilevel converters," in *41st Annual Conference of the IEEE Industrial Electronics Society (IECON)*, Nov. 2015, pp. 000 180–000 185.



- [116] J. Sun and H. Liu, "Impedance modeling and analysis of modular multilevel converters," in *IEEE 17th Workshop on Control and Modeling for Power Electronics (COMPEL)*, Jun. 2016, pp. 1–9.
- [117] G. Stamatiou, "Analysis of vsc-based hvdc systems," PhD thesis, Department of Energy and Environment, Chalmers University of Technology, Gothenburg, Sweden, 2016.
- [118] N. Cherix, "Functional description and control design of modular multilevel converters-towards energy storage applications for traction networks," PhD thesis, École Polytechnique Fédérale de Lausanne, 2015.
- [119] J. Liu, X. Feng, F. C. Lee, and D. Borojevich, "Stability margin monitoring for dc distributed power systems via perturbation approaches," *IEEE Transactions on Power Electronics*, vol. 18, no. 6, pp. 1254–1261, Nov. 2003.
- [120] A. Antonopoulos, L. Ångquist, L. Harnefors, K. Ilves, and H. P. Nee, "Global asymptotic stability of modular multilevel converters," *IEEE Transactions on Industrial Electronics*, vol. 61, no. 2, pp. 603–612, Feb. 2014.
- [121] P. Münch, D. Görge, M. Izák, and S. Liu, "Integrated current control, energy control and energy balancing of Modular Multilevel Converters," in *36th Annual Conference of the IEEE Industrial Electronics Society (IECON)*, Nov. 2010, pp. 150–155.
- [122] K. Sharifabadi, L. Harnefors, H.-P. Nee, R. Teodorescu, and S. Norrga, *Design, Control and Application of Modular Multilevel Converters for HVDC Transmission Systems*. John Wiley & Sons, 2016.
- [123] M. D. Jaksic, "Identification of small-signal dq impedances of power electronics converters via single-phase wide-bandwidth injection," PhD thesis, Virginia Tech, 2015.
- [124] M. Amin, M. Zadeh, J. A. Suul, E. Tedeschi, M. Molinas, and O. B. Fosso, "Stability analysis of interconnected ac power systems with multi-terminal dc grids based on the cigré dc grid test system," in *3rd Renewable Power Generation Conference (RPG)*, Sep. 2014, pp. 1–6.
- [125] G. O. Kalcon, G. P. Adam, O. Anaya-Lara, S. Lo, and K. Uhlen, "Small-signal stability analysis of multi-terminal vsc-based dc transmission systems," *IEEE Transactions on Power Systems*, vol. 27, no. 4, pp. 1818–1830, Nov. 2012.
- [126] J. Arocas-Pérez and R. Griño, "A local stability condition for dc grids with constant power loads," in *International Federation of Automatic Control (IFAC)-PapersOnLine*, vol. 50, Elsevier, Jul. 2017, pp. 7–12.
- [127] S. F. G. Graham C. Goodwin and M. E. Salgado, *Control System Design*. Prentice Hall, 2001.
- [128] R. C. Dorf and R. H. Bishop, *Modern control systems*. Pearson, 2011.
- [129] F. D. Freijedo, A. Vidal, A. G. Yepes, J. M. Guerrero, Ó. López, J. Malvar, and J. Doval-Gandoy, "Tuning of synchronous-frame pi current controllers in grid-connected converters operating at a low sampling rate by mimo root locus," *IEEE Transactions on Industrial Electronics*, vol. 62, no. 8, pp. 5006–5017, Aug. 2015.
- [130] C. Desoer and Y.-T. Wang, "On the generalized nyquist stability criterion," *IEEE Transactions on Automatic Control*, vol. 25, no. 2, pp. 187–196, Apr. 1980.
- [131] L. Harnefors and H. P. Nee, "Model-based current control of ac machines using the internal model control method," *IEEE Transactions on Industry Applications*, vol. 34, no. 1, pp. 133–141, Jan. 1998.
- [132] F. D. Freijedo, U. Javaid, and D. Dujic, "Conformal mapping of impedance stability models for system-level dynamics assessments," in *International Symposium on Power Electronics (Ee)*, Oct. 2017, pp. 1–6.
- [133] F. E. Cellier and E. Kofman, *Continuous system simulation*. Springer Science & Business Media, 2006.



# Curriculum Vitae

Uzair Javaid

✉ uzairchaudhary@gmail.com  
born 02.27.1989  
Pakistani

*Doctoral Assistant - Power Electronics Laboratory*

## EDUCATION

École Polytechnique Fédérale de Lausanne, Lausanne, Switzerland

2014 – 2018 Ph.D., *Electrical Engineering Doctoral School*, Power Electronics Laboratory

(exp.) *MVDC Distribution Fed High Power Multi-Motor Drives* Funded by ABB MV Drives

2011 – 2013 M.Sc., *Energy Management and Sustainability*

M.Sc. thesis *Pilot Bus Selection for Tertiary Level Control of Voltage Regulation to Increase Voltage Stability Margin*

University of Engineering and Technology, Lahore, Pakistan

2006 – 2010 B.Sc., *Electrical Engineering*

B.Sc. thesis *Load Frequency Control (Automatic Generation Control) of an Inter-connected Hydro-Thermal System Using Fuzzy Logic Controller*

## TEACHING AND SUPERVISION

2014 – 2017 Assistant for the master course *Industrial Electronics II* (Control and modeling of high performance variable speed drives)

2016 Two MSc semester projects supervision (*Impedance modeling of power electronic systems*)

2015 Two MSc semester projects supervision (*High performance variable speed drives, HIL simulation of variable speed drives*)



